INTERPRETATION OF THE HLEM SURVEY WITH MULTIPLE SEPARATION

K. KIM

Abstract

Dimensional analysis is applied to the electromagnetic problem of a sheet-like conductor of finite dimensions and conductivity in order to reduce the number of variable parameters associated with the secondary electromagnetic field. Through model work the relations among these parameters are investigated with horizontal loop EM system by varying the thickness, depth, depth extent, conductivity and dip angle, to make a set of master curves for interpretation of field results

In order to establish the usefulness of these master curves, field data from several areas in Saskatchewan and Quebec were interpreted by this method and the results compared to those obtained from standard characteristic curves. The method is also applied to the results from three other surveys.

Interpretation of the Horizontal loop EM Survey with Multiple Separation

by

Kwang-Kook Kim B.Sc. in Eng.

A thesis submitted to the Faculty of Grauate Studies and Research in partial fulfilment of the requirements for the degree of Master of Science.

Department of Mining
and Metalurgical Engineering,
McGill University,
Montreal, Quebec, Canada

June, 1973

Acknowledgements

I am indebted to some fellow graduate students who answered my questions, and this thesis reflects strongly the suggestions made by them. In particular, I wish to acknowledge the financial support made by the National Research Council of Canada, during the period September, 1971 to April, 1973. The author is grateful to Dr. W. M. Telford who led me by endless suggestion and discussion to make this thesis. I thank T - R Yu and Russell Parrott who prepared the experimental equipment and gave helpful suggerstions for the experimental work. I express my thanks to my wife, Chung-Ja, and my daughter, Grase, for encouragement and patience for my work. I wish my wife could have the degree which is sought by this thesis !

Table of Contents

Table of Illustrations

List of Tables

Chapter 1. Introduction

In mineral exploration, geophysical prospecting has played an important role in explaining subsurface structure, so that a geophysicist may establish detailed plans of the next step of the survey procedure. Using certain of the electromagnetic (EM) prospecting techniques, one may obtain some idea of the electrical and geometrical parameters, such as conductivity, location, dip-angle, etc. Therefore, many geophysicists have attacked this problem.

Looking into EM interpretation theory, it is obviously very difficult to perform theoretical or numerical derivations of the electromagnetic response in the case in which we have finite conductivity. In fact, analytical solutions may be obtained for only a few simple geometries where the conductivity is infinite. These include:

1) Sphere (cylinder) in AC and dipole field,
2) Horizontal thin sheet in AC and dipole field,
3) Infinite half space in AC and dipole field,
4) Half plane in dipole field.

See, for example, Wait(1951, 1954, 1955, 1956), Slichter & Knopoff(1959), Grant & West(1965), Ward(1967). Wesley(1958) has published an approximate solution for the case of a vertically dipping dyke. Grant & West(1965) obtained solutions using

Green's functions in the problem which had been dealt with by Wesley.

On the other hand, because of the complexity involved in deriving numerical solutions for typical field conditions, some people, such as Hedstrom and Parasnis(1959), and Paterson (1961) have approached the electromagnetic problem with model studies. Strangway(1966) conducted a series of model experiments as an aid to the interpretation of the horizontal loop E.M. survey, showing results similar to Parasnis(1959). Again Parasnis(1971) issued a cautionary note, based on some full scale data of multi-frequency, multi-separation methods in E.M. surveys, against the blind use of vector diagrams and also discussed the extent of the extra information and interpretation aid provided by such surveys.

In different manner, Koefoed and Kegge(1969) calculated the electrical current pattern on a thin sheet using the development by Wesley(1958), and Koefoed and Struyk(1969) determined the electrical current distribution by measuring the tangential component of the magnetic field strength very close to the metal plate that simulated the vertical conductive dyke.

By considering the conductor to be equivalent to a coil one can obtain some important and useful parameters, such as the relation of in-phase and out-of-phase component of the secondary magnetic field to the response parameter $\alpha = \omega L/R$, for analysis of the EM response.

For the present study, the author has investigated the electromagnetic response of the horizontal loop EM system using a thin plate with variable dip-angle, depth, conductivity, depth extent and separation, applying dimensional analysis to the results of model work to calculate new factors, such as $\sigma\mu\omega$, t/l, d/l, s/l and θ under consideration in electromagnetic surveys. The relations between the new factors have been compared with field results to get more information than from conventional interpretation. The results of dimensional analysis with five parameters as described have been studied through numerical analysis, by which mutual and self-inductances among three coils, say, transmitter, receiver and a conducting coil have been obtained. The conductor is simulated by an elliptical coil. In order to reduce the number of parameters, the conductor is assumed to be very thin, having initially infinite conductivity and vertical attitude so that one may have some idea about the relation of the five parameters.

Following the numerical analysis, model work has been carried out to determine the size of conductor and its conductivity by considering the relations between the new factors from the model experiments. In addition, by plotting the data in vertical pseudo section as in the method developed by Hallof for dipole-dipole I.P. surveys, we may obtain the location and estimate the dip angle of the target directly.

Chapter 2. Dimensional Analysis of Electromagnetic Response over the Tabular Dipping Body

In Canada, we have a large Precambrian area which is composed of igneous and meta-sedimentary rocks. In this geology, many mineral deposits are due to hydrothermal processes, since the geological age is very great and in that period many complicated geological movements have changed the structure in various ways. Thus, cavity filling and replacement by economic minerals have frequently occurred in dyke or sheet structures. This type of mineral deposit is commonly associated with intrusion of igneous rocks and with faulting of geological formations. In prospecting for the mineral deposit, the problem is to determine the electrical properties of the conductor as well as information about its structure.

Suppose we carry out a horizontal loop E.M. traverse over a dyke or sheet conductor shown in Fig. 1. In the horizontal loop EM survey, the transmitter (Tx) produces a primary electromagnetic field which induces currents in the conductor and we measure the secondary EM field produced by the induced currents, as a fraction of the primary transmitted field, at the receiver (Rx). The secondary EM field, $H^{(s)}$, depends upon the electrical and geometrical properties of the conductor,

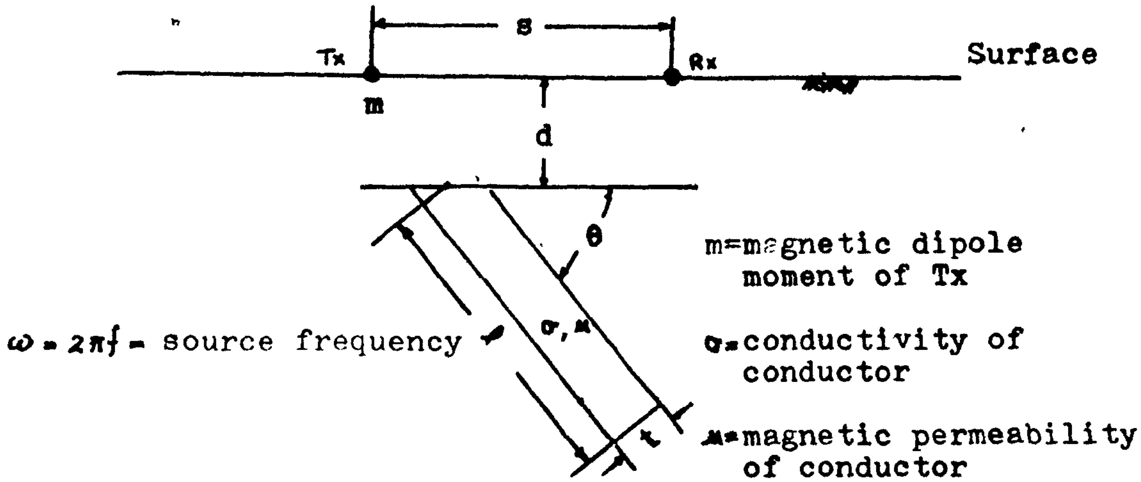

Fig. 1. The horizontal loop survey system

as well as the geometry of the survey system. Now we have a formula in terms of the variables described in Fig. 1, which expresses the secondary field, $H^{(s)}$.

$$H^{(s)} = f(\, l, \sigma, \mu, \omega\ s, d, t, \theta, m) \quad \ldots\ldots\ldots\ldots\ldots(1)$$

The primary field of the transmitter at the receiver is obtained from the expression for the magnetic field of a small loop (Grant and West, 1965) as follows:

$$H^{(P)} = -\frac{\pi I a^2}{4\pi s^3} = -\frac{m}{4\pi s^3} \quad \ldots\ldots\ \ldots\ldots(2)$$

where I= current in the transmitter

a = radius of the transmitter coil

$m = \pi I a^2$, magnetic dipole moment of Tx., as in Fig. 1.

Therefore we have the ratio of $H^{(s)}$ to $H^{(p)}$ for the survey system;

$$H = H^{(s)}/H^{(p)} = -\frac{4\pi s^3}{m} f(l, \sigma, \mu, \omega, s, d, t, \theta, m) \qquad (3)$$

Let us investigate the secondary electomagnetic field measured by the receiver, employing dimensional analysis. Writing down the variables related to $H^{(s)}$ with dimensional formulae in terms of the Giorgi unit system(Duncan, 1953), we have

$H^{(s)}$: $MT^{-1}Q^{-1}L^{2}$

l : L

σ : $Q^2 TM^{-1}L^{-3}$

μ : MLQ^{-2}

ω : T^{-1}

s : L

t : L

d : L

θ : dimensionless

m : $ML^2 T^{-1}Q^{-1}$

where M = unit of mass

L = unit of length

T = unit of time

Q = unit of electrical charge.

From equation(1) we now have

$$H^{(s)} = \text{const}\ (\ell)^{\alpha}\ (\sigma)^{\beta}\mu^{\gamma}\omega^{\delta}\ s^{\varepsilon}d^{\zeta}t^{\eta}m^{\lambda}\cdot f(\theta) \qquad \ldots(4)$$

which leads to the dimensional relation

$$MT^{-1}Q^{-1} \triangleq L^{\alpha}(Q^{2}TM^{-1}L^{-3})^{\beta}(MLQ^{-2})^{\gamma}(T^{-1})^{\delta}(L)^{\varepsilon}(L)^{\zeta}(L)^{\eta}(ML^{3}T^{-1}Q^{-1})^{\lambda} \qquad \ldots\ldots(5)$$

where "≙" denotes that the two sides are equal dimensionally.

The indicial equations are

$$\begin{aligned}
&(L) \quad 0 = \alpha - 3\beta + \gamma + \varepsilon + \zeta + \eta + 3\lambda\\
&(Q) \quad -1 = 2\beta - 2\gamma - \lambda\\
&(T) \quad -1 = \beta - \delta - \lambda\\
&(M) \quad 1 = -\beta + \gamma + \lambda
\end{aligned} \qquad (6)$$

Assuming that $\delta, \varepsilon, \zeta$ and η are known, we have finally

$$\alpha = 2\delta - \varepsilon - \zeta - \eta - 3 \qquad (7a)$$

$$\beta = \delta \qquad (7b)$$

$$\gamma = \delta \qquad (7c)$$

$$\alpha = 1 \qquad (7d)$$

Substitute the above values into equation(4), and we have

$$H^{(s)} = \text{const.} \frac{m}{l^3} \left(l^2\sigma\mu\omega\right)^{\delta} \left(\frac{s}{l}\right)^{\epsilon} \left(\frac{d}{l}\right)^{\zeta} \left(\frac{t}{l}\right)^{\eta} f(\theta) \qquad (8)$$

where $\delta, \epsilon, \zeta, \eta$ are arbitrary values.

Since $H^{(p)}$ = const. m/s^3 , the measured value

$$H = \frac{H^{(s)}}{H^{(p)}} = \text{const.} \frac{s^3}{l^3} \left(l^2\sigma\mu\omega\right)^{\delta} \left(\frac{s}{l}\right)^{\epsilon} \left(\frac{d}{l}\right)^{\zeta} \left(\frac{t}{l}\right)^{\eta} f(\theta) \qquad (9)$$

Because the value of the indices are arbitrary, equation(9) becomes

$$H = \text{const.} \frac{s^3}{l^3} \sum_i \left(l^2\sigma\mu\omega\right)^{\delta_i} \sum_j \left(\frac{s}{l}\right)^{\epsilon_j} \sum_k \left(\frac{d}{l}\right)^{\zeta_k} \sum_p \left(\frac{t}{l}\right)^{\eta_p} f(\theta) \qquad (10)$$

Rearranging this equation we have

$$H\left(\frac{l}{s}\right)^3 = f\left(l^2\sigma\mu\omega,\ s/l,\ d/l,\ t/l,\ \theta\right) \qquad (11)$$

Now we have an unknown function whose variables are $l^2\sigma\mu\omega$, s/l, d/l, t/l and θ. The dimensional analysis has reduced the number of variables related to $H^{(s)}$ from nine to five and all the new variables are dimensionless. The use of l, the depth extent of the sheet, as a scaling factor follows naturally from equations(7) and (8), because from equation(7)

$$l^{\alpha} = l^{2\delta - \epsilon - \zeta - \eta - 3}$$

$$= (l^2)^{\delta}(1/l)^{\epsilon}(1/l)^{\zeta}(1/l)^{\eta}(1/l^3)$$

and it is substituted into equation(4). Furthermore, although it is a dimension which we cannot measure directly, it is not a critical parameter; that is, changes in the magnitude of l do not affect the system response particularly.

With the usual measuring system, we obtain the value of H as a complex number corresponding to the real or in-phase component and imaginary or out-of-phase component. In the dimensional analysis, we consider the magnitude of H or $[(\text{in-phase})^2 + (\text{out-of-phase})^2]^{1/2}$, in which both components appear.

Chapter 3. Electromagnetic Response of Thin Sheet of Infinite Conductivity

We will now consider the problem in terms of a simplified model. The dimensional analysis reduced the number of variables considerably. However, in order to determine the function $f(\sigma\mu\omega l^2, s/l, d/l, t/l, \theta)$ in equation(11) it is necessary to reduce the five variables still further by fixing some of them.

Suppose we have a very thin vertical sheet conductor, of semi-infinite dimensions and infinite conductivity, whose geometry is shown in Fig. 2. Here we have maximum coupling between the EM system and the conductor, which is midway between the transmitter and the receiver. The electrical current pattern, induced by the primary field from the transmitter, has an elliptical shape on the face of the sheet, the upper and lower edges of the ellipse being at distances of s/8 and s/2, respectively, below the top of the sheet. (Koefoed & Kegge, 1968) This pattern is shown in Fig. 2.

Now we may consider the secondary electromagnetic field from a loop conductor formed by the concentration of the induced currents, in terms of mutual inductance and self inductance.

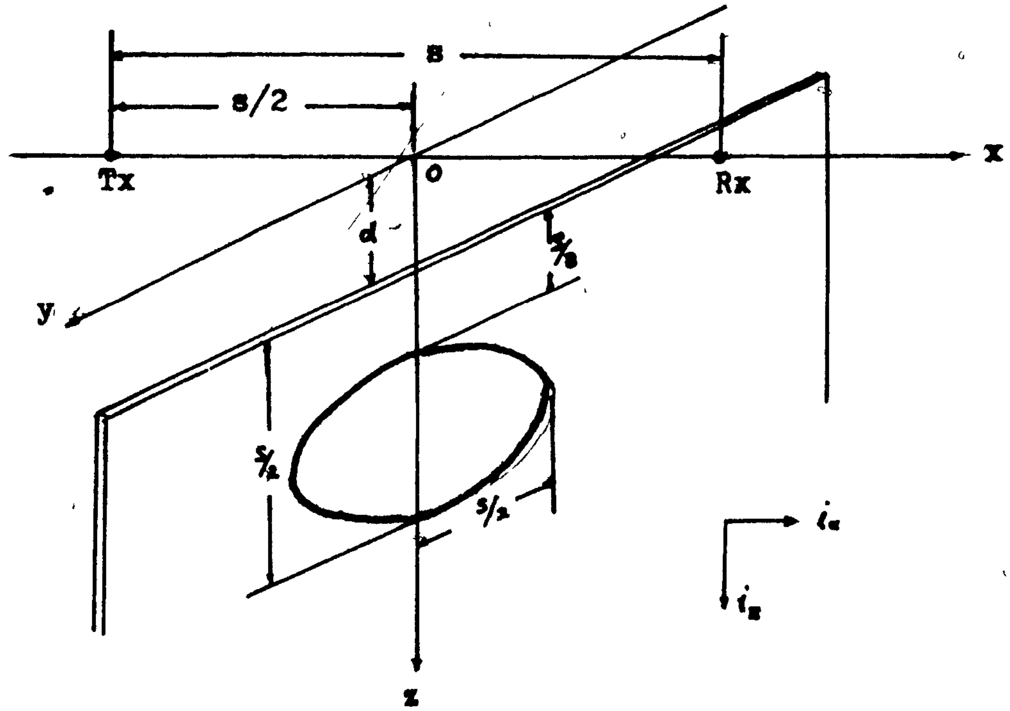

Fig. 2. The electrical current pattern in the thin plate

The response with the situation shown by Fig. 2 is as follows: (Grant & West, 1965)

$$\frac{\mathcal{E}_2^{(S)}}{\mathcal{E}_2^{(P)}} = -\frac{M_{01} M_{12}}{M_{02} L} \left(\frac{\alpha^2 + i\alpha}{1+\alpha^2} \right) \tag{12}$$

where $\mathcal{E}_2^{(S)}$ = the secondary electromotive force at the receiver, due to the conductor loop,

$\mathcal{E}_2^{(P)}$ = the primary electromotive force at the receiver, due to the transmitter loop,

M_{01} = the mutual inductance between the transmitter and the conductor coil -- that is, the conducting sheet,

M_{12} = the mutual inductance between the conductor coil and the receiver,

M_{02} = the mutual inductance between the transmitter and the receiver,

L = the self inductance of the conductor coil,

R = the resistance of the conductor coil,

ω = the angular frequency of the transmitter

and $\alpha = \omega L/R$.

We have assumed that the magnetic permeability of the conductor, $\mu = \mu_0 = 4\pi \times 10^{-7}$ henry/m, that is, the value in free space.

To solve equation(12), we must determine the mutual inductances between the three coils and the self inductance of the elliptical coil which simulates the conductor. The calculation of M_{02} is not difficult since the transmitter and reciver coils are coplanar and separated by a distance much larger than their radii, which are generally equal. The value is

$$M_{02} = -\frac{\mu_0 \pi a^4}{4 s^3} \tag{13}$$

where a = radius of each coil.

For more complex geometry the exact expression for mutual inductance is given by the Neumann formula

$$M = \frac{\mu_0}{4\pi}\oint\oint \frac{d\vec{l}_1 \cdot d\vec{l}_2}{r}$$

where we have two coils shown below.

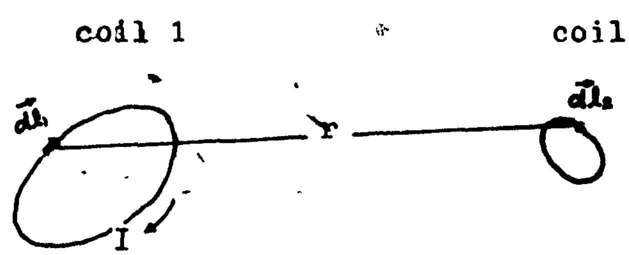

Generally the integration must be done numerically. As an approximation we use the following relation

$$M = \frac{\Phi}{I} = \frac{1}{I}\int_S \vec{B}\cdot d\vec{S}$$

where Φ = flux linking two coils,

I = current in coil 1,

$\vec{B}$ = magnetic induction in coil 2,

S = area of the coil 2,

We assume that $\vec{B}$ may be approximated by B_c, the axial value at the center of coil 2. Then we have

$$M = \frac{1}{I}\int_S B_c \, dS = \frac{B_c S}{I} \qquad (14)$$

The magnetic induction due to the transmitter at the center of the conductor loop can be derived from the expression

$$\vec{H} = \frac{Ia^2}{4}\left[\frac{3\rho z}{(\rho^2+z^2)^{5/2}} i_\rho + \frac{2z^2-\rho^2}{(\rho^2+z^2)^{5/2}} i_z\right] \qquad (15)$$

when the coordinate system is as follows

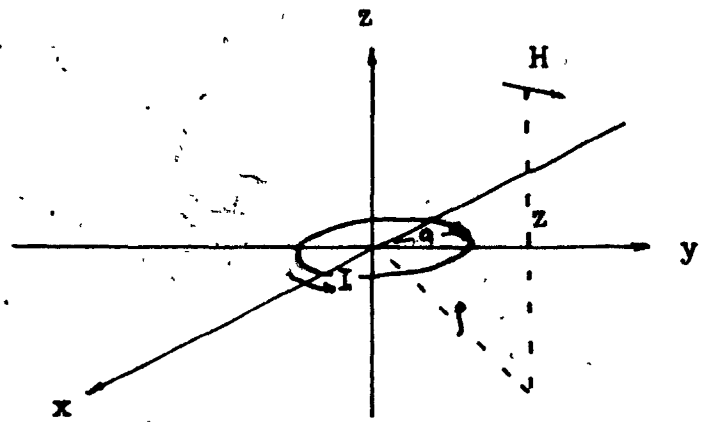

Then, the magnetic induction B_{e1} is

$$B_{e1} = \frac{\mu_0 I a^2}{4}\left[\frac{3\frac{s}{2}(d+\frac{5}{16}s)}{\left\{(\frac{s}{2})^2+(d+\frac{5}{16}s)^2\right\}^{5/2}} i_x + \frac{2(d+\frac{5}{16}s)^2-(\frac{s}{2})^2}{\left\{(\frac{s}{2})^2+(d+\frac{5}{16}s)^2\right\}^{5/2}} i_z\right] \qquad (16)$$

When the magnetic flux Φ_{e1} is computed, only the x component of the magnetic induction is considered (since the sheet is vertical), as below,

$$\Phi_{01} = \frac{\mu_0 I a^2}{4} \frac{\frac{3}{2} s \left(d + \frac{5}{16} s\right)}{\left\{\left(\frac{s}{2}\right)^2 + \left(d + \frac{5}{16} s\right)^2\right\}^{5/2}} \pi \cdot \frac{3}{16} s \frac{3}{2}$$

$$= \frac{9}{16^2} \mu_0 I \pi a^2 s^3 \frac{\left(d + \frac{5}{16} s\right)}{\left[\left(\frac{s}{2}\right)^2 + \left(d + \frac{5}{16} s\right)^2\right]^{5/2}} \qquad (17)$$

Then, the mutual inductance M_{01}, between the conductor coil and the transmitter becomes

$$M_{01} = \frac{9}{16^2} \mu_0 \pi a^2 \frac{s^3 \left(d + \frac{5}{16} s\right)}{\left[\left(\frac{s}{2}\right)^2 + \left(d + \frac{5}{16} s\right)^2\right]^{5/2}} \qquad (18)$$

In order to compute the mutual inductance between the conductor and the receiver, the magnetic induction at the receiver has to be calculated as follows

$$\vec{B}_{12} = \frac{\mu_0 I' \frac{3}{16} s \cdot \frac{3}{2}}{4\pi} \left[\frac{s\left(d + \frac{5}{16} s\right) \frac{3}{2}}{\left\{\left(d + \frac{5}{16} s\right)^2 + \left(\frac{s}{2}\right)^2\right\}^{5/2}} (-i_z) + \frac{2 \cdot \left(\frac{s}{2}\right)^2 - \left(d + \frac{5}{16} s\right)^2}{\left\{\left(d + \frac{5}{16} s\right)^2 + \left(\frac{s}{2}\right)^2\right\}^{5/2}} i_x \right] \qquad (19)$$

where I' = current induced in the conductor coil.

As before, the magnetic flux linking the conductor loop with the receiver is given by

$$\Phi_{12} = -\frac{\mu_0 I' a^2 \frac{3}{16} s \cdot \frac{3}{2} \pi}{4} \left[\frac{\frac{3}{2} s \left(d + \frac{5}{16} s\right)}{\left\{\left(d + \frac{5}{16} s\right)^2 + \left(\frac{s}{2}\right)^2\right\}^{5/2}} \right]$$

Therefore, the mutual inductance between the conductor loop and the receiver is

$$M_{12} = -\frac{9}{16^2}\pi\mu_0 a^2 \frac{s^3(d+\frac{5}{16}s)}{\left[(d+\frac{5}{16}s)^2+(\frac{s}{2})^2\right]^{5/2}} \qquad (20)$$

To calculate the self inductance of the conductor loop, we use a formular from Grover(1946) which is suitable for any plane figure

$$L = 0.002\,l\left[\log_e\frac{2l}{\rho} - \left(2\log_e\frac{l}{\sqrt{S}} + \varphi\right) + \frac{1}{4}\right]$$

where l = perimeter of the loop,

S = area of the loop,

ρ = cross section radius of the loop,

φ = constant, related to the geometry.

For the ellipse, assuming that $\rho = t/2$, where t is the sheet thickness, and converting to MKS units, this expression becomes

$$L = 0.378\,\mu_0 s\left[\log_e\frac{9.5s}{t} - 2.63\right]$$

The term in the bracket is only approximately a constant. We have assumed t to be small and constant, while s may vary in practice by no more than a factor of 4 or 5. Under these conditions we can write

$$L \approx ks. \qquad (21)$$

The error is about ±15%

Therefore, using all these approximations, the geometrical factor of the response when the survey system straddles the sheet conductor, becomes

$$G = \frac{M_{12}\,M_{01}}{L\;\;M_{02}} = \frac{9^2 \times 4\,\mu_0 \pi}{16^4\;\;k}\;\frac{s^8\left(d + \frac{5}{16}s\right)^2}{\left[\left(\frac{s}{2}\right)^2 + \left(d + \frac{5}{16}s\right)^2\right]^5} \qquad (22)$$

The approximation for the mutual inductance in equation(14) should be investigated to check its accuracy by comparision with known results for a simple geometry. Suppose we have two circular coils in the configuration below

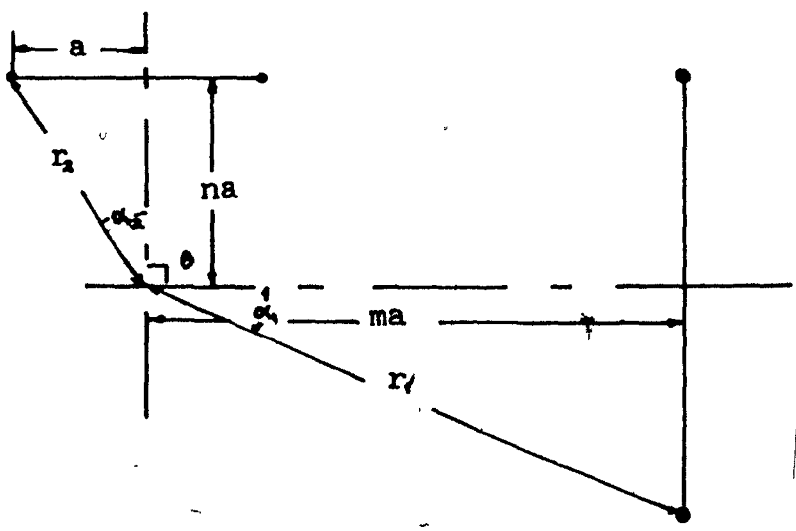

The exact expression, using a series of Legendre polynomials, is given by(Grover, 1946)

$$M = 0.002\,\pi^2 \frac{n^2 a^4}{r_1^3}\left[\frac{1}{3}\frac{r_2}{r_1} P_2(\cos\theta)\,P_2'(\cos\alpha_1)\,P_2'(\cos\alpha_2) + \frac{1}{6}\left(\frac{r_2}{r_1}\right)^2 P_3(\cos\theta)\,P_3'(\cos\alpha_1)\,P_3'(\cos\alpha_2)\right.$$

$$\left. + \cdots \frac{2}{(l+1)(l+2)}\left(\frac{r_2}{r_1}\right)^l P_{l+1}(\cos\theta)\,P_{l+1}'(\cos\alpha_1)\,P_{l+1}'(\cos\alpha_2) + \cdots\right]$$

For the same geometry, the approximation is

$$Mc = \frac{\mu_0 \pi a}{4} \frac{3mn}{(m + n)}$$

For example, when m = 10, n = 1

$$\frac{M}{Mc} = 0.95$$

and when m = n = 10

$$\frac{M}{Mc} = 1.25$$

Thus the approximation for calculating M is reasonably good.

With regard to the value of L used in equation(21), it has been shown that the approximation is reasonably good within the range of the parameters s and t. Consequently, equation(22) depends entirely upon the function

$$F(s,d) = \frac{s^6\left(d+\frac{5}{16}s\right)^2}{\left[\left(\frac{s}{2}\right)^2+\left(d+\frac{5}{16}s\right)^2\right]^5} \tag{23}$$

which is shown in Fig. 3, where F(s,d) is given in terms of s for various depths d. (For details see Appendix A)

Fig. 3 shows that the function F(s,d), which controls the geometrical factor G of the response, initially increases with the transmitter - receiver separation and reaches a certain asymptotic value for large s, and that F(s,d) varies inversely with the value of d.

Recalling that the anomaly due to the conductor coil is

$$\frac{\mathcal{E}_2^{(S)}}{\mathcal{E}_2^{(P)}} = -\frac{M_{01}M_{12}}{M_{02}L}\left(\frac{\alpha^2+i\alpha}{1+\alpha^2}\right)$$

$$= -\frac{4\times 9^2\mu_0}{16^2\times k}\;\frac{s^6\left(d+\frac{5}{16}s\right)^2}{\left[\left(\frac{s}{2}\right)^2+\left(d+\frac{5}{16}s\right)^2\right]^5}\left(\frac{\alpha^2+i\alpha}{1+\alpha^2}\right) \tag{24}$$

from equations(12) and (22), we can proceed a little further to make comparison with the result of the dimensional analysis. If we assume the conductor has an infinite conduct-ivity, the real part of $\left(\frac{\alpha^2+i\alpha}{1+\alpha^2}\right)$ is 1 and the imaginery part is zero. Therefore the factor $\left(\frac{\alpha^2+i\alpha}{1+\alpha^2}\right)=1$. Then, $\frac{\mathcal{E}^{(S)}}{\mathcal{E}^{(P)}}$ is a function of s and d so that

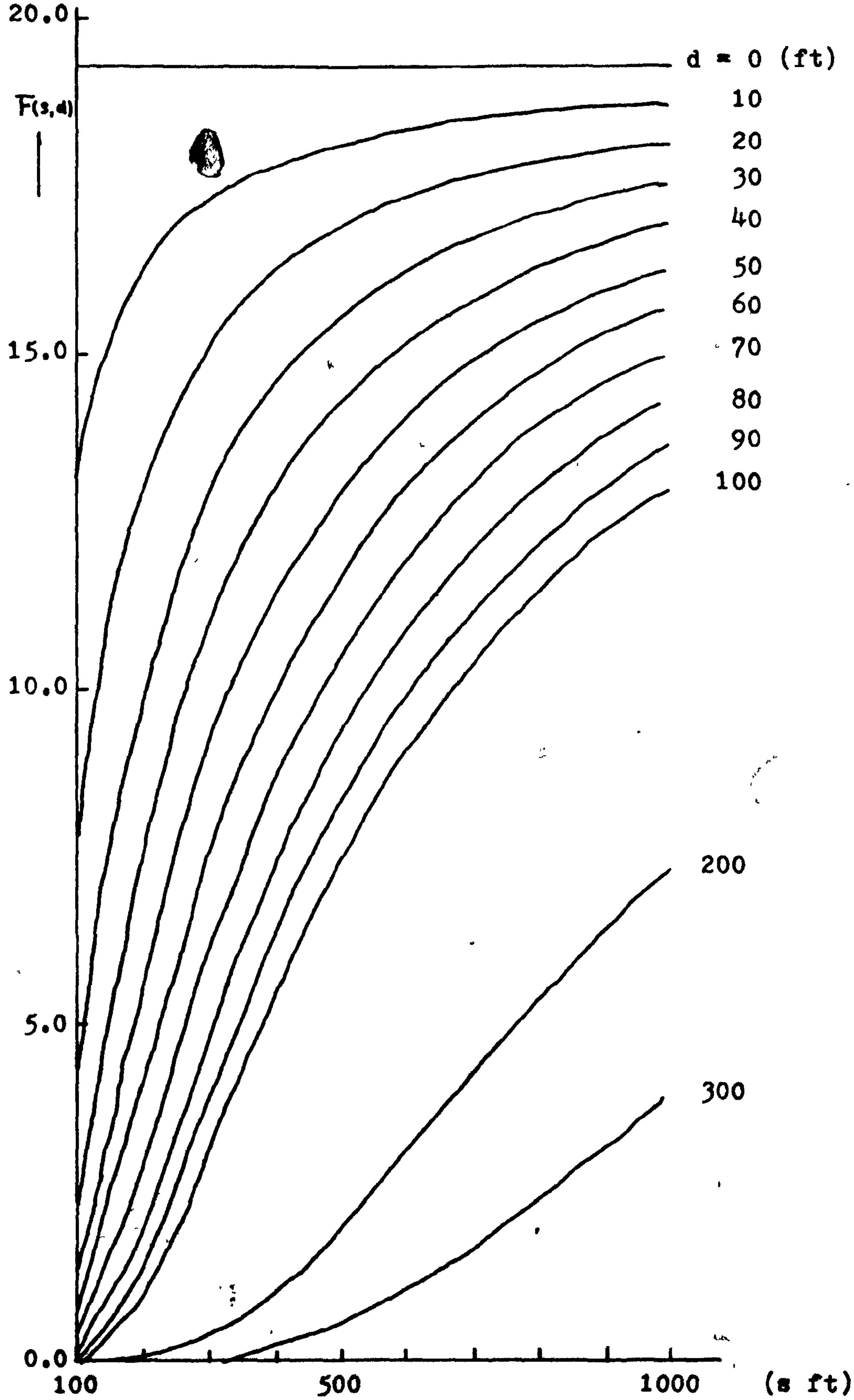

Fig. 3. F in terms of s at various depths

we have $\frac{\mathcal{E}_x^{(s)}}{\mathcal{E}_x^{(p)}} = f(s, d)$ (25)

where $\frac{\mathcal{E}_x^{(s)}}{\mathcal{E}_x^{(p)}}$ corresponds to H in equation(11).

Comparing equation(25) with equation(11) both express the physical phenomena but equation(25) was obtained with a thin vertical sheet of infinite conductivity ($\theta = 90°$, $t/l \rightarrow 0$, $l^2\sigma\mu\omega \rightarrow \infty$). Therefore, equation(11) under these conditions becomes

$$H(l/s)^3 = f(s/l,\ d/l) \qquad (26)$$

On the other hand, equation(26) may be derived from equation(25) by multiplying both sides by $(1/s)^3$. In order to illustrate equation(26) we have plotted $H(1/s)^3$ vs. s/l for a range of values of d/l, as shown in Fig. 4, using the curves of F(s,d) vs. s with various values of d and assuming that all the conditions required so far are simulated.

The curves show that $H(1/s)^3$ decreases with increasing d/l as would be expected. When d/l is zero, the relation appears practically linear for the range plotted. For d/l bigger than 0.02, the curves all have maxima which are located approximately where $s/l \approx d/l$ that is, the maxima move

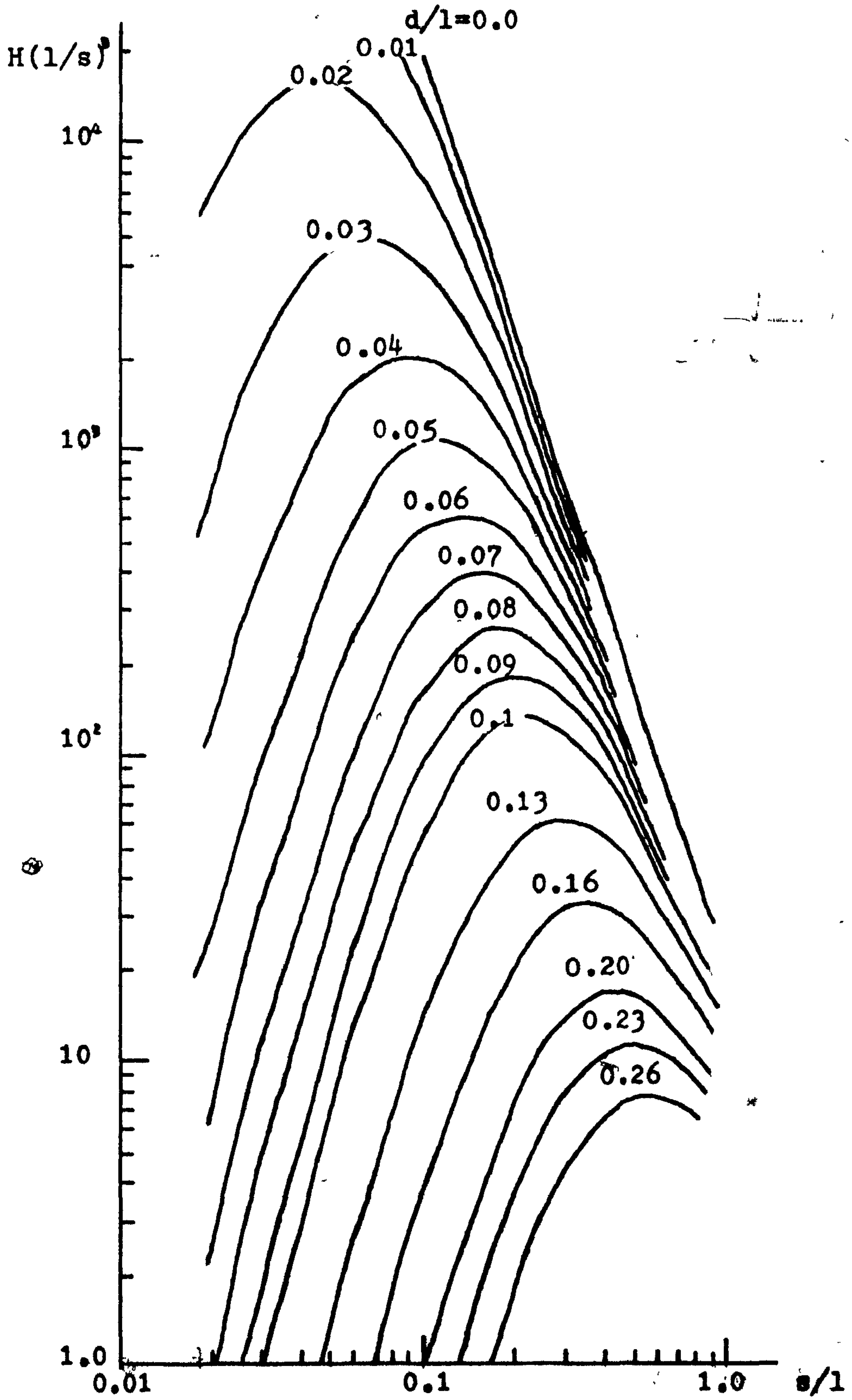

Fig. 4. H(l/s)³ - s/l curves from equation(26)

towards increasing s/l with increasing d/l. Then, the shape and axial location of the curve provide some information about d/l, from which d may be estimated. It should be kept in mind that the survey system straddles the sheet, that is, the response is maximum.

Chapter 4. Model Work

1. Introduction

In addition to the data from the dimensional analysis and its application to the case of a very thin vertical sheet of infinite conductivity and of semi-infinite dimensions, model work has been carried out for the purpose of applying this information to a more realistic type of conductor in field conditions.

The model work employs conductors such as aluminum, copper, stainless steel and lead sheets, of various dimensions and dip-angles. Since the samples are non-magnetic we assume throughout that $\mu = \mu_0$.

Two sets of instruments were employed for measurement, the one being an early model horizontal loop EM system receiver manufactureed by Huntec Ltd., Toronto, the other constructed by Russell Parrott in the Geophysical Laboratory, McGill University.

Considering the former model unit, the transmitter and receiver coils have the following specifications;

effective radius of coil = $\frac{1}{2}$"

radius of wire =0.006"

No. of turns of wire = 2700.

For the latter, the specifications are

effective radius of coil = $\frac{1}{4}$" (cored by ferrite)

radius of wire = 0.006"

No. of turns of wire = 1600.

The transmitter was excited at 876 Hz. by a Hewlett Packard Audio Oscillator which produce 0.1 - 0.15 amperes in the transmitter coil at 4 - 6 volts.

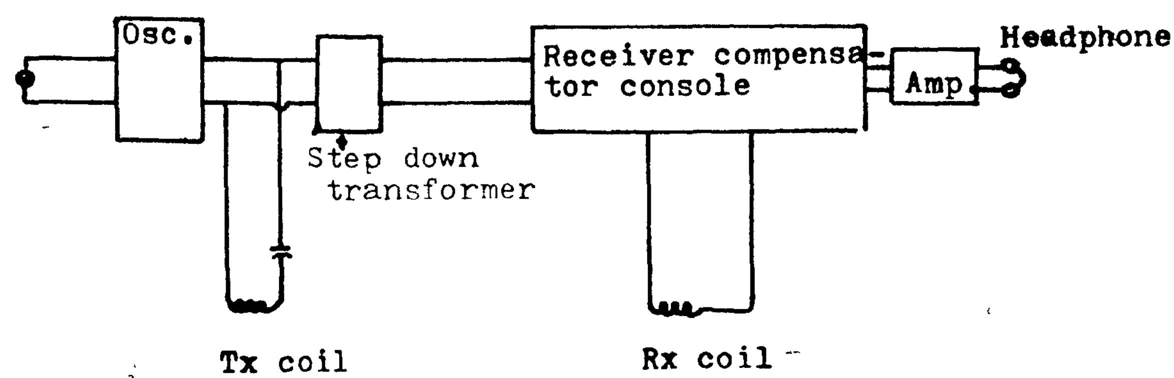

Fig. 5 Schematic of equipment for model work

Fig. 5 shows a schematic of the model equipment. In the second arrangement, the above setup was modified by adding a band pass filter to a homemade receiver amplifier and using small($\frac{1}{4}$" radius) transmitter and receiver coils with ferrite cores in order to obtain essentially the same sensitivity, despite the smaller dimensions. Otherwise, it is similar to Fig. 5. With these instruments, the model horizontal loop EM system measured in-phase and out- of-phase components of the secondary field.

2. Discussion of the results

The results obtained with various model plates indicate the effect of varying s/l, t/l, d/l, θ and σ (and hence the dimensionless parameter $l^2\sigma\mu\omega$) and made it possible to calculate $H(l/s)^3$. In addition, s was varied directly to produce pseudo vertical sections, as shown in Fig. 6.

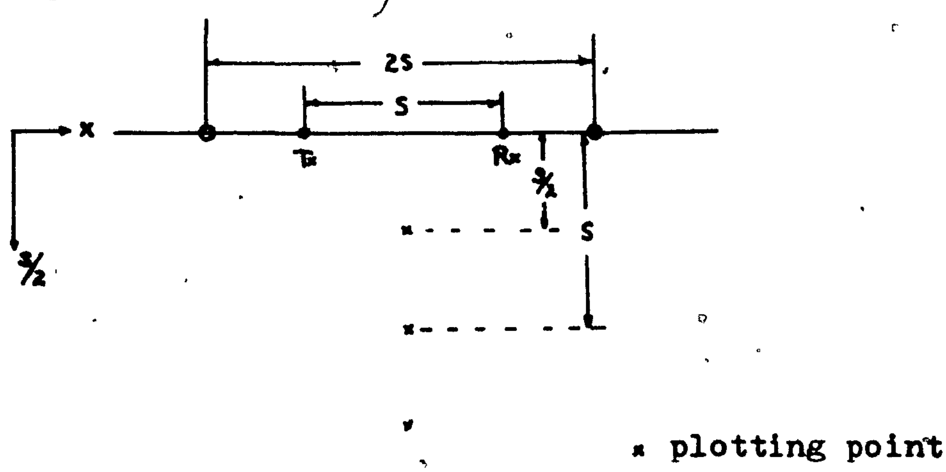

Fog. 6 Data-representation in vertical pseudo section

The representation of the data in vertical pseudo section shows the dependence of system response on x (distance of transmitter-receiver midpoint from origin directly above the top of the conductor) and s, as the geometry and conductivity of the conductor are varied. Several suites of these curves are included in Appendices C, D and E. Model measurements were made with sheets of Cu, Al, Pb by varying thickness, depth, depth extent and dip-angle. In-phase (Appendix C) and quadrature (Appendix D) values were obtained for four s values —6", 9", 12", 15"— by expanding the transmitter-receiver spacing symmetrically about successive stations on the x-axis. Total field results are shown in Appendix E. Note that in the diagrams of the appendices the vertical scales are twice the horizontal. A discussion of these results follows.

A. First we plot the in-phase component of the secondary field.(See Appendix C) The characteristics of the vertical pseudo-sections, with one particular parameter varied and the others fixed, are described in the following.

1). <u>Variation of depth extent</u> (Cu sheets)

For $\theta = 90°$, as the value of l decreases in steps from 24" to 2", the peak in-phase response decreases, from 35 % to 1.5 %, as one might expect. However, the position of the peak varies in a rather peculiar fashion. For l = 24", 18" and 12", it is located at depths of 6", 4½" and 3" respectively. But for l = 10" the peak drops to a depth of 6" and again moves up as l is decreased further, until it is at 3" for l = 6". Again the peak moves down to 4½" for l = 5" and rises to 3" at l = 2". (Presumably in the last case the magnitude might be larger if it was possible to use a smaller value of s.) Thus the proper transmitter-receiver separation to produce maximum response is controlled to some degree by the depth extent of the conductor. In addition, we see that for sheet conductors of large depth extent the induced current pattern is centered at a fairly constant position in the sheet, about 1/5 of its depth extent below the top. But for conductors of limited depth extent, the current is induced at a much greater depth relative to the sheet dimension.

There is very little difference between the results for $\theta = 60^\circ$ and $\theta = 90^\circ$. When $\theta = 30^\circ$, however, there are two maxima, except for $l \geqslant 18"$. The larger is located slightly up dip and the smaller down dip, both at depth. Thus the contours have the appearance of two conductors dipping in opposite directions and converging near surface at the correct location of the top of the conductor, the one with the shallower attitude being the correct dip direction.

2). Variation of conductivity

Two conductors, aluminum and lead sheets with the same dimensions, are compared. The peak values are larger for the better conductor(aluminum) and are located at shallower depths; the contours for lead appear more diffuse. For $\theta = 30°$ the double peaks are not present as in the case (1) for the copper sheets.

3). Variation of depth

Increasing the depth of burial of an aluminum sheet decreases the maximum response and moves it down, as might be expected, except for $\theta = 30°$, where the peak decreases in magnitude but remains at 4½". Again there is no evidence of two maxima at shallow dip.

4). Variation of thickness

Two aluminum sheets, 0.026" and 0.090" thick with other dimensions identical, were used. Clearly there is very little difference between these results, since both are essentially thin sheets. However, the thicker one appears to have a mild second maximum at depth for $\theta = 90°$ and $60°$; this is not apparent where $\theta = 30°$.

B. Quadrature or out-of-phase pseudo depth plots are shown in Appendix D. There are some fundamental differences in the results compared to the in-phase data.

1). Variation of depth extent

$\theta = 90°$. Although the peak response falls off with decreasing depth extent, the overall change is much smaller, 8.5 % to 5.5 %, and possibly not uniform, although this is not clear for such small variations. For l = 24", 18" and 12", the location of the peak moves up, but remains at 3" for smaller values of l. As a result, the ratio of in-phase to quadrature response, used as an indicator of relative conductivity in horizontal loop interpretation, varies in a rather complicated way. In general one may say that this ratio decreases with l, but it also varies directly with s, the transmitter-receiver spacing, unless $l \leq s$, when it decreases again. The plots for dipping sheets are similar to those in Appendix C, showing a double peak developing for shallow dip angles and decreasing l values.

2,3,4). Variation of conductivity, depth and thickness

Similar remarks apply here as in A. Clearly the ratios of in-phase to quadrature are larger for aluminum than for lead.

C. Pseudo sections of magnitude, that is $[(\text{in-phase})^2 + (\text{quadrature})^2]^{1/2}$, are shown in Appendix E, since this is the quantity that is used to develop the characteristic curves described in the next chapter.

From the vertical pseudo sections it is possible to locate the conductor, to determine the dip direction and possibly something of the depth extent. The horizontal loop technique is not particularly sensitive to dip, so an estimate of the actual dip angle is difficult. Presumably conductor thickness may also be estimated but no thick sheet was tested.

Using the in-phase and quadrature sections of Appendices C and D we can also get some idea of the relative conductivity. Although a single traverse with fixed s value would be sufficient to give a ratio of RE/IM for this purpose, it is interesting to note that there is a large variation in this ratio with s. For sheets of great depth extent RE/IM increases with s; if the transmitter-receiver spacing is larger than about 2l, it decreases.

Figures 7 - 12 are a representative sample of the collection in the appendix. Here the total field values have been plotted in pseudo section for sheets of Cu, Al and stainless steel, using s values of 6", 7.5", 9" and 10.5".

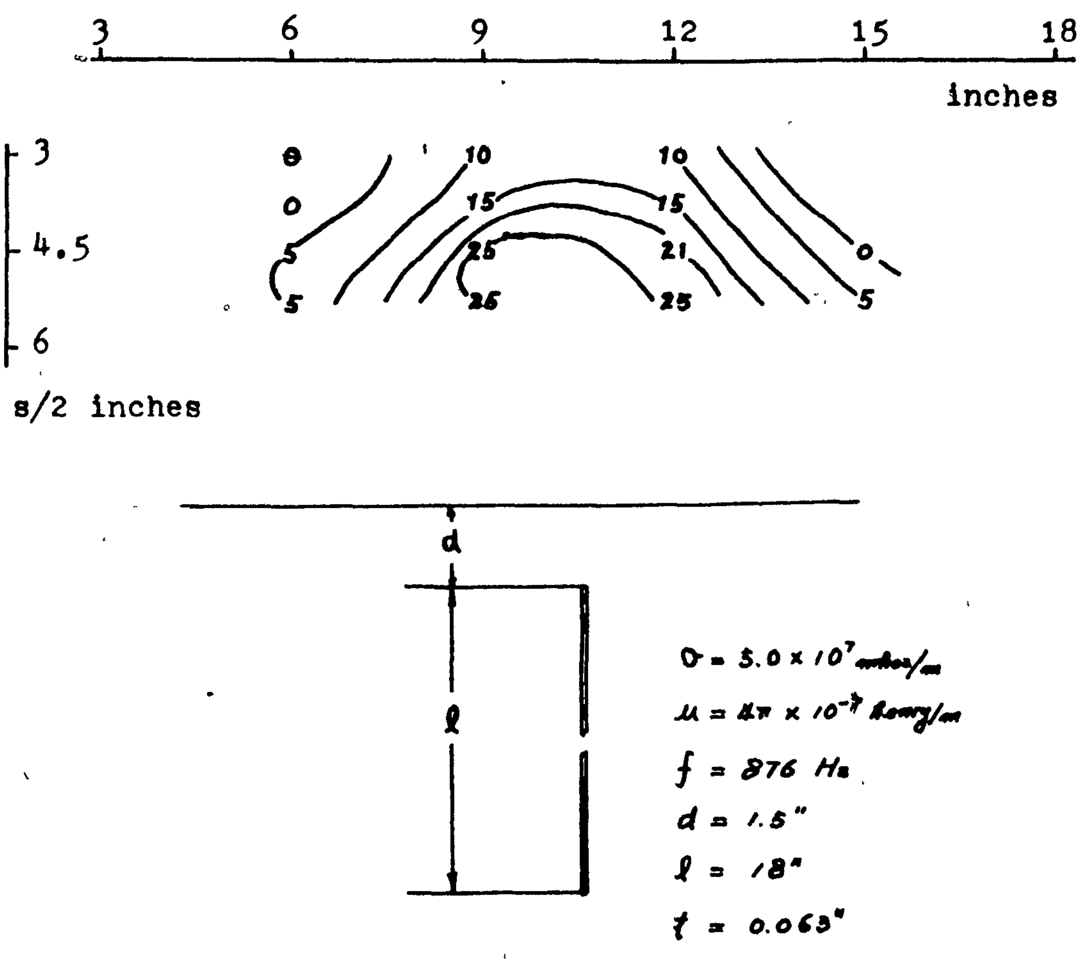

Fig. 7 Vertical pseudo section of magnitude from experiments

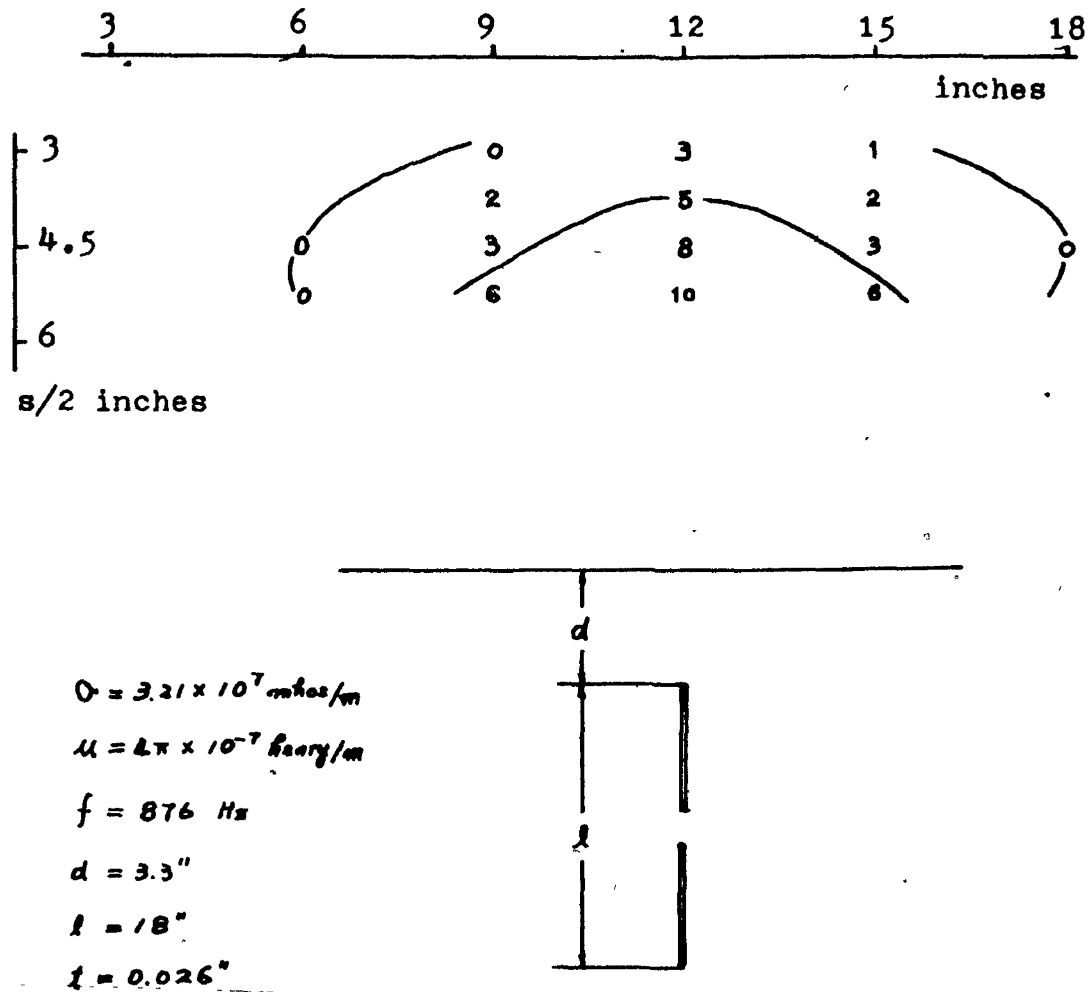

Fig. 8. Vertical pseudo section of magnitude from experiments

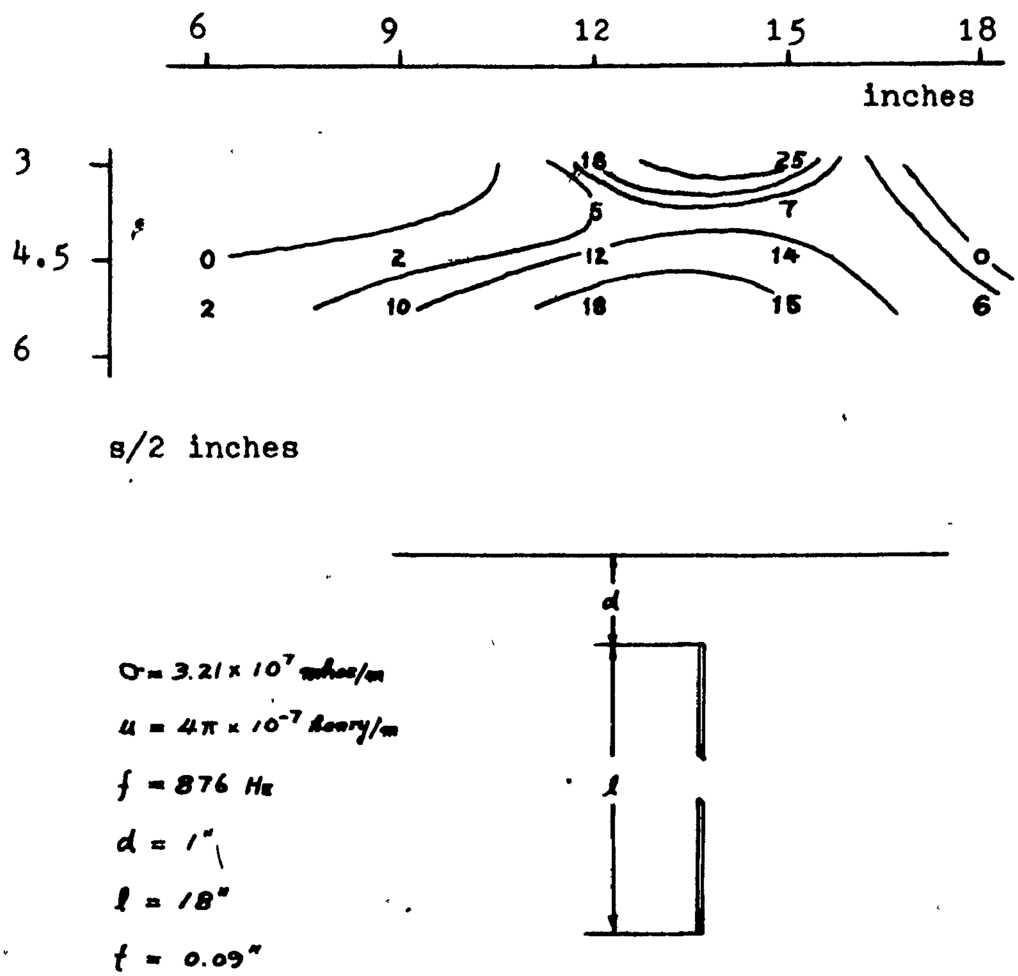

Fig. 9. Vertical pseudo section of magnitude from experiments

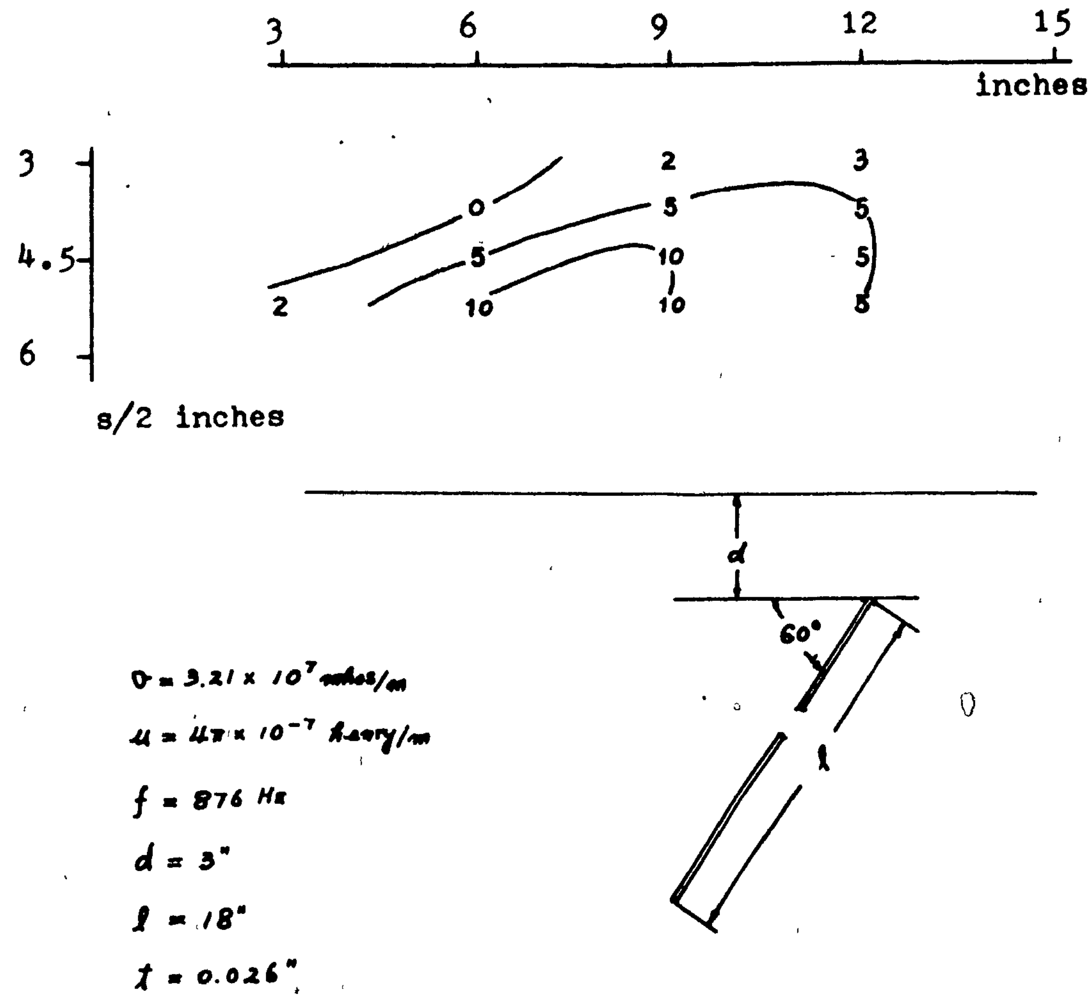

Fig. 10. Vertical pseudo section of magnitude from experiments

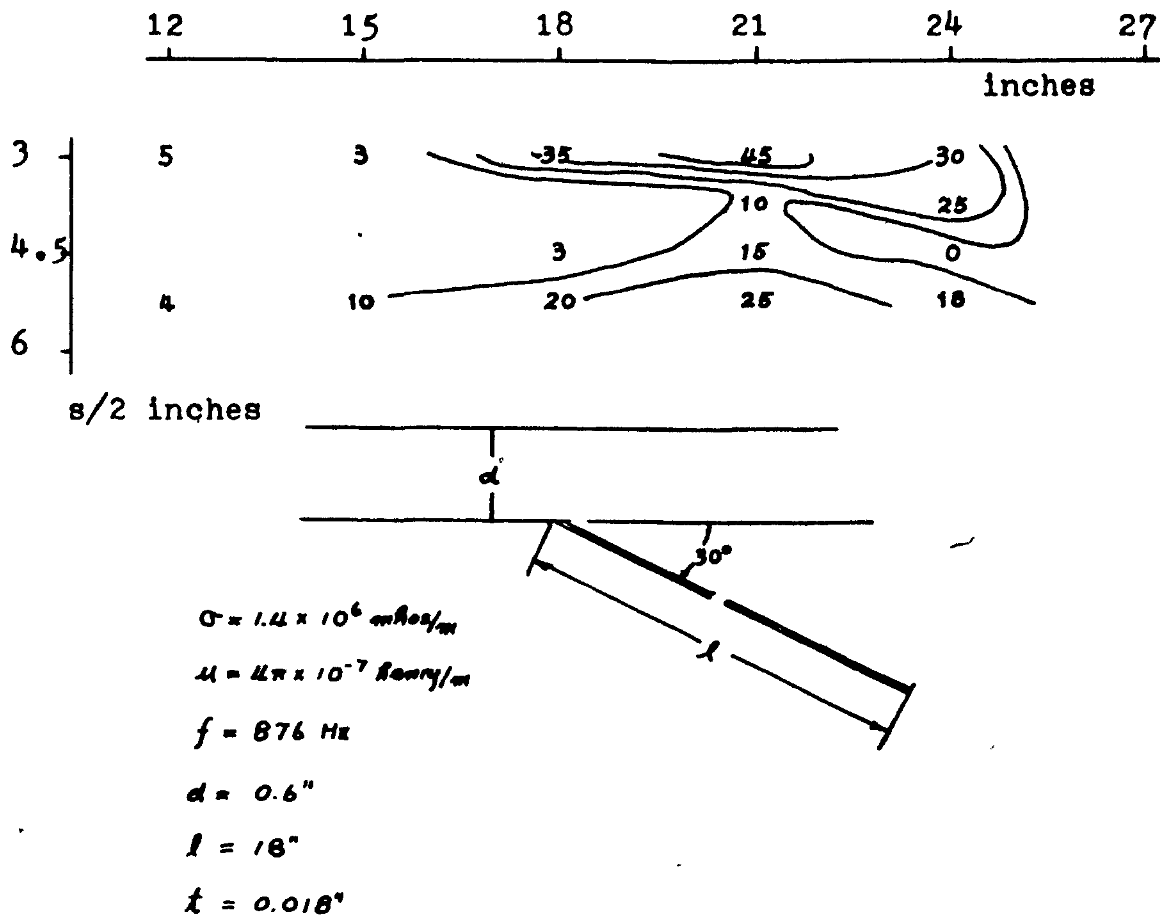

Fig. 11. Vertical pseudo section of magnitude from experiments

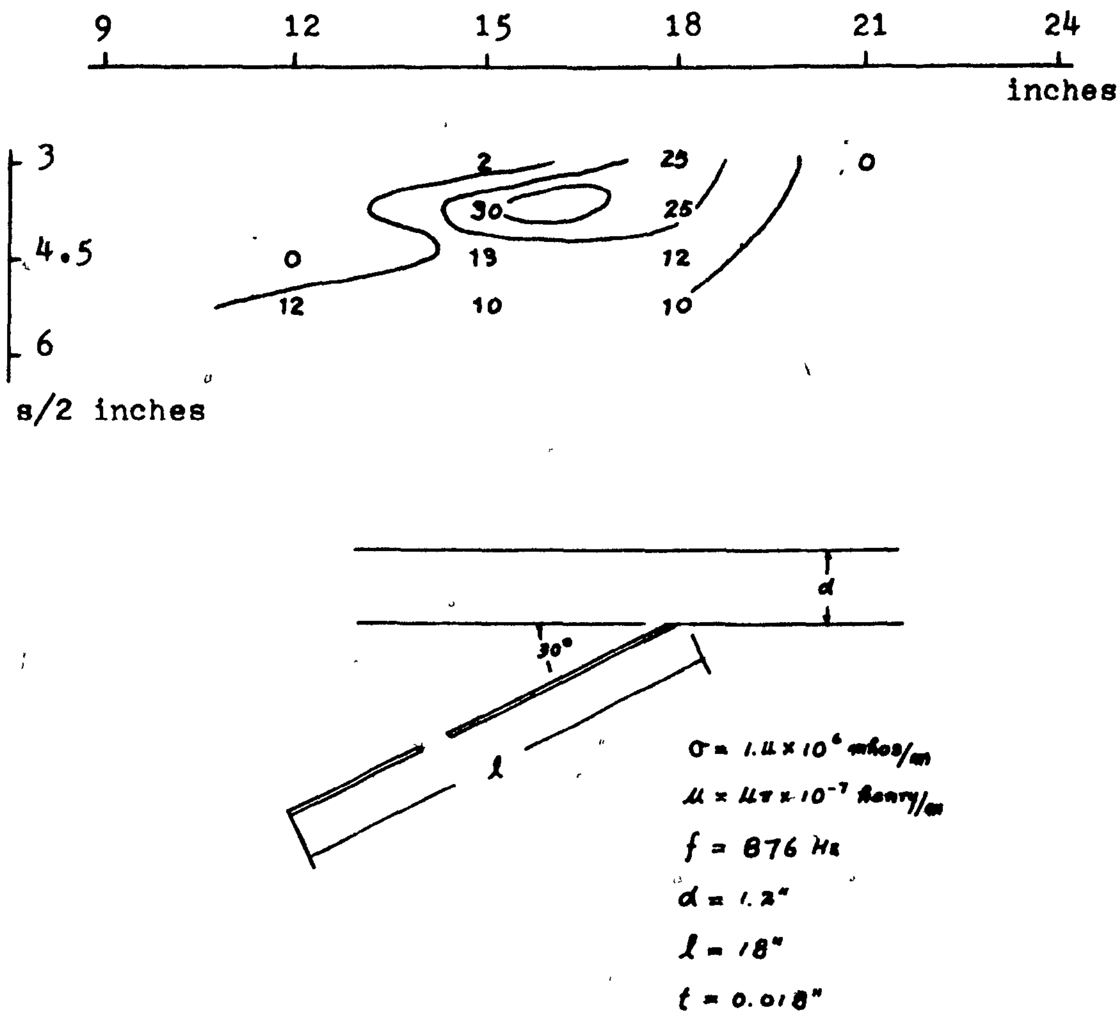

Fig. 12. Vertical pseudo section of magnitude from experiments

Chapter 5. Preparation of Characteristic Curves

We now proceed to develop characteristic curves for the horizontal loop EM system, using the results of the dimensional analysis from chapter 2. and the model measurements with multiple transmitter-receiver spacing in chapter 4. These curves have been prepared from the data obtained when the EM system is located with its midpoint directly over the top of the conductor. The values of $H(l/s)^3$ are plotted against s/l on log-log paper for variations in d/l, $\sigma\mu\omega l^2$, t/l and θ. A discussion of the curves follows.

1. $\theta = 90°$. The effect of d on $H(l/s)^3$ vs. s/l

These curves are shown in Figures 13 - 18. From the results of the dimensional analysis,

$$H(l/s)^3 = \text{const.} \sum_i (\sigma\mu\omega l^2)^{\delta_i} \sum_j (s/l)^{\epsilon_j} \sum_k (d/l)^{\zeta_k} \sum (t/l)^{\eta} f(\theta) \qquad (10)$$

$H(l/s)^3 = \text{const.} \sum_j (s/l)^{\epsilon_j}$, for a particular value of d/l, if we fix the values of $\sigma\mu\omega l^2$, t/l and θ.

This function $H(l/s)^3$, in general, may be of a quadratic form on the log-log paper, but in any case the shape of the curves

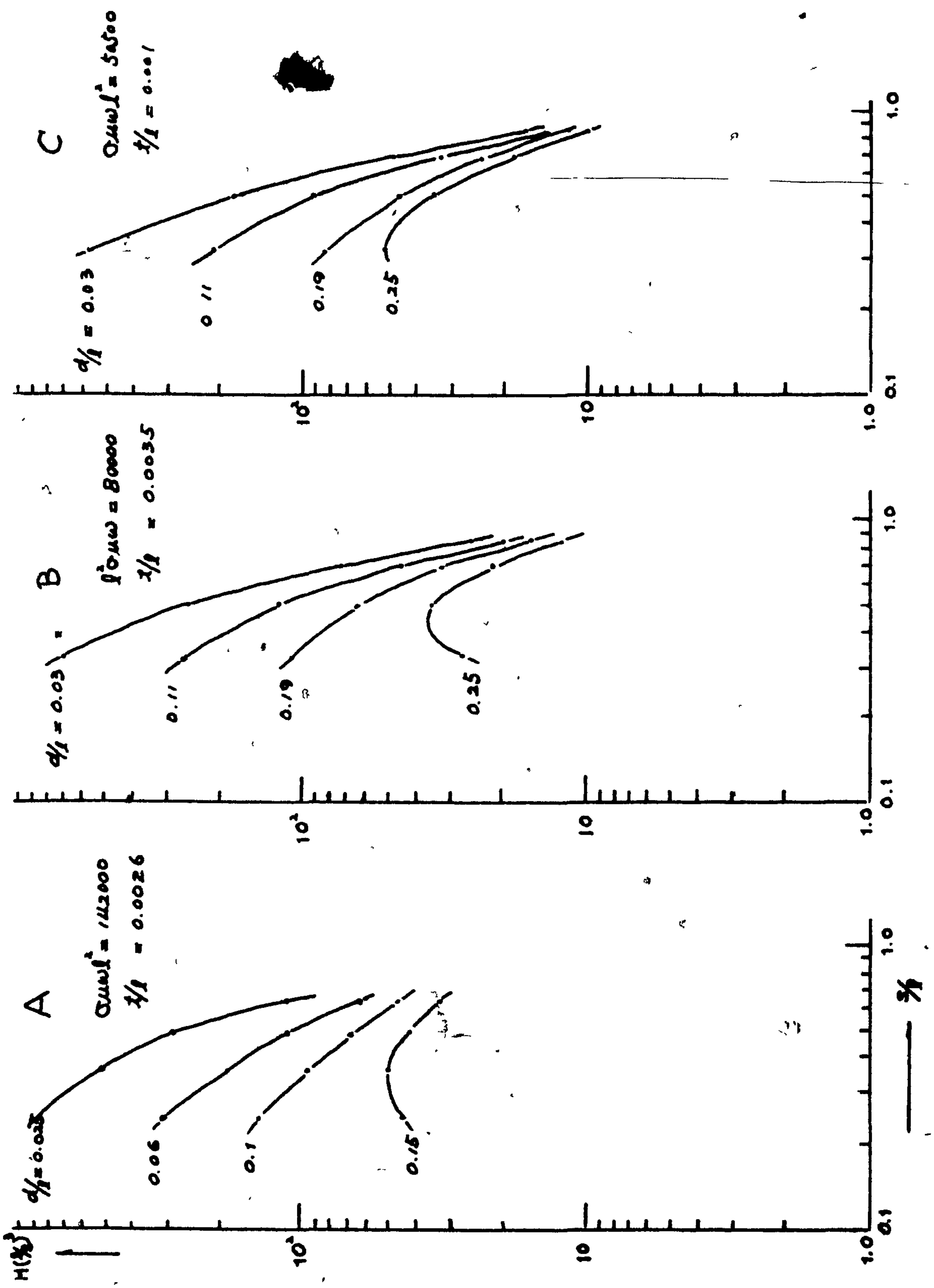

Fig. 13. $H(l/s)^3$ - s/l curves for $\theta = 90°$ from experiment (I)

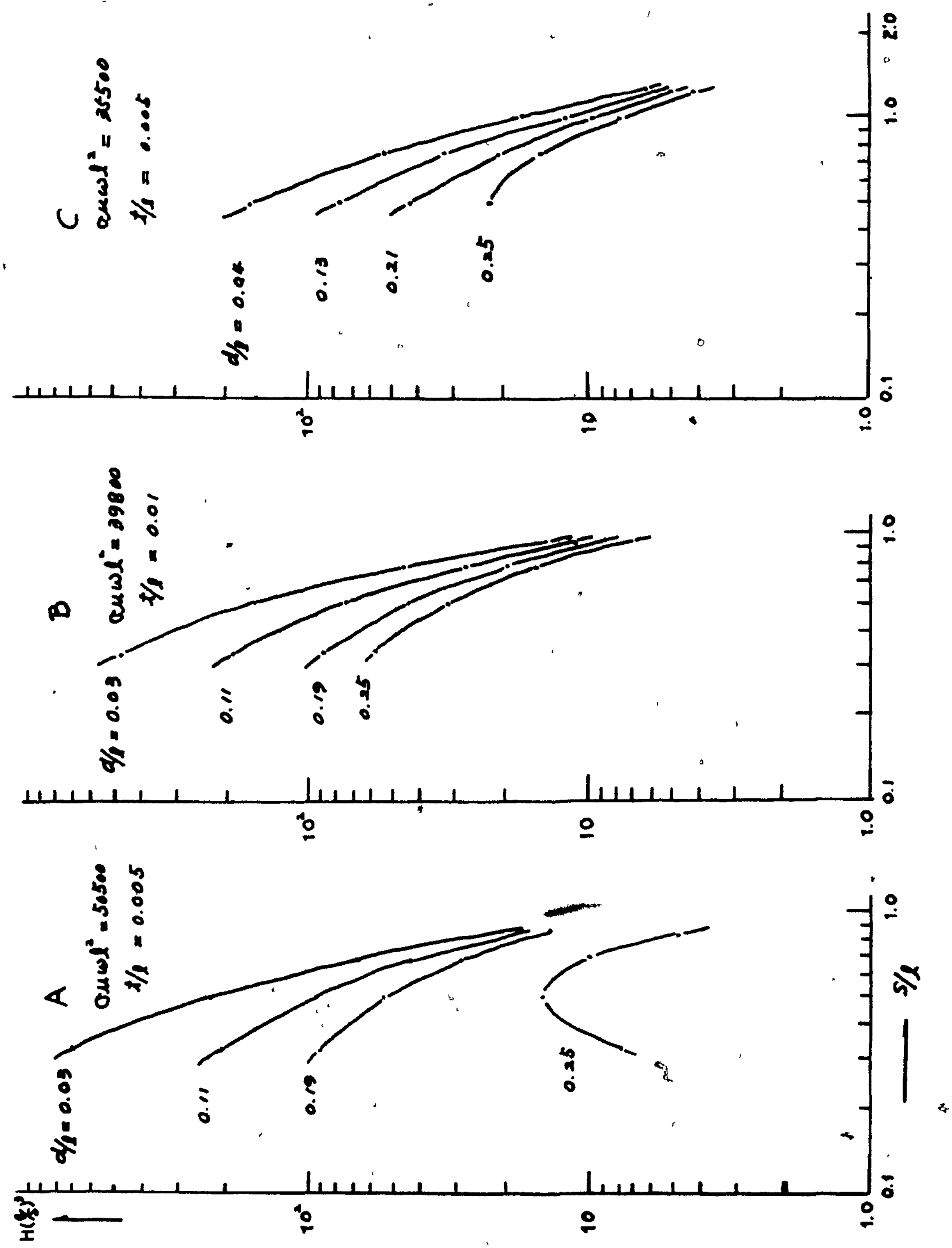

Fig. 14. H(1/s)³ - s/1 curves for θ = 90° from experiments (II)

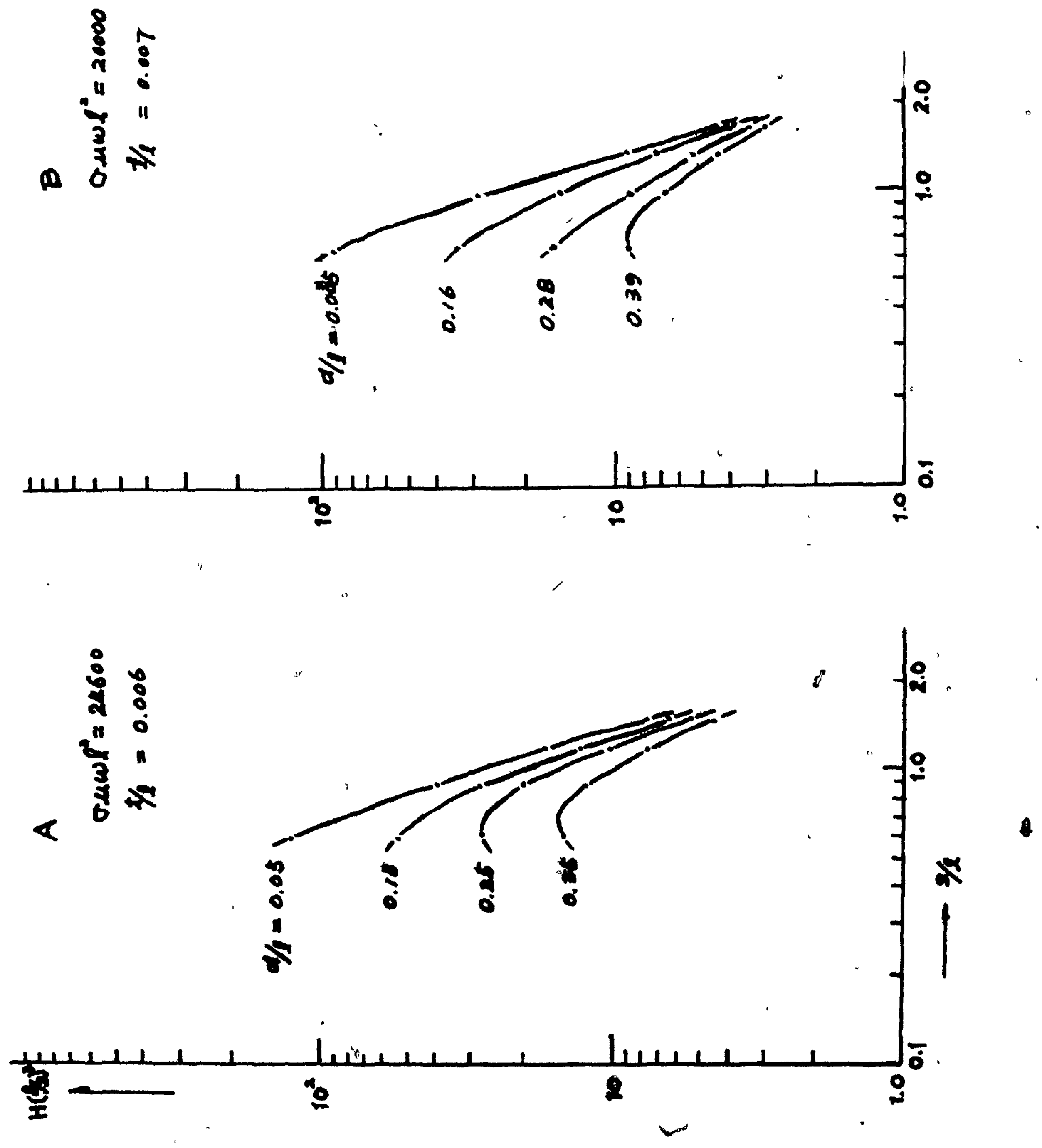

Fig. 15. $H(l/s)^3$ - s/l curves for $\theta = 90°$ from experiments (III)

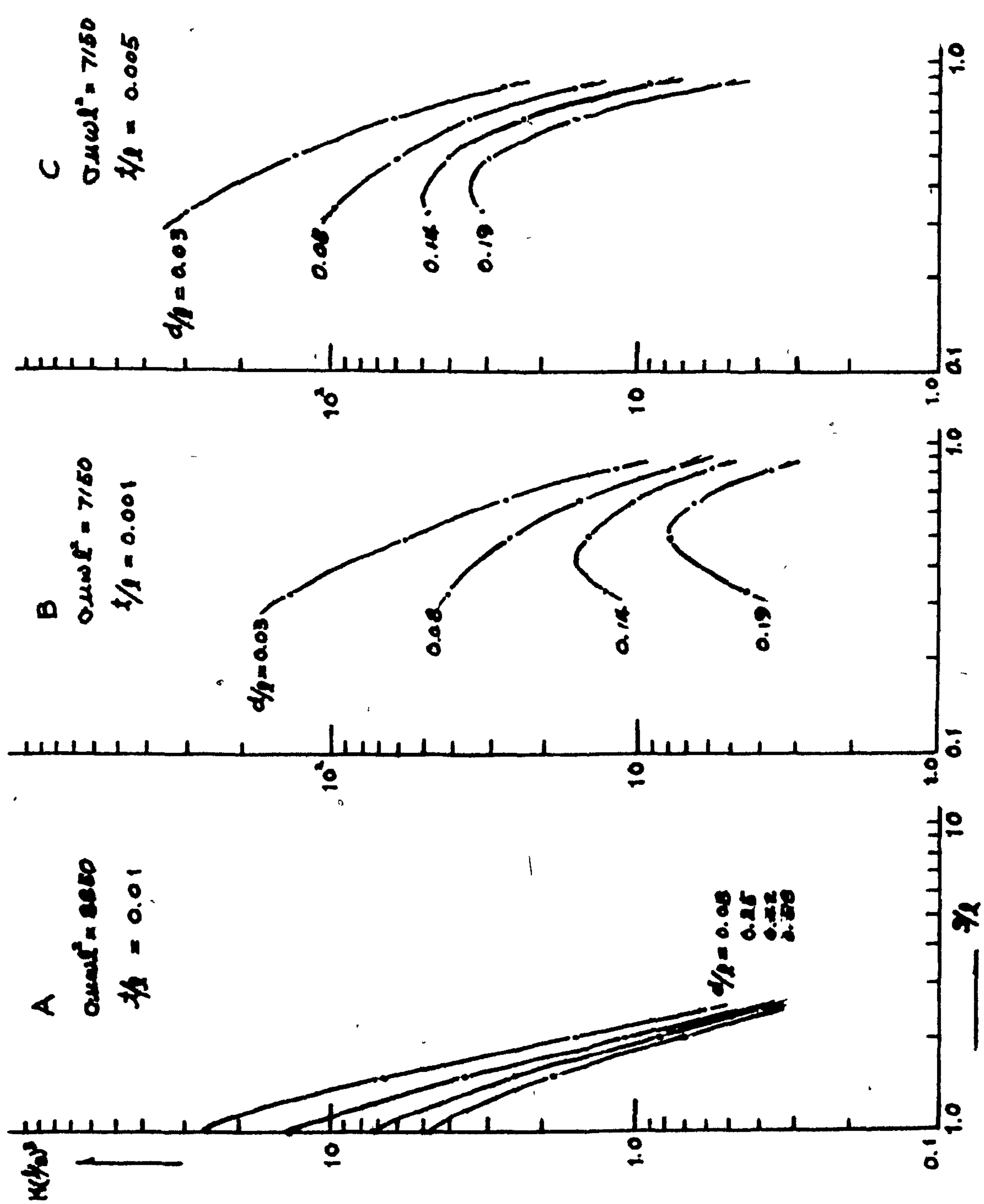

Fig. 16. $H(l/s)^3$ - s/l curves for $\theta = 90°$ from experiments (IV)

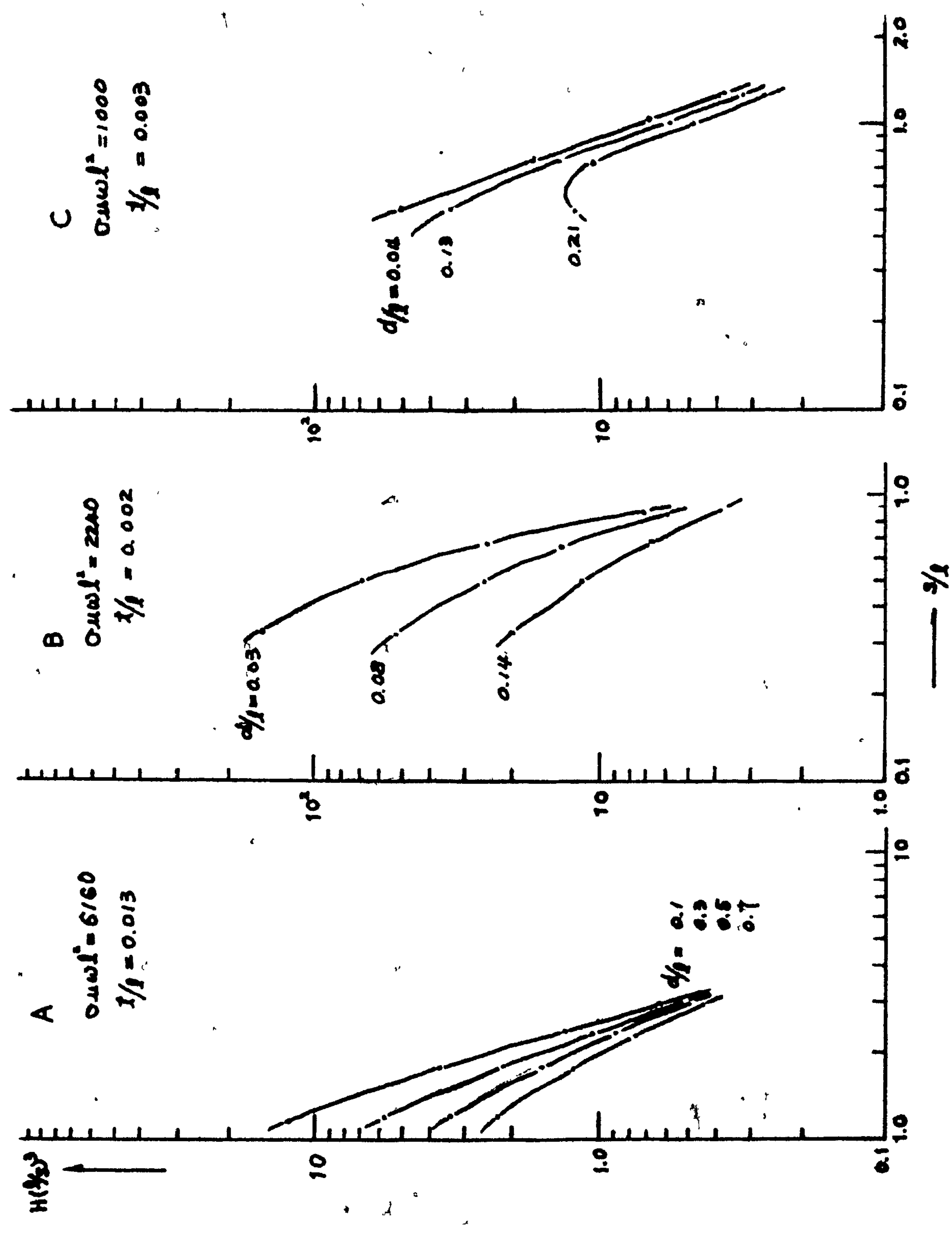

Fig. 17. H(l/s)^3 - s/l curves for θ = 90° from experiments (V) .

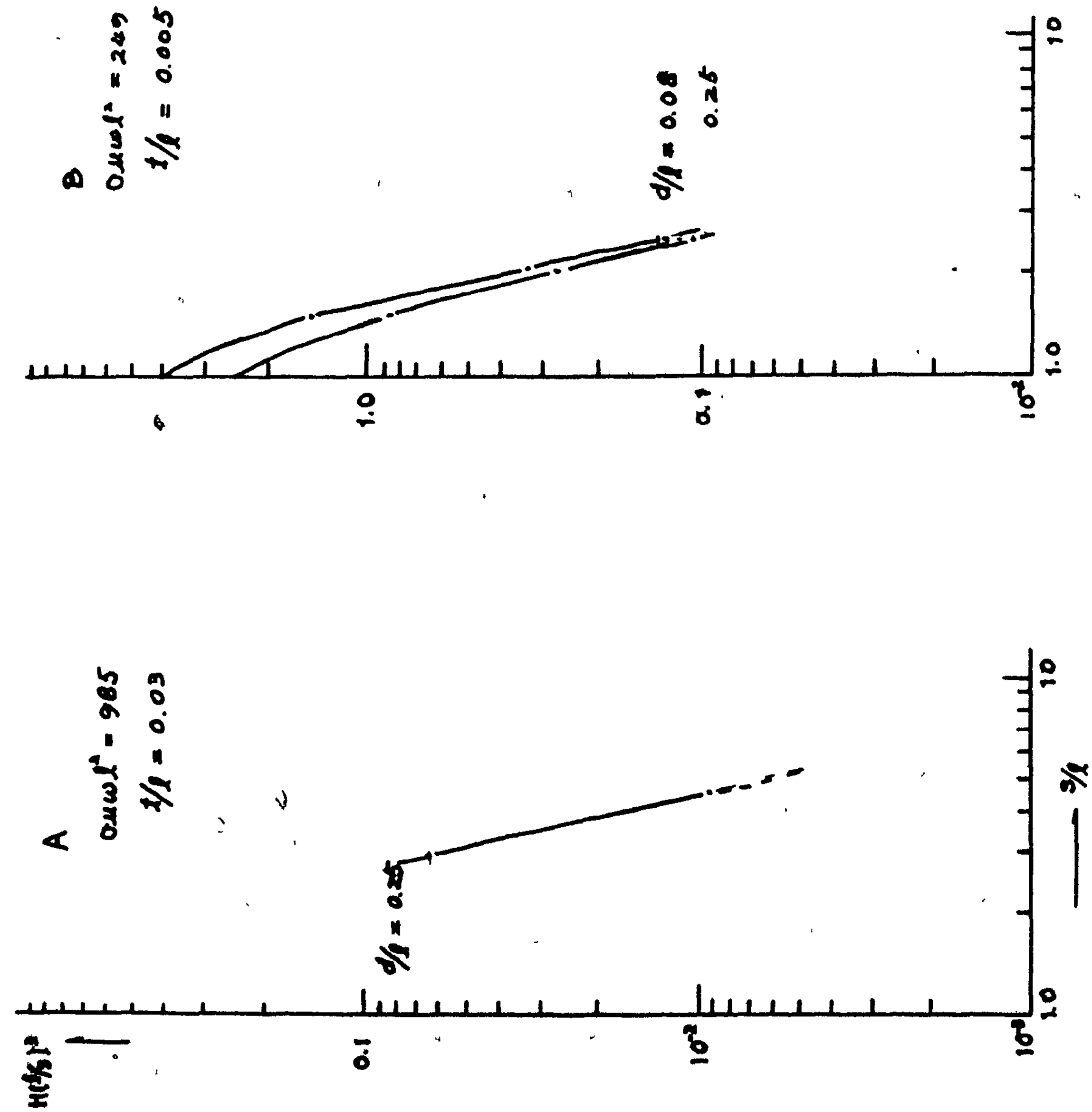

Fig. 18. $H(l/s)^{3}$ - s/l curves for $\theta = 90^{\circ}$ from experiments(VI)

varies in the same fashion as those in Fig. 4. The magnitude of $H(l/s)^3$ is decreased and the rate of change in $H(l/s)^3$ with s/l is also decreased as d (or d/l, provided l is constant) is increased up to a certain value of d/l. Beyond this value of d/l, the slope has both positive and negative signs, that is, the value of $H(l/s)^3$ reaches a maximum and then decreases for larger values of s/l.

2. $\theta = 90°$. The effect of σ on $H(l/s)^3$ - s/l

In order to consider the effect of σ on the curve $H(l/s)^3$ - s/l, the dimensionless parameter $\sigma\mu\omega l^2$ is related to the penetration distance in electromagnetic theory. The so-called skin depth -- that is, the distance for which the EM field is reduced to 1/e of its original amplitude -- is defined as

$$\delta = \sqrt{\frac{2}{\sigma\mu\omega}}$$

$$\text{or} \quad \sigma\mu\omega l^2 = 2l^2/\delta^2 \tag{27}$$

The skin depth effect controls the concentration of the induced current in the conductor along the imagined coil. From Fig. 19, when the magnetic induction $\vec{B}$ encounters the sheet as shown, the electric field $\vec{E}$ is

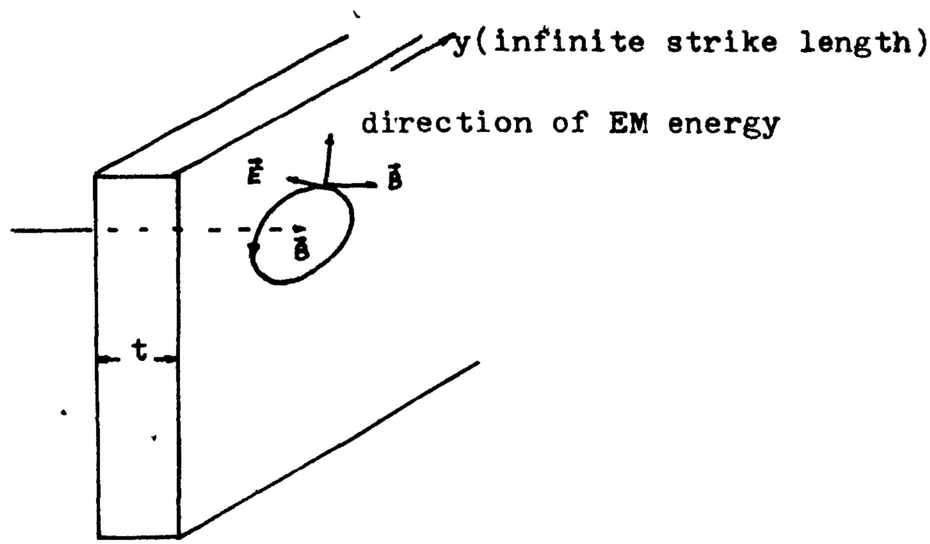

Fig. 19   Electromagnetic phenomenon in the plate

tangent to the coil, and the propagation of electromagnetic energy is in all direction radially from the coil. Thus if the skin depth is very small in the direction of propagation, the current density along the coil is very high. For a larger skin depth the current would be distributed over a wider region. When Figs. 14A and 16C, which are identical in all the parameters excpt for σ, are compared, we find that the values of $H(l/s)^3$ for the same s/l are decreased and the rate of change is decreased as the conductivity is decreased, because the induced current is distributed over wider range. These curves are for Al and stainless steel sheets of the same dimensions.

3. The effect of t on the curve $H(l/s)^3$ - s/l

When the effect of t is considered, the propagation of the secondary electromagnetic wave in the direction parallel to the thickness is significant. Let us consider Fig. 20 where the loop represents the induced current in the sheet conductor and its thickness is in the x direction.

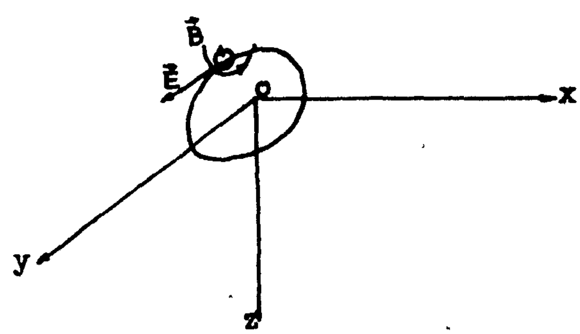

Fig. 20 Electromannetic phenomenon in the conductor coil

In the diagram $\hat{B}$ is the secondary magnetic field whose direction determines the coil orientation. In this case, the energy propagation is in all directions around the sectional area of the loop. Of all the directions of propagation, only the x component is affected by the thickness t.

Thus, we would expect that the secondary field at the receiver would vary in some fashion with thickness of the conductor. That this is indeed the case may be seen by comparing Figs. 13C with 14A, for Al sheets and Figs. 16B and 16C for stainless steel sheets. In both examples only the thickness has been varied, by a factor of 5, other parameters remaining constant. The H values increase with t, although the increase is not proportional to t and it is larger for the stainless steel sheets (≈ 2.2) than for the aluminum (≈ 1.2). This is to be expected, since the attenuation is larger in the aluminum. However, no quantitative relation between t and H seems possible.

4. The effect of l on $H(l/s)^3 - s/l$. $\theta = 90$.

From equation(27), it has been shown that the factor $\sigma\mu\omega l^2$ is a function of l and δ. In considering only the l effect, by use of Fig. 19, the EM phenomenon is concentrated within a certain area of the plate conductor. The depth extent of the conductor is related to the area which is energized by the magnetic field from the transmitter, unless l is considerably larger than the transmitter-receiver spacing.

Consider the curves in Figs. 17B and 17C which show the effect of varying l on $H(l/s)^3 - s/l$, when the value of t/l is slightly changed by appropriete variation of l for Pb sheets. The results demonstrate that the change of l is equivalent to sliding along the curve shown below.

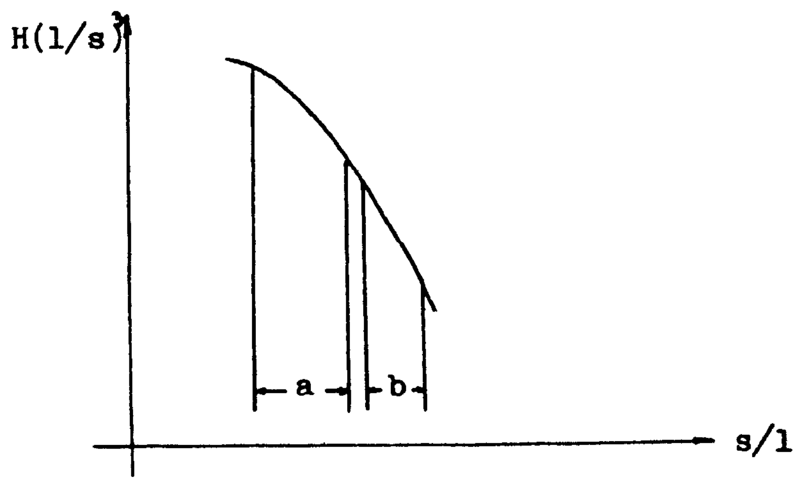

Fig. 21 The effect of l on the H(l/s) - s/l curve

If l is increased or s/l is decreased, the part of the curve marked "b" is moved to "a", for fixed values of $\sigma\mu\omega l^2$. The latter is maintained constant by suitable variation of σ.

5. The effect of θ on $H(l/s)^3$ - s/l

A collection of curves for $\theta = 60°$ and $30°$ is shown in Figs. 22 - 31. As the dip angle decreases from the vertical attitude the value of $H(1/s)^3$ is increased and the rate of the change is also increased. For large values of $\sigma\mu\omega l^2$ and small d/l, the curves are almost identical to their equivalent for $\theta = 90^\circ$, as can be seen by comparing Figs. 13B, C, 14A with 22B, C,23A and 27B, C, 28A. This is to be expected because of the insensitivity of the horizontal loop system to dip angle. For smaller values of $\sigma\mu\omega l^2$ and larger d/l, however, the differences are quite distinct.

The problem of selecting the dip angle of the sheet conductor, in order to use the proper characteristic curve, is not as difficult in this method as it is with the conventional sets of characteristic curves, since pseudo depth dections provide a more reliable estimate than a single profile.

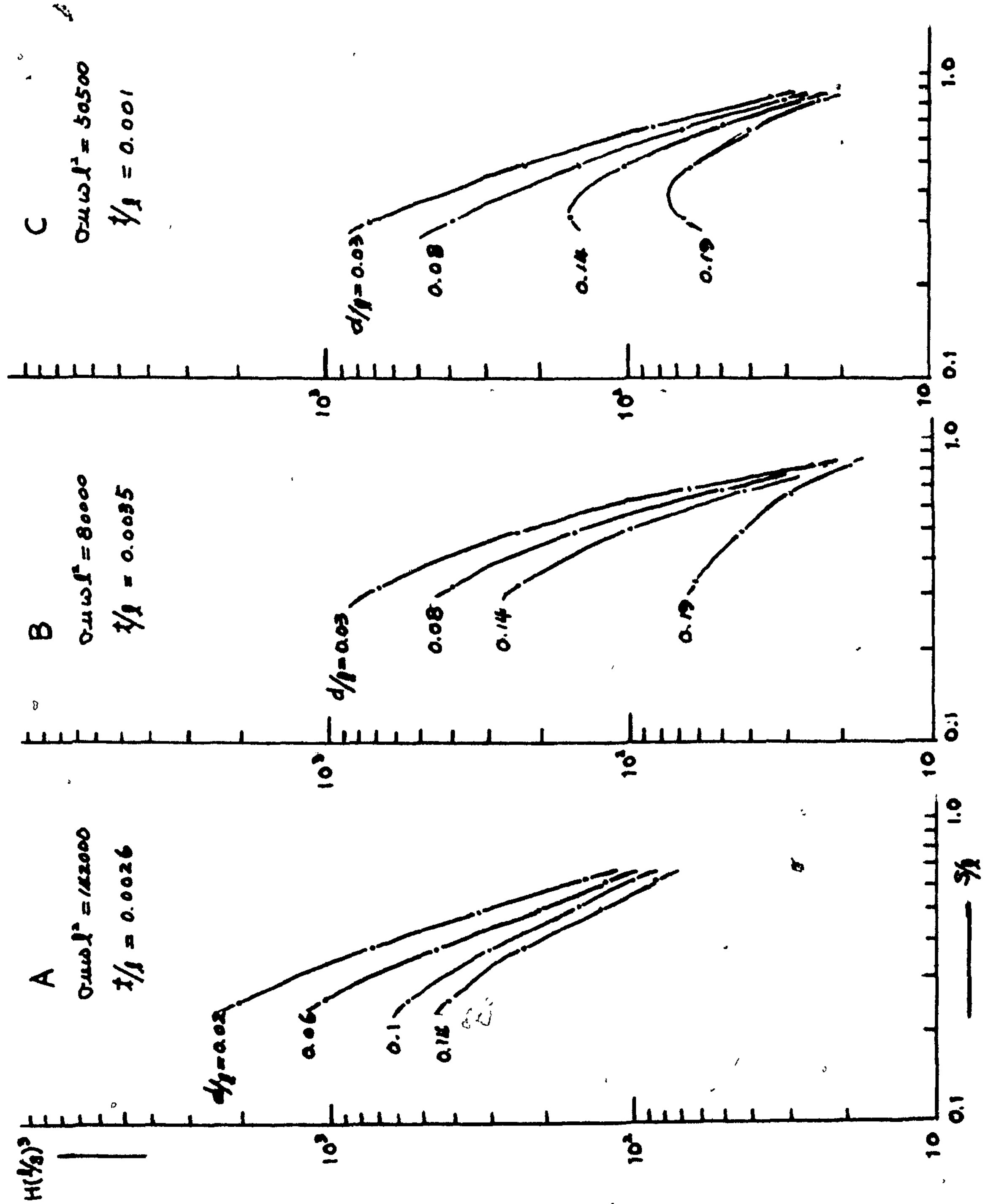

Fig. 22. $H(l/s)^3$ - s/l curves for $\theta = 60°$ from experiments(I)

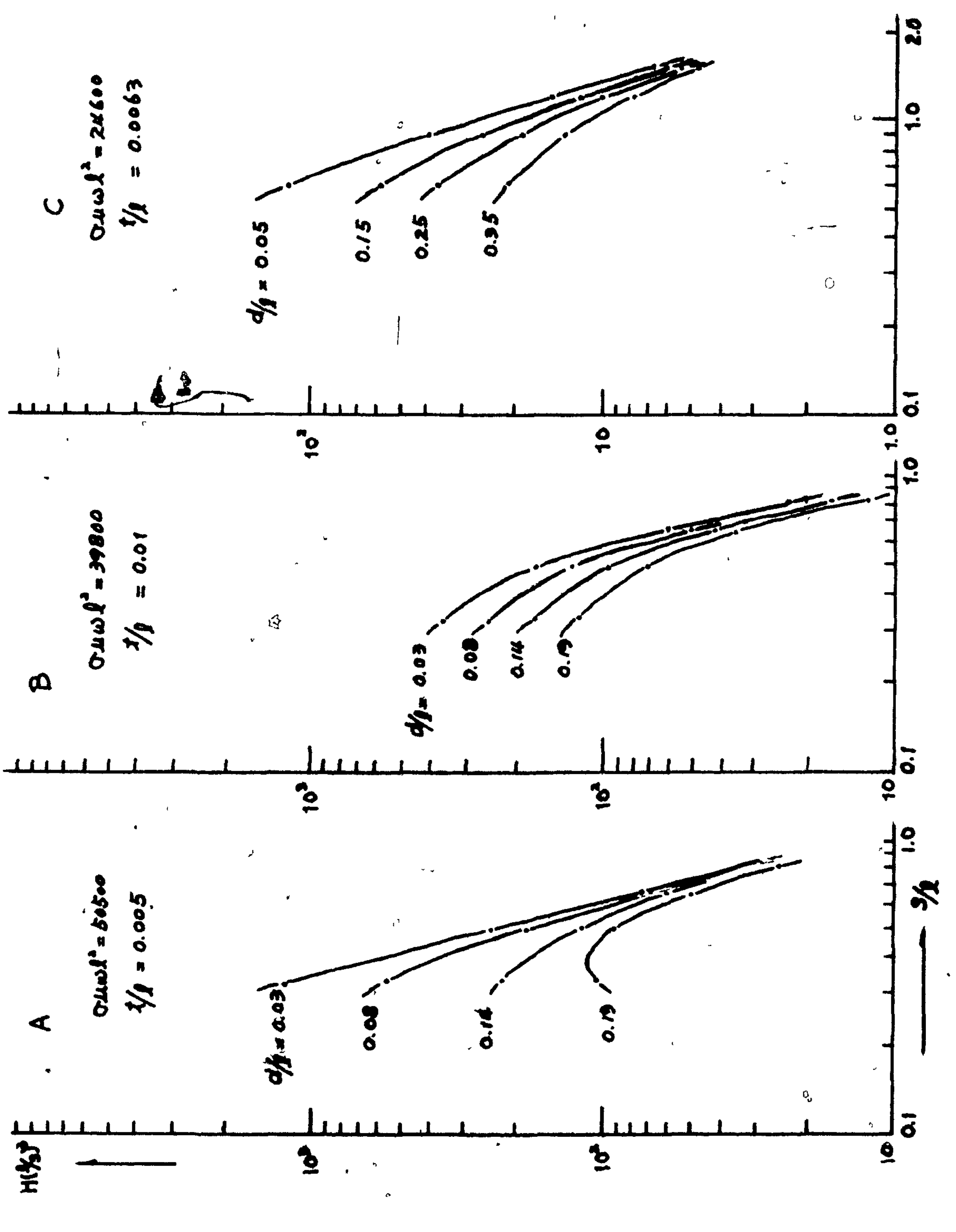

Fig. 23. H(1/s)³ - s/1 curves for θ = 60° from experiments(II)

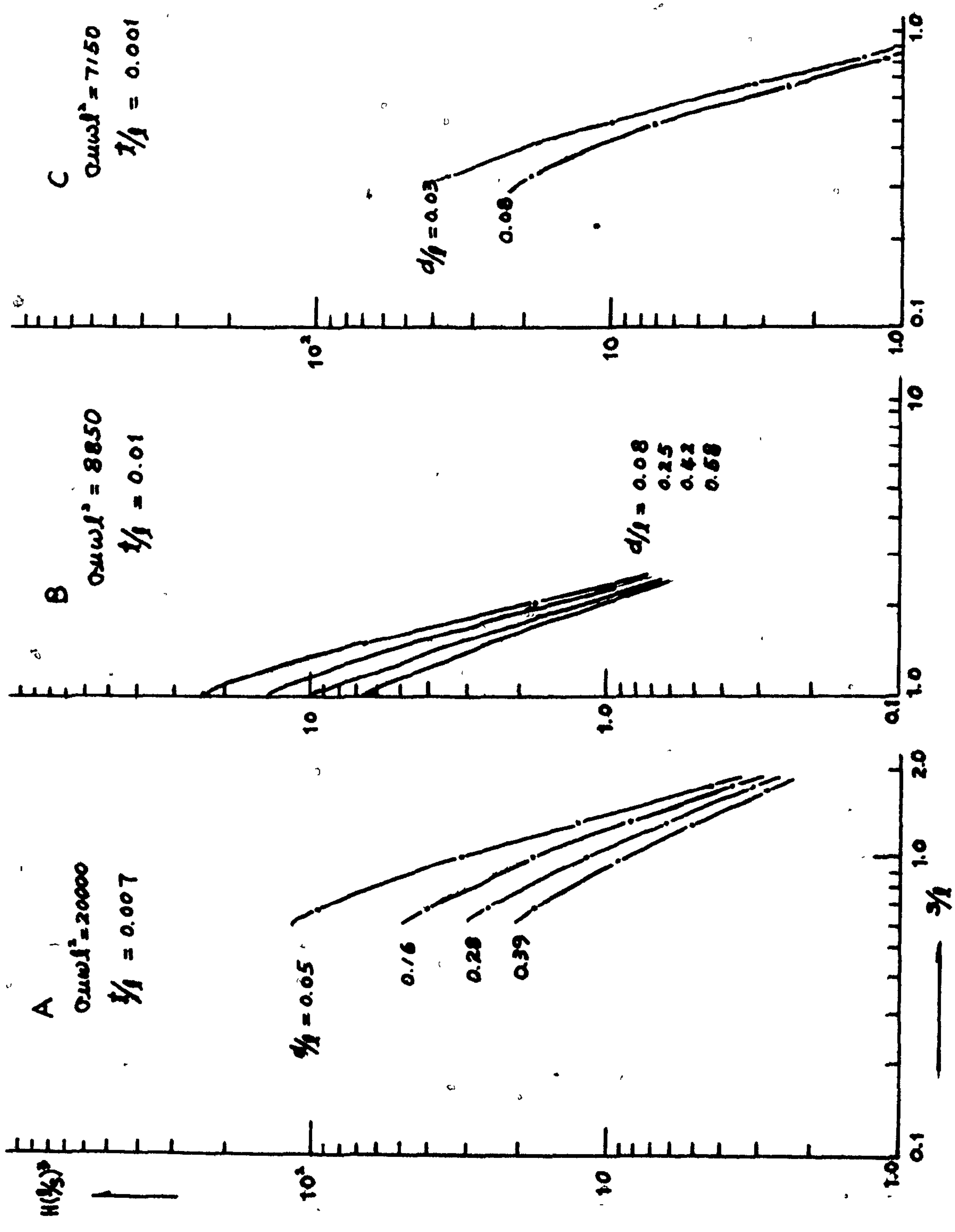

Fig. 24. $H(l/s)^3$ - s/l curves for $\theta = 60°$ from experiments (III)

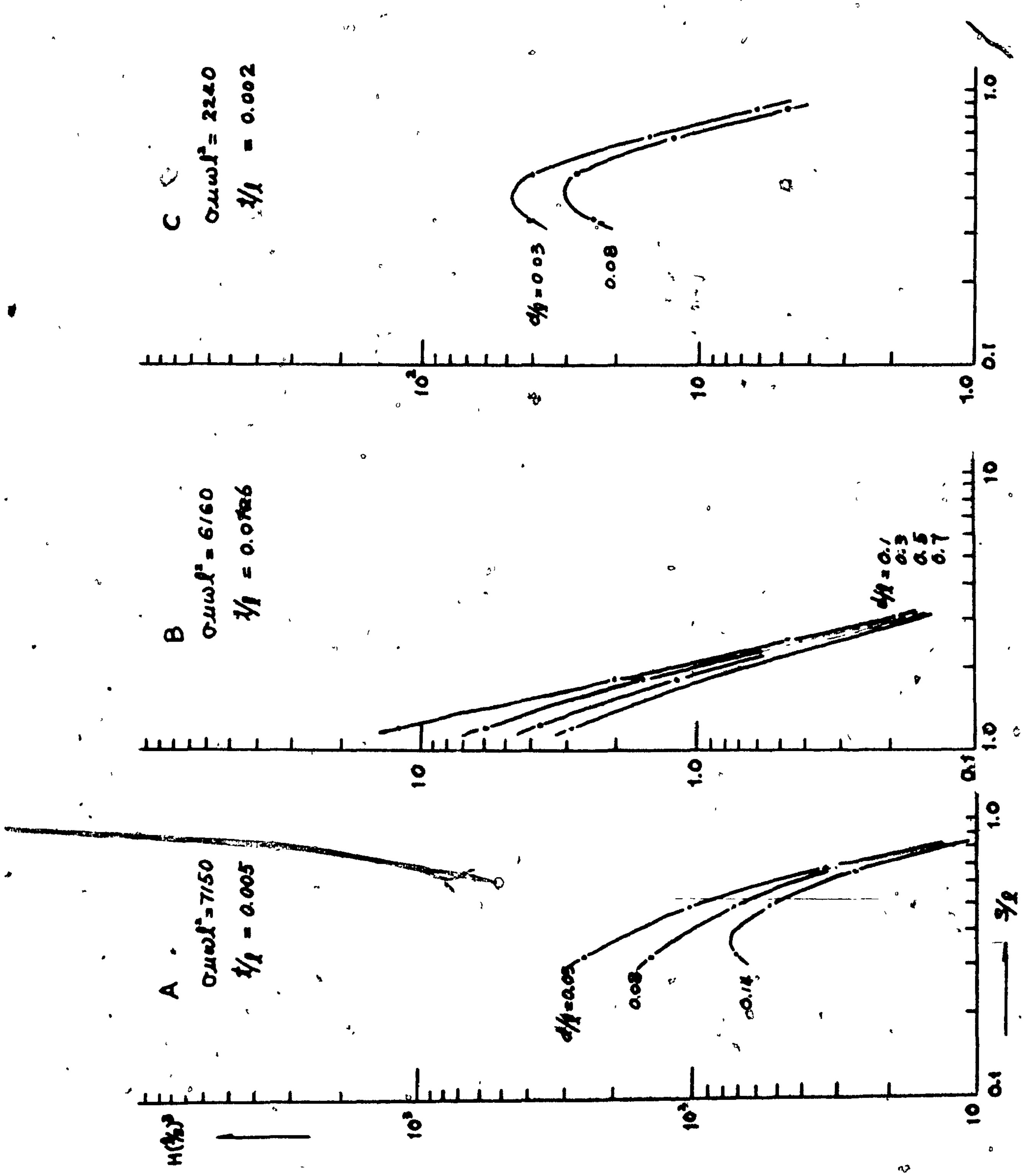

Fig. 25. $H(l/s)^3$ - s/l curves for θ = 60° from experiments(IV)

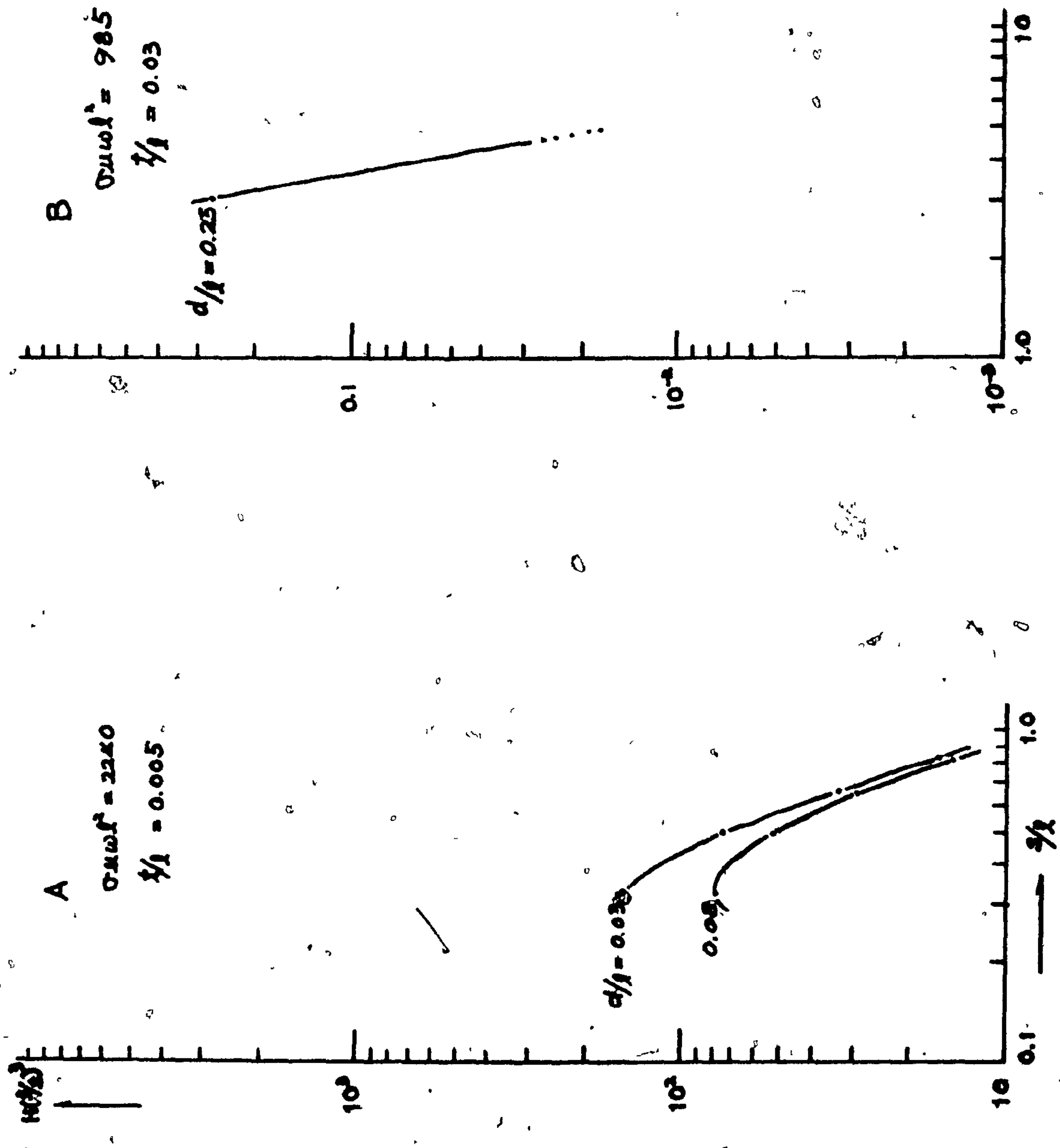

Fig. 26. H(1/s)^{3} - s/1 curves for θ = 60° from experiments (V)

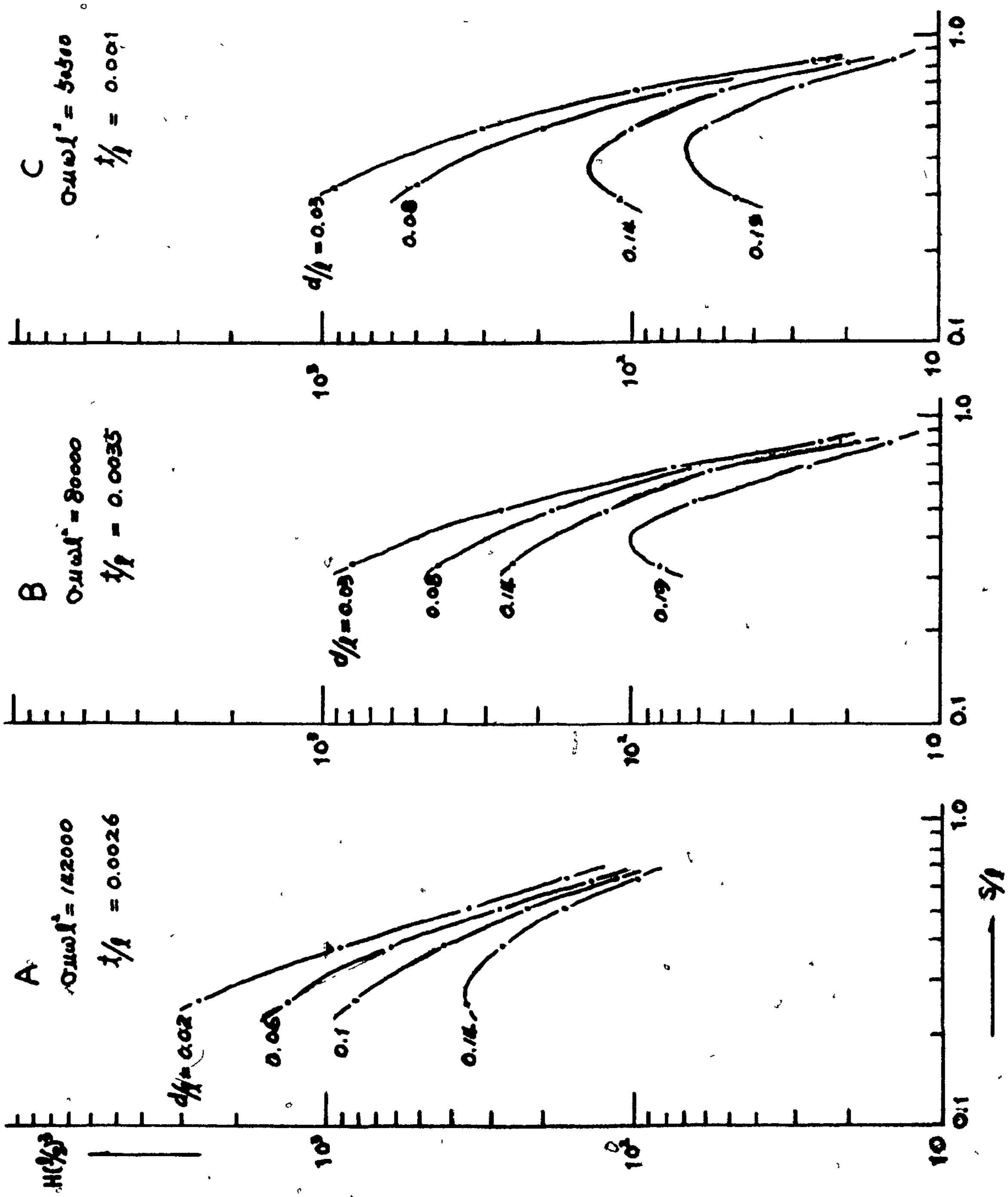

Fig. 27. $H(l/s)^3$ - s/l curves for θ = 30° from experiments(I)

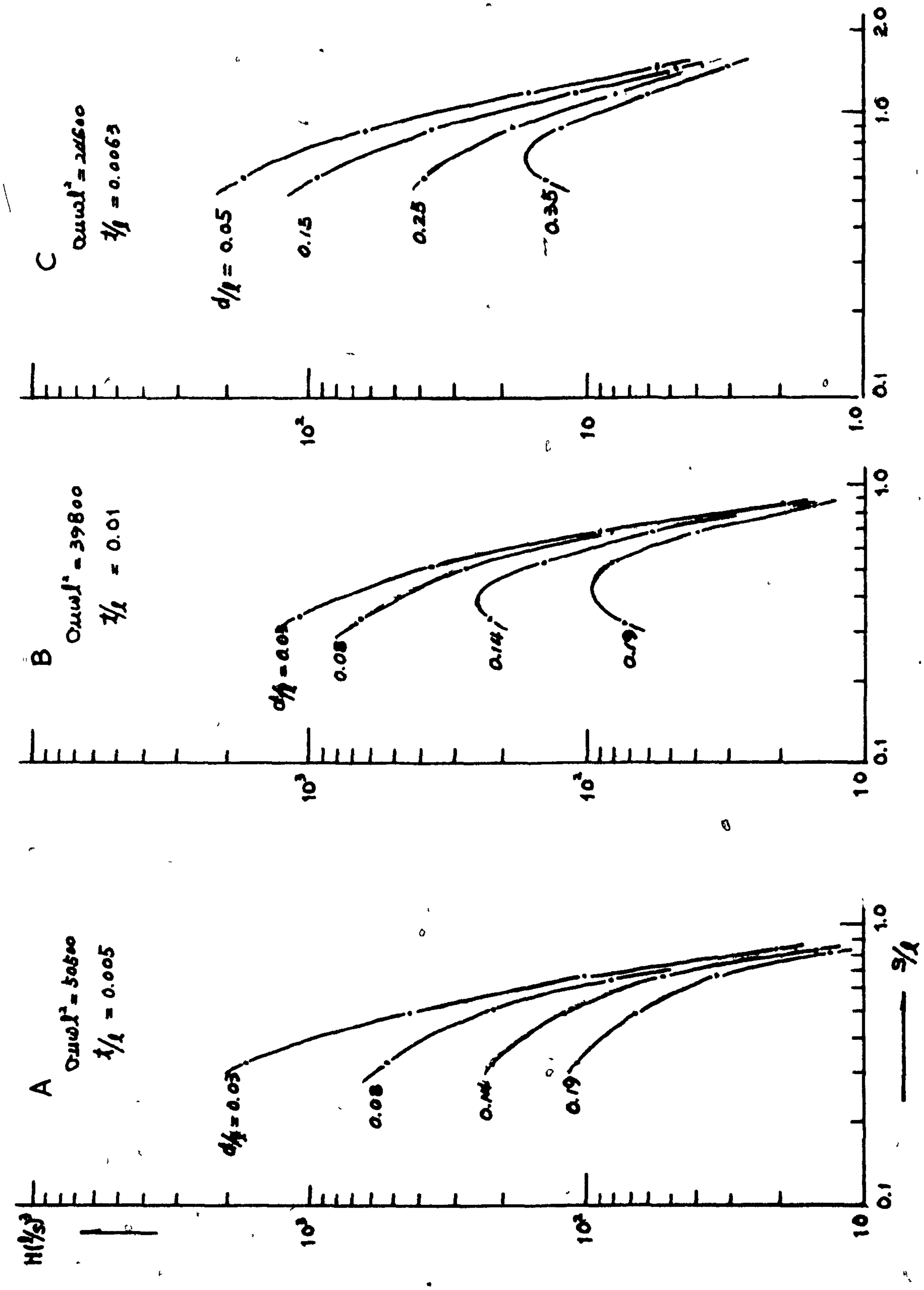

Fig. 28. $H(l/s)^3$ - s/l curves for $\theta = 30°$ from experiments(II)

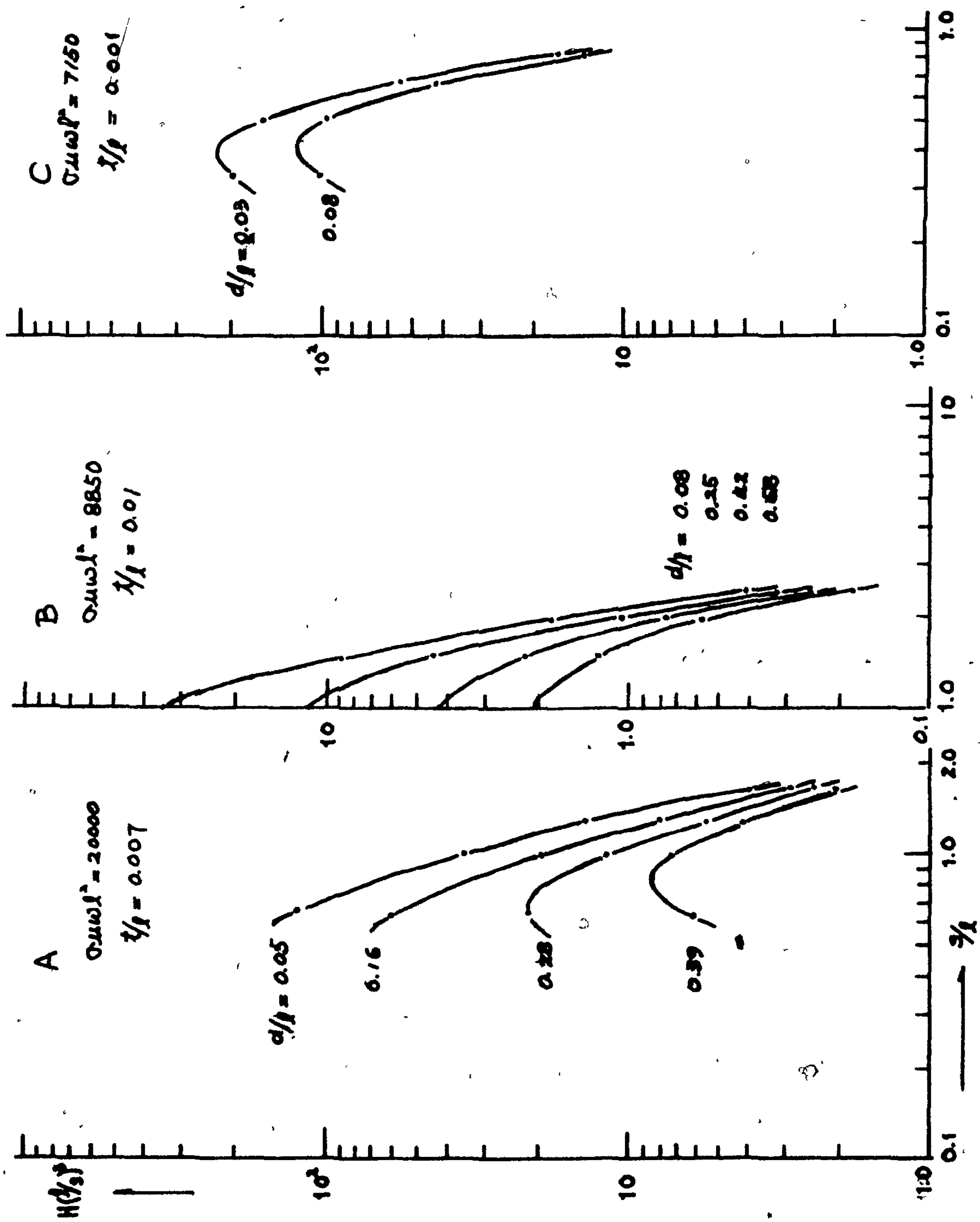

Fig. 29. $H(1/s)^3$ - s/l curves for θ = 30° from experiments (III)

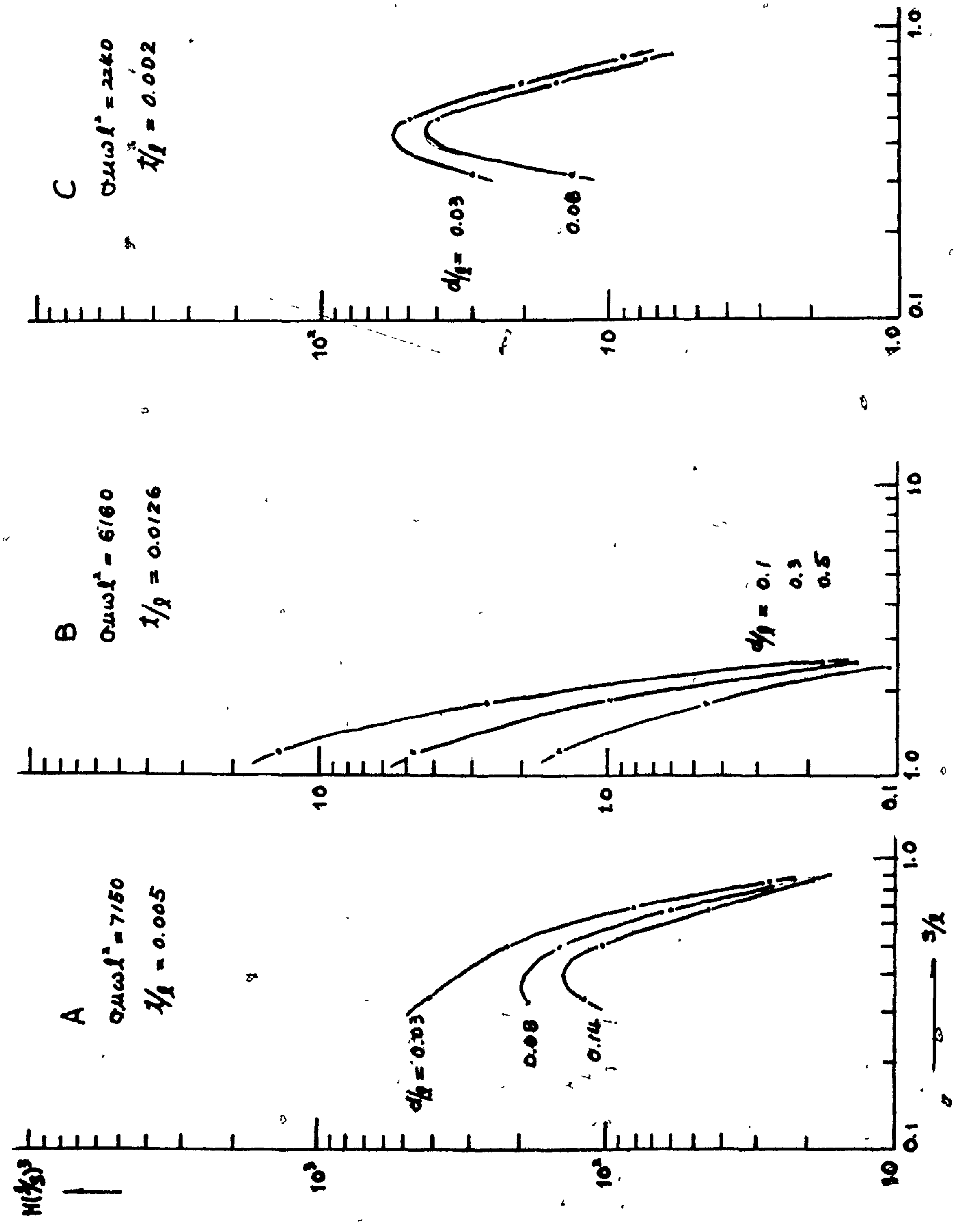

Fig. 30. $H(l/s)^3$ - s/l curves for $\theta = 30^\circ$ from experiments (IV)

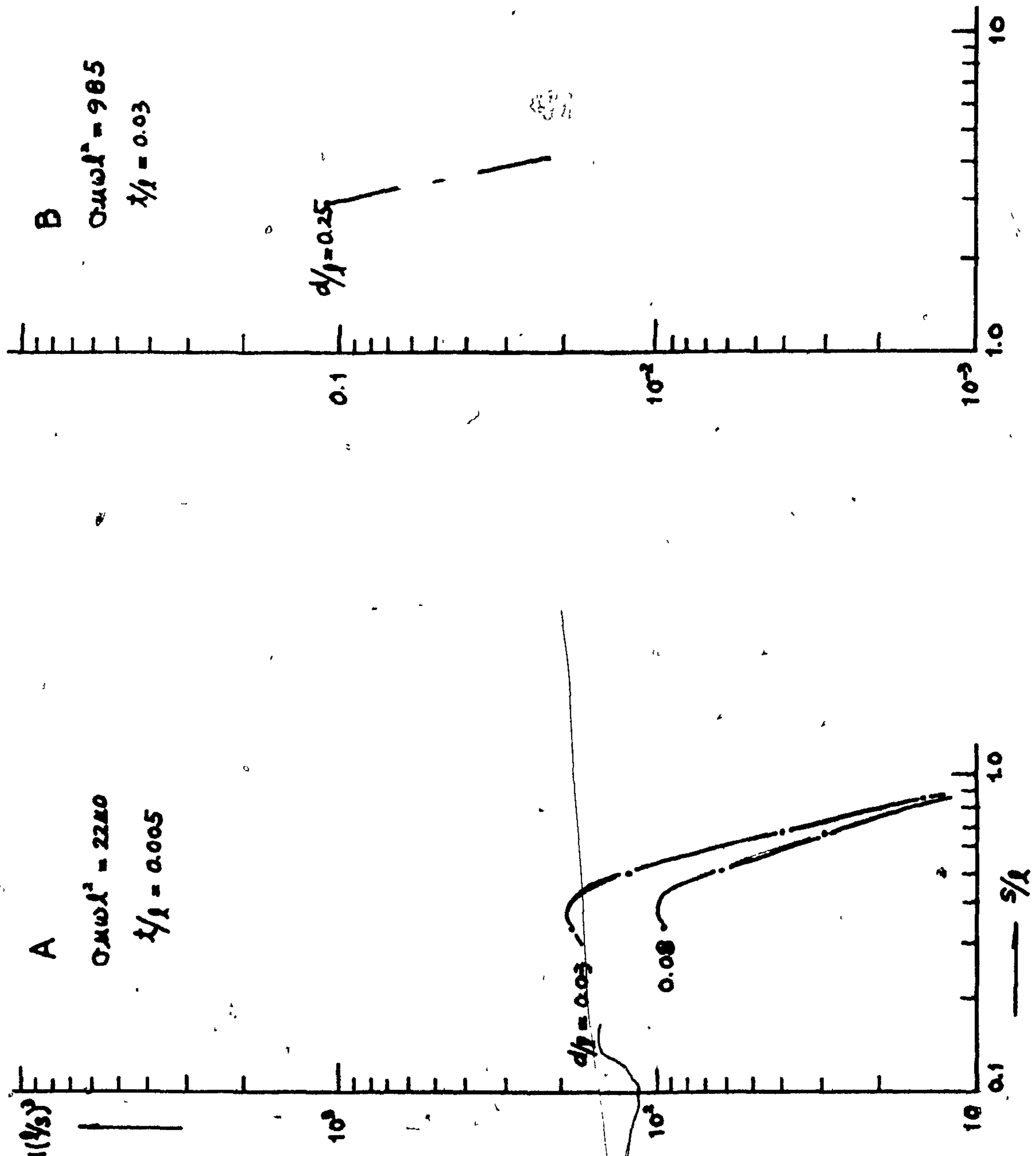

Fig. 31. $H(1/s)^3$ - s/l curves for θ = 30° from experiments (V)

Chapter 6. Field Work

1. Introduction

From the model work, we have found that the contours in the vertical pseudo section have distinguishable characteristics from which some information can be obtained about the geometry of the conductor, for example, location and dip, and that depth, depth extent, thickness and conductivity may be found from the characteristic curves.

The field results were obtained in 1970 and 1972 at four areas in Saskatchewan and Quebec, and have been used for investigating how the characteristic curves from the model work are applied to interpretation of the horizontal loop EM survey with multiple separation. In 1970 the author was employed by Donald Fisher & Associates as a geophysicist conducting various EM surveys in Saskatchewan. Multiple separation horizontal loop EM was done at three locations, two on Hicks Island and one at Uranium Valley, in the La Ronge area north of Saskatoon, where geological mapping and a self potential survey had previously been carried out. In 1972, a similar type of EM survey was made near Demers Creek in Ham Township, one hundred miles northeast of Montreal.

During the 1970 work in Saskatchewan, the EM field units employed were the Geonics EM 17 and McPhar VHEM, while the Demers Creek survey was made with the McPhar VHEM equipment. The EM 17 transmitter is excited at 1600 Hz, while the VHEM uses two frequencies, 2400 Hz and 600 Hz.

The results of the horizontal loop EM survey with multiple separation were analyzed by plotting the vertical pseudo sections and matching the characteristic curves obtained from model work. This technique, to be described later in detail, offers more information about geometrical properties of the conductor and less ambiguity than conventional interpretation techniques. A comparison of the results obtained with the two interpretation methods (and with other data available at the same sites) shows reasonable agreement.

2. Geophysical surveys

A. Hicks Island

1) Location and general geology

Hicks Island is bounded by latitude 55 degrees 44 minutes and 55 degrees 46 minutes north and by longitude 105 degrees

54 minutes and 105 degrees 55 minutes west, and is approximately 60 miles northwest of the village of La Ronge, Saskatchewan (Fig. 32). This area is readily acessible from the Churchill River, upon which a float-equipped aircraft may land.

The consolidated rocks in this region are of Precambrian age and composed of intrusive and/or plutonic rocks in the western part and metasomatized and migmatic rocks in the eastern part. The intrusive and/or plutonic rocks are mainly composed of "Eastern Granitic Rocks" which are, in general, medium to coarse grained equigranular and either lack foliation or have a weak, irregular foliation, composed mainly of biotite-quartz-diorite, while the metasomatic and migmatic rocks occur as migmatite which is considered to be derived from garnet-cordierite-biotite rocks. (Fig. 33)

2) Geophysical results

In this area, two survey lines, the first a claim line crossed by L-35S, the second being L-30S, were selected as test traverse lines, since trenching had been previously carried out nearby to find mineralized rocks. The EM 17 was used on the claim line and VHEM unit on L-30S.(See Fig. 34)

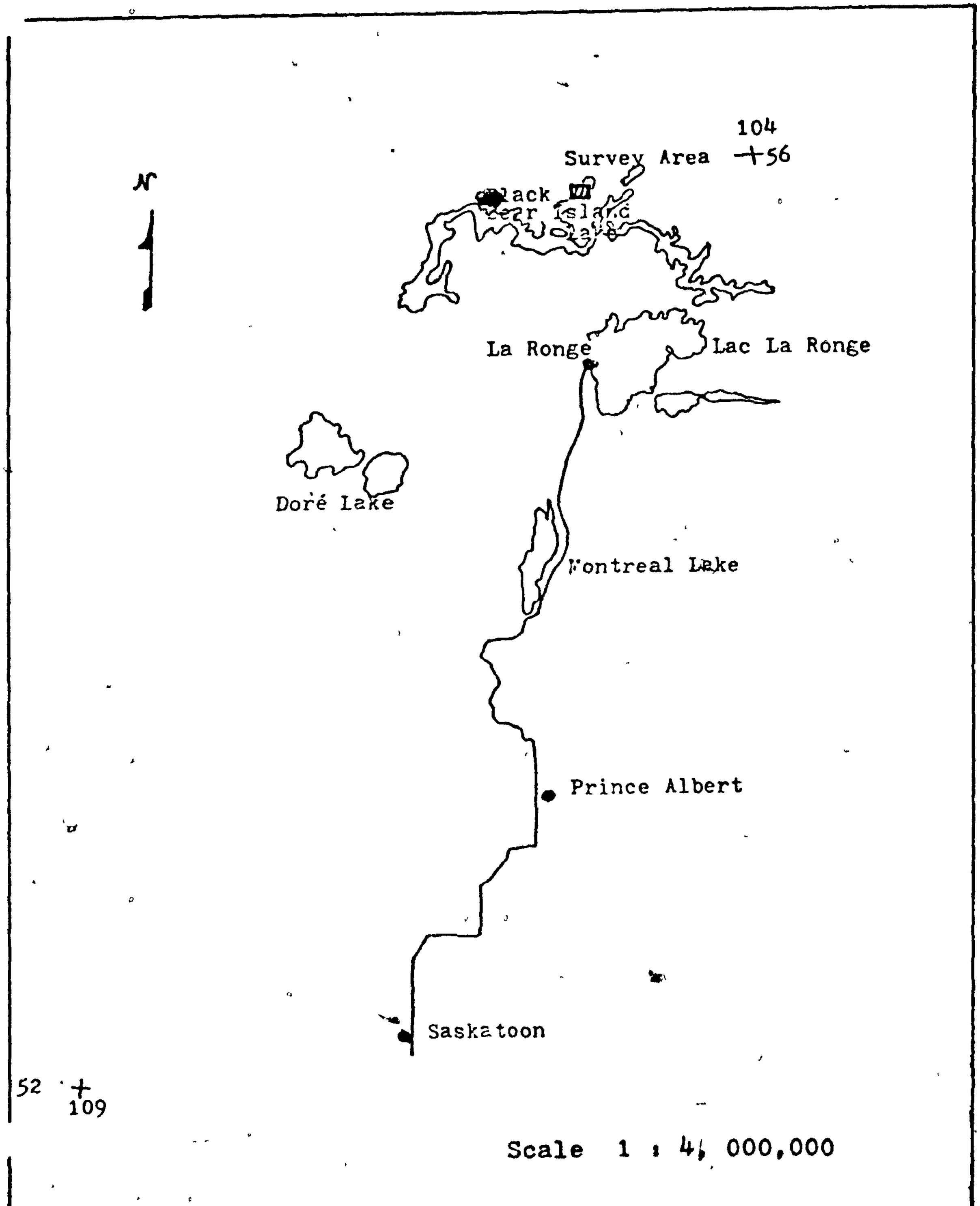

Fig. 32. Location map of Hicks Island

Geologic Map of Hicks Island

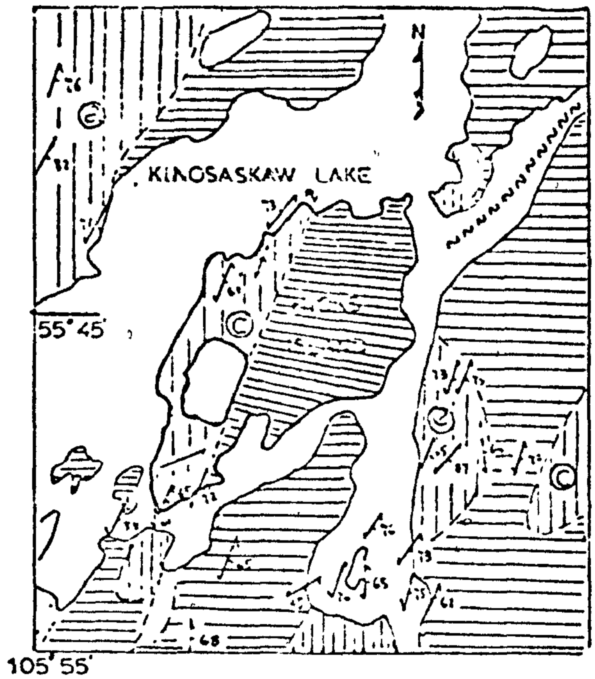

LEGEND

Eastern granitic rocks (probably Hudso ian); equigranular, mainly grey granodiorite and biotite quartz diorite, in part quartz monzonite.

Porphyroblastic potassium feldspar gneiss-augen gneiss-migmatite complex, probably derived mainly from hornblendic and biotitic rocks.

migmatite derived mainly from hornblende and hornblende-biotite rocks.

migmatite derived from garnet-biotite and garnet-cordierite-biotite rocks.

migmatite derived mainly from biotitic rocks.

SYMBOLS

FAULT, SHEAR ZONE (POSITION DEFINED, APPROXIMATE, ASSUMED)

SCHISTOSITY AND GNEISSOSITY (INCLINED, VERTICAL)

LINEATION: AXIS OF MINOR SYNCLINE (INCLINED, HORIZONTAL)

Py MINERALIZATION: PYRITE

Scale 1" = 1.6 mile

Fig. 33. Geological map of Hicks Island

Location of Survey Lines

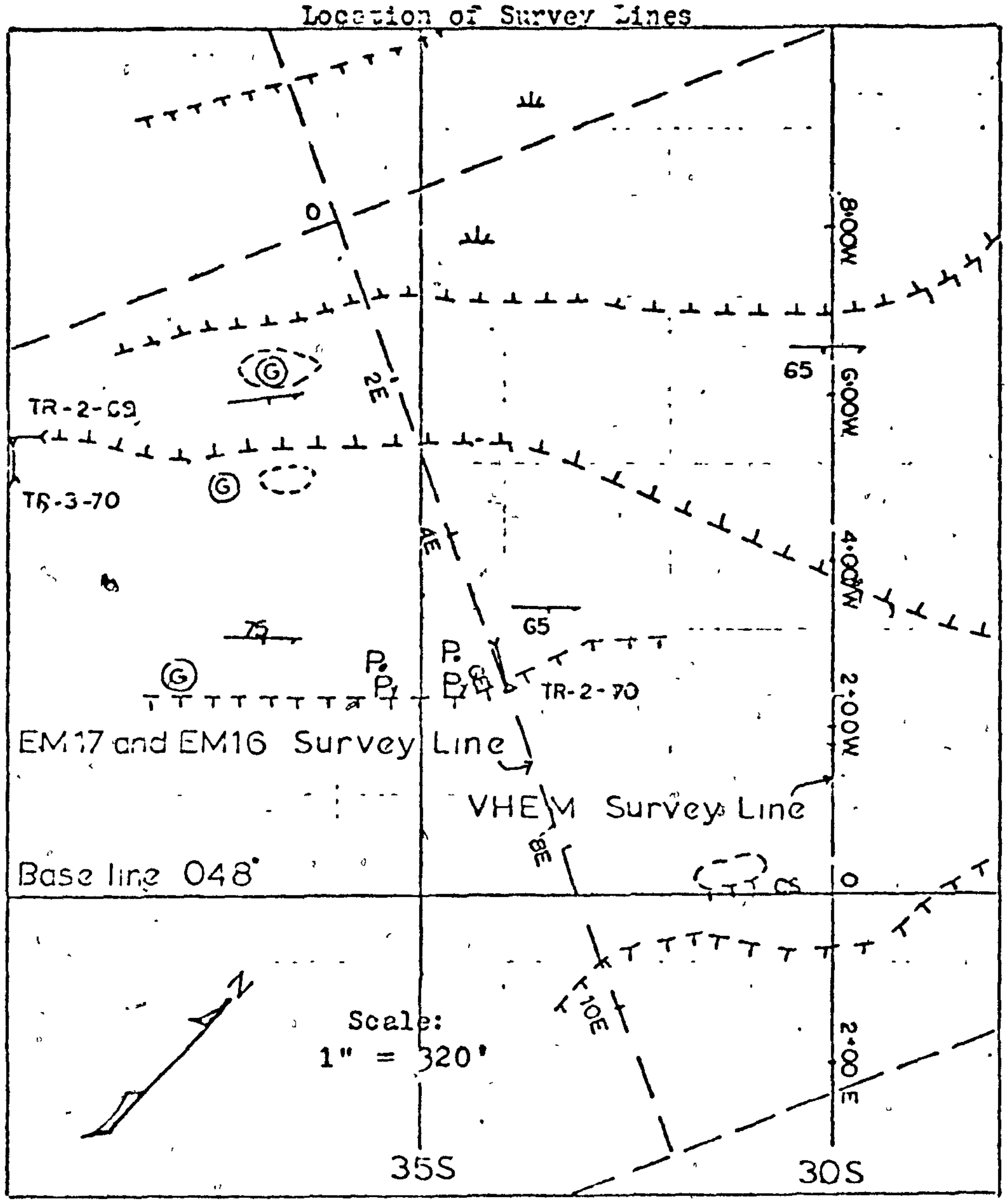

LEGEND

CS	Calc-silicate gneiss containing hornblende and/or diopsite locally containing pyrite and pyrrhotite
G	Gossan
	pyrrhotite, pyrite.
	scarn
	Rock Trench
	Claim Line
	Foliation and/or gneissosity inclined, vertical.
	Muskeg

Fig. 34. Location of survey lines

a) Claim line

The horizontal loop EM survey was carried out at coil-separations of 100' and 200' with station interval of 100' and the profiles are shown in Fig. 35. The data are also displayed in vertical pseudo sections in Fig. 36. The contours show two anomalies, one at 3E, the other at 7E. The former appears to dip to the east (actually SE), while the latter appears to be almost vertical, when the trend of the contours is indicated.

Since only two transmitter-receiver separations have been used, the vertical pseudo section is hardly complete enough for the present type of interpretation; however, an attempt has been made, by drawing curves on log-log paper, to indicate the relation between H/s^3 and s, and by matching them to the model curves for $H(l/s)^3 - s/l$. These are shown in Fig. 37. First an estimate of l is obtained, which is equivalent to the inverse of the horizontal displacement and to the cube root of the vertical displacement. If the l values are not approximately equal, the matching should be adjusted to minimize the difference between them.

Having obtained l, it is possible to estimate σ and d,

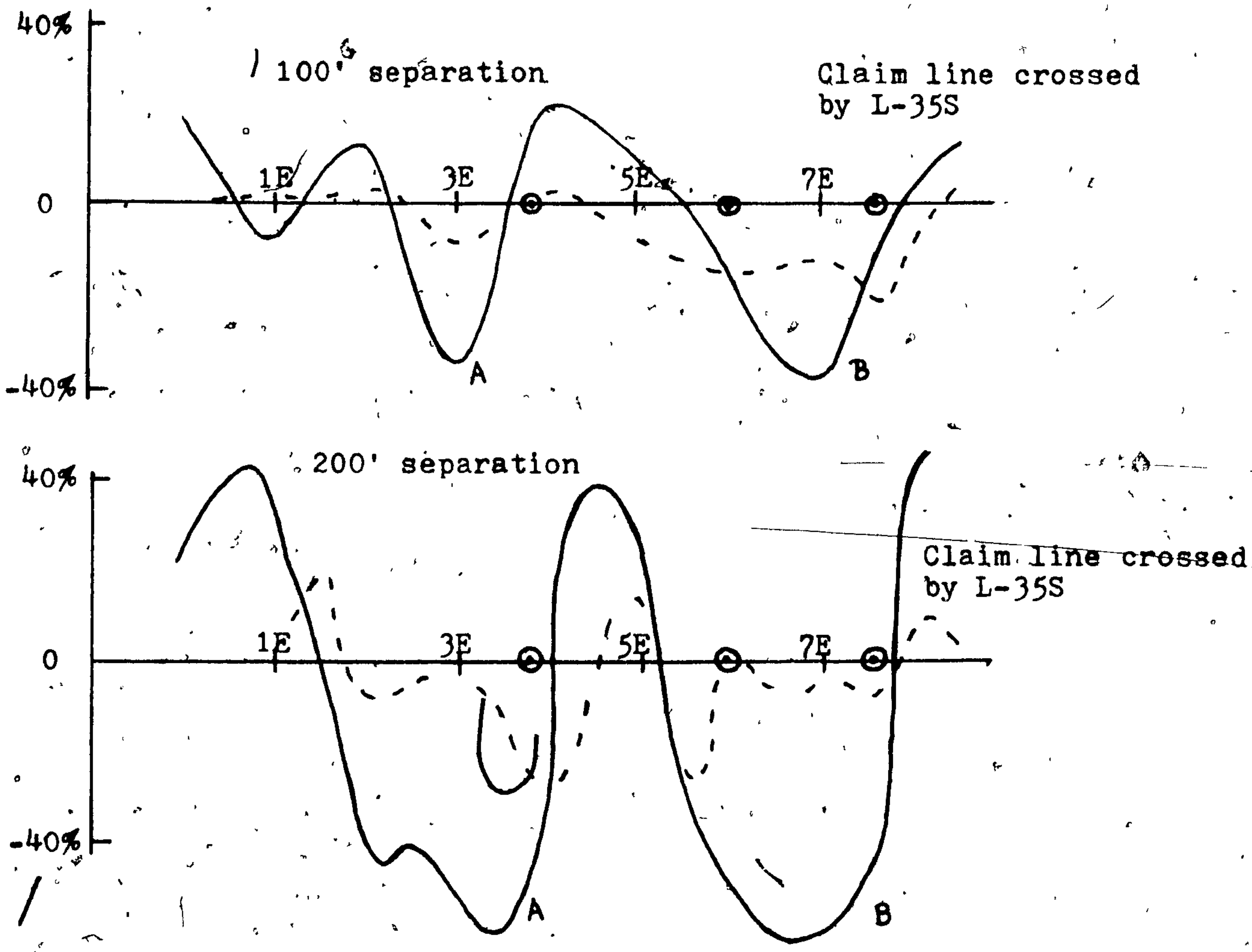

——— in-phase

- - - out-of-phase

⊙ location of S.P. anomaly

Scale 1"=200' Frequency 1600 Hz

Fig. 35. Horizontal Loop Profiles of Hicks Island (I)

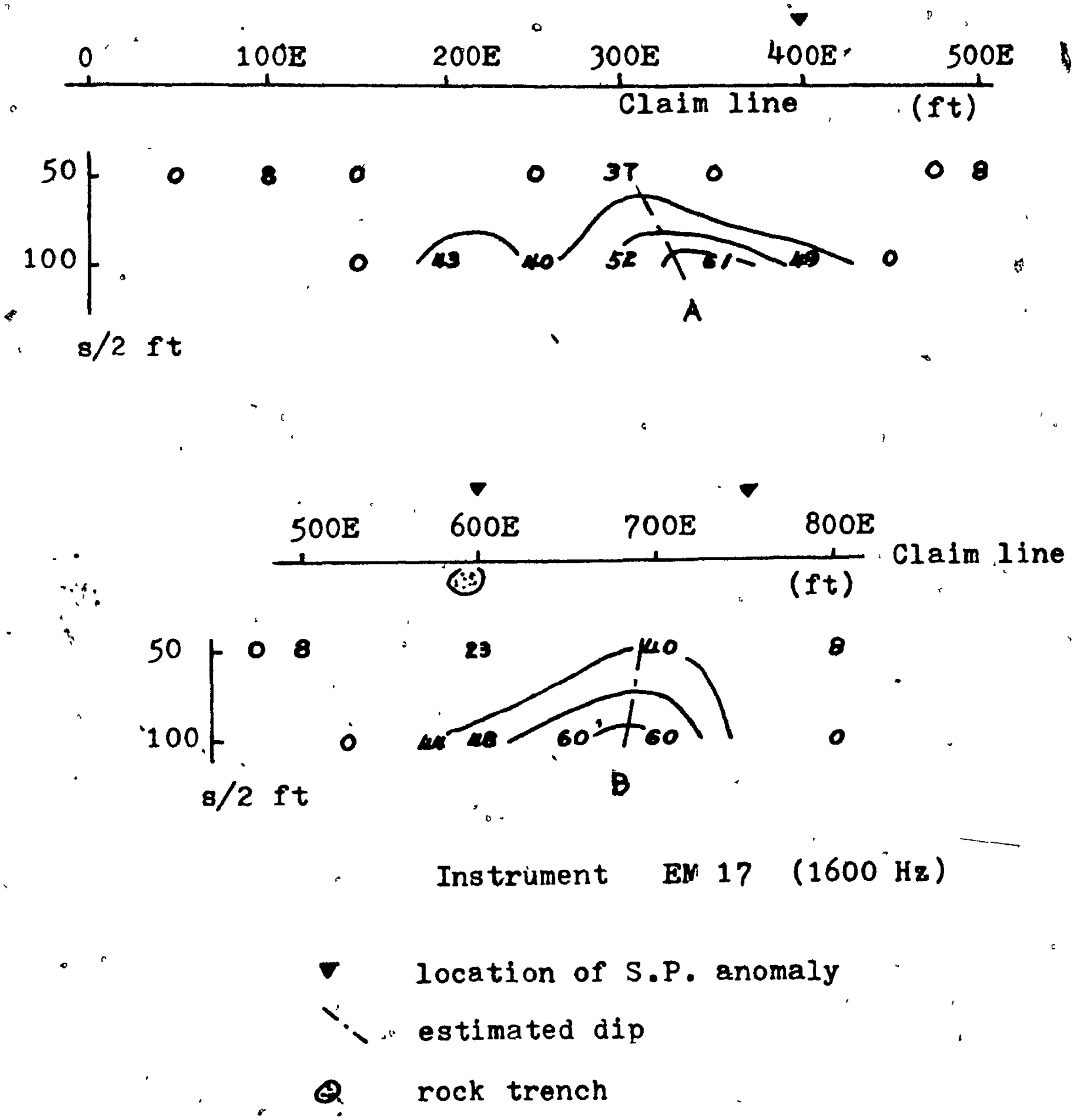

Fig. 36. Vertical pseudo section of Hicks Island (I)

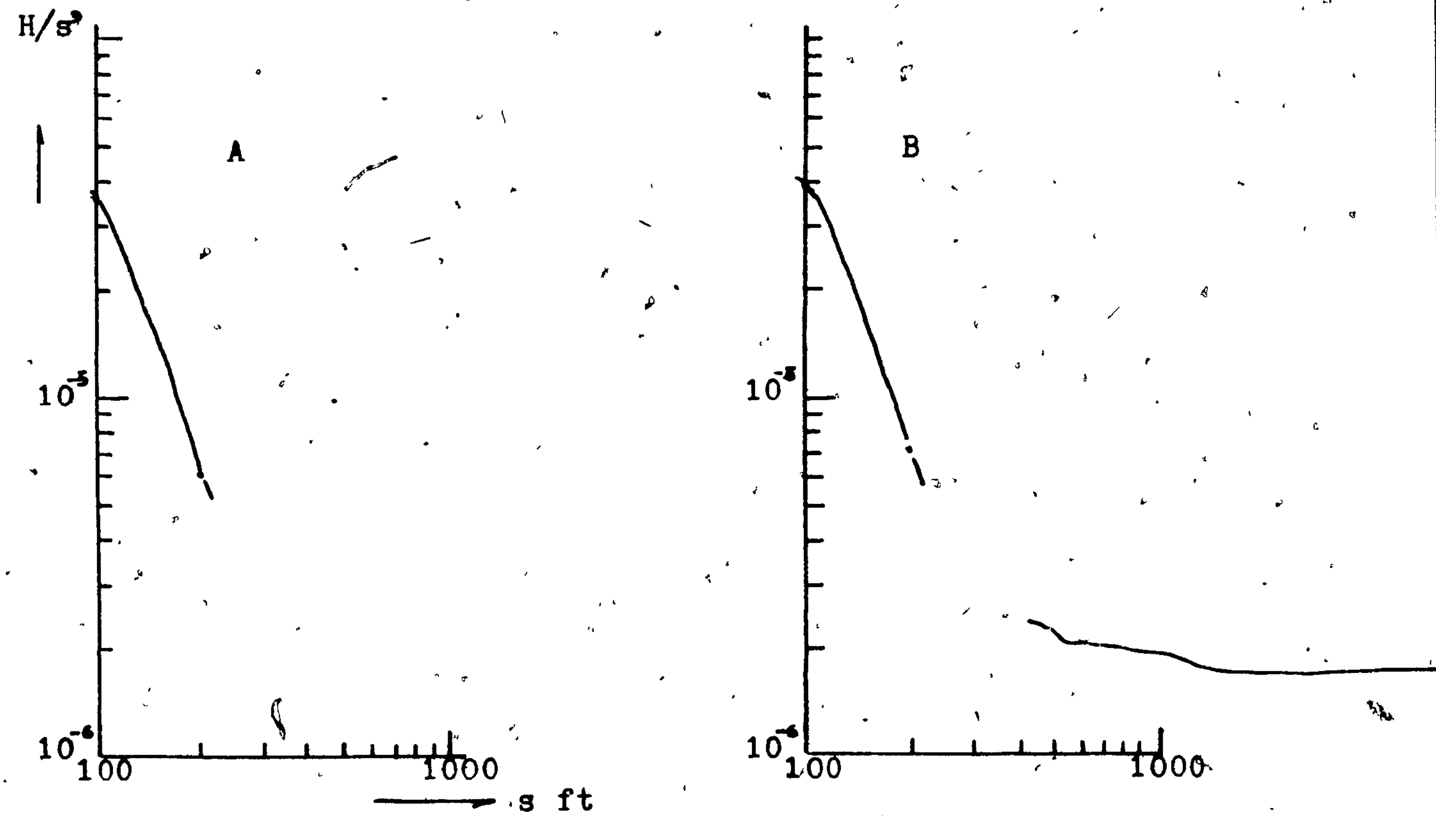

Parameters of matched curves:

$\sigma\mu\omega l^2 = 20{,}000$
$t/l = 0.007$
$d/l = 0.05$
$\theta = 60°$

$\sigma\mu\omega l^2 = 6160$
$t/l = 0.013$
$d/l = 0.3$
$\theta = 90°$

Fig. 37. H/s^3 - s curves of Hicks Island (I)

from the values of $\sigma\mu\omega l^2$ and d/l, on the appropriate model curve. Finally, the value of t may be estimated from the characteristic curve, provided the field curve matches it reasonably well.

The interpretation technique is carried out in the following steps. First, the curves of the relation $H/s^3 - s$ are plotted as mentioned above, putting the midpoint of the separations at the assumed location of the suspected conductor to produce the two curves, labelled "A" and "B", in Fig. 37.

For anomaly "A", the field curve is matched to the following curves to estimate l values from the horizontal and vertical displacements, l_h and l_v, respectively.

$\sigma\mu\omega l^2$	t/l	d/l	s/l	$H(l/s)^3$	$s_{(ft)}$	H/s^3	$l_{h(ft)}$	$l_{v(ft)}$
142,000	0.0026	0.02	0.23	2.6×10^3	100	3.6×10^{-5}	436	416
		0.06	0.26	1,000	100	3.6×10^{-5}	384	302
80,000	0.0035	0.03	0.3	780	100	3.6×10^{-5}	333	278
		0.08	0.3	500	100	3.6×10^{-5}	333	240
		0.14	0.35	220	100	3.6×10^{-5}	398	183
50,500	0.001	0.03	0.27	970	100	3.6×10^{-5}	370	300
		0.08	0.31	360	100	3.6×10^{-5}	322	216
		0.14	0.43	140	100	3.6×10^{-5}	232	140
		0.19	0.6	44	100	3.6×10^{-5}	167	107

$\alpha\mu\omega l^2$	t/l	d/l	s/l	H(l/s)	$s_{(ft)}$	H/s^3	$l_{h(ft)}$	$l_{v(ft)}$
50,500	0.005	0.14	0.4	170	100	3.6×10^{-5}	250	168
		0.19	0.45	100	100	3.6×10^{-5}	222	141
24,600	0.0063	0.05	0.5	170	100	3.6×10^{-5}	200	168
		0.15	0.7	45	100	3.6×10^{-5}	143	107
		0.25	0.9	20	100	3.6×10^{-5}	111	82
20,000	0.007	0.05	0.57	150	100	3.6×10^{-5}	175	162
		0.16	0.73	35	100	3.6×10^{-5}	137	99
8,850	0.001	0.08	0.8	22	100	3.6×10^{-5}	125	85
7,150	0.001	0.03	0.25	62	100	3.6×10^{-5}	400	120
		0.08	0.3	22	100	3.6×10^{-5}	333	85
6,160	0.0126	0.3	0.8	14	100	3.6×10^{-5}	125	73
		0.5	0.8	10	100	3.6×10^{-5}	125	65
		0.7	0.85	5.5	100	3.6×10^{-5}	118	54

(The above model curves are for $\theta = 60^\circ$)

From the above list, it appears that, for the suite of curves available, the best fit of the field curve is obtained with that of Fig. 24A, which is specified by:

$$\alpha\mu\omega l^2 = 20{,}000, \quad t/l = 0.007, \quad d/l = 0.05 \text{ and } \theta = 60^\circ .$$

The calculated value of l from the horizontal displacement is

$$l_h = 100/0.57 = 175',$$

while the calculated value of l from the vertical displacement is $\quad l_v = \left[150/(3.6 \times 10^{-5})\right]^{1/3} = 162$ (ft),

so that the difference between l_h and l_v is a minimum, for the curves which appear to match reasonably well. However, this match does not give the same value of l for both displacements. In order to have the same value of l, the model curve should have higher values of $H(l/s)^3$ than those in Fig. 24A. This departure of $H(l/s)^3$ is assumed to be due to the difference of t. Therefore, the matched value of s/l may be assumed to be a good value, since s/l is not affected by t. From the value of s/l or the horizontal displacement, we have found l = 175' or 53 m. Since the value of t/l should be higher than 0.007 due to the fact that the value of $H(l/s)^3$ should be 195 at s/l = 0.57, when H/s^3 is 3.6×10^{-5}, s = 100'; in order to have the same value of l (l = 175'), the results of the interpretation on the anomaly A are: l = 175', σ = 760 mhos/m, t > 1.2 ft, d ≑ 9 ft.

As for t, it is expected to be almost five times the above value, from the fact that $H(l/s)^3$ should be 1.25 times the matched value and a relatively good conductor is indicated from Fig. 35. From the model work, when we vary the thickness of a good conductor (aluminum) by a factor of five, the value of $H(l/s)^3$ changes by 1.2, while a poorer conductor (stainless steel) changes $H(l/s)^3$ by a factor of 2.2 for the same change of thickness. Then, $t \doteqdot 6$ ft and $\sigma t \doteqdot 1370$ mhos.

From the vertical pseudo section in Fig. 36, θ is estimated to be about $70°$.

Finally, the interpretation of the anomaly A is as follows:

$l = 175'$, $\sigma = 760$ mhos/m, $t \doteqdot 6$ ft, $d = 9$ ft, $\theta \doteqdot 70°$ and $\sigma t = 1{,}370$ mhos.

From the two profiles in Fig. 35, the one at 100 ft separation and the other at 200 ft separation, it is possible to get two results from anomaly A by the conventional interpretation technique in which the characteristic curves of Strangway are employed.

For 100' separation, θ may not be defined, because the right hand side shoulder of anomaly A is not only due to the anomaly A but also to anomaly B. When θ is assumed to be $60°$, since the assumed dip angle is close to the estimated one from the vertical pseudo section, $\sigma\mu\omega s t = 53$ and $d \doteqdot 0.19s$, because $Re)_{max}$ = -36%, $Im)_{max}$ = -8 %. Then d ≑ 19 ft and σt = 129 mhos. If the thickness t is assumed to be the difference between the separation of zeros in the profile and the separation of coils (p 556, Grant & West, 1965), t ≑ 30 ft so that σ ≑ 14 mhos/m.

For 200' separation, θ may not be defined for the same reason as above. When θ is assumed to be 60°, $\sigma\mu\omega st$ = 35 and d ≪ 0.1s, because $Re)_{max}$ = -60 %, $Im)_{max}$ = -26 %. Then, d ≪ 20 ft and σt = 46 mhos. Using the same method as for 100' separation, t ≑ 60 ft and σ = 2.6 mhos/m.

From the above two results, the averages are: d ≪ 20 ft, σt ≑ 88 mhos, t ≑ 45 ft and σ ≑ 8 mhos/m.

Comparing the results obtained by the conventional interpretation with those using the present technique, θ is not well defined by the former method, but by the latter method, some estimate may be made from vertical pseudo section. There are large differences in the values of σt, t and d, since the conventional method gives larger values of t and d, but smaller value of σt than the present method. Therefore, the conventional method indicates that the conductor is of rather low conductivity and is considerably wider ($t \doteqdot 45$ ft), while the method described in this thesis shows the conductor is of good conductivity and thin.

For anomaly B, when the technique described in this thesis is aporlied in the same fashion as for anomaly A, the results are;

$l = 83$ ft, $\sigma \doteqdot 780$ mhos/m, $d \doteqdot 25$ ft, $t \doteqdot 11$ ft and $\sigma t = 2{,}600$ mhos. θ is estimated from the vertical pseudo section to be about $80°$.

From the horizontal profiles, θ may not be defined for the same reason as for anomalv A, that the left hand side shoulder of the anomaly B is not only due to the anomaly B but also the anomaly A. Using the characteristic curves of Strangwav, for 100' separation, $\sigma\mu\omega st = 20$ and $d < 0.1s$.

Then, $\sigma t = 53$ mhos, $d < 10$ ft, $t \doteqdot 140'$ and $\sigma \doteqdot 1$ mho/m,

and for 200' separation, $\sigma\mu\omega t = 25$ and $d < 0.1s$, so that $\sigma t = 33$ mhos, $d < 20$ ft, $t \doteqdot 60$ ft and $\sigma = 2$ mhos/m.

When these are averaged, $d < 15$ ft, $\sigma t = 43$ mhos, t = 100', so that σ = 1 mho/m.

Comparing these results with those at the top of page 78, there are also large differences in the values of σt, t and d in the two results, that indicate the same characteristics as for anomaly A in σ, σt and t. However, the d value appears larger in the present method than in the conventional one for this anomaly.

When we consider the mineralization exposed in the trench(TR-2-70) at 600E (Fig. 37), we find that;
$\theta = 60^\circ - 70^\circ$, d ≃ 5 - 6 ft, t = 2 - 3 ft with massive sulphide mineralization of pyrite and pyrhotite (50 - 60 %). The method described in this thesis gives better values of t but d is too large.

In addition, S.P. anomalies are not coincident with the locations indicated by the vertical pseudo section (Fig. 36) but one of the S.P. anomalies (600E) coincides with the trench.

b) L - 30S

The results on this line were obtained with the VHEM unit and coil-separations 100', 200' and 300', and the data are displayed in the horizontal profiles of Figs. 38 - 40. Again, the data are plotted in vertical pseudo section in Fig. 41. Two anomalies labelled "A" and "B" appear at 560W and 100W in Fig. 41, while the locations of the peaks of EM anomalies vary from separation to separation. Furthermore, the dip angles appear to be steep in Fig. 41. The anomaly A is assumed to be composed of two adjacent conductors, located at 600W and 500W, respectively.

Applying the same technique as described in the preceding, we have obtained the following results; Ref. Fig. 41 and Fig. 42.

Anomaly	l	σ (mhos/m)	d	t	σt (mhos)	θ
A - 1	330'	110	20'	5'	170	70°
A - 2	120'	270	40'	3'	290	90°
B	50'	860	40'	10'	2600	70°

However, the anomalies A-1 and A-2 are not independent but affected by each other. Then, the interpretation of the

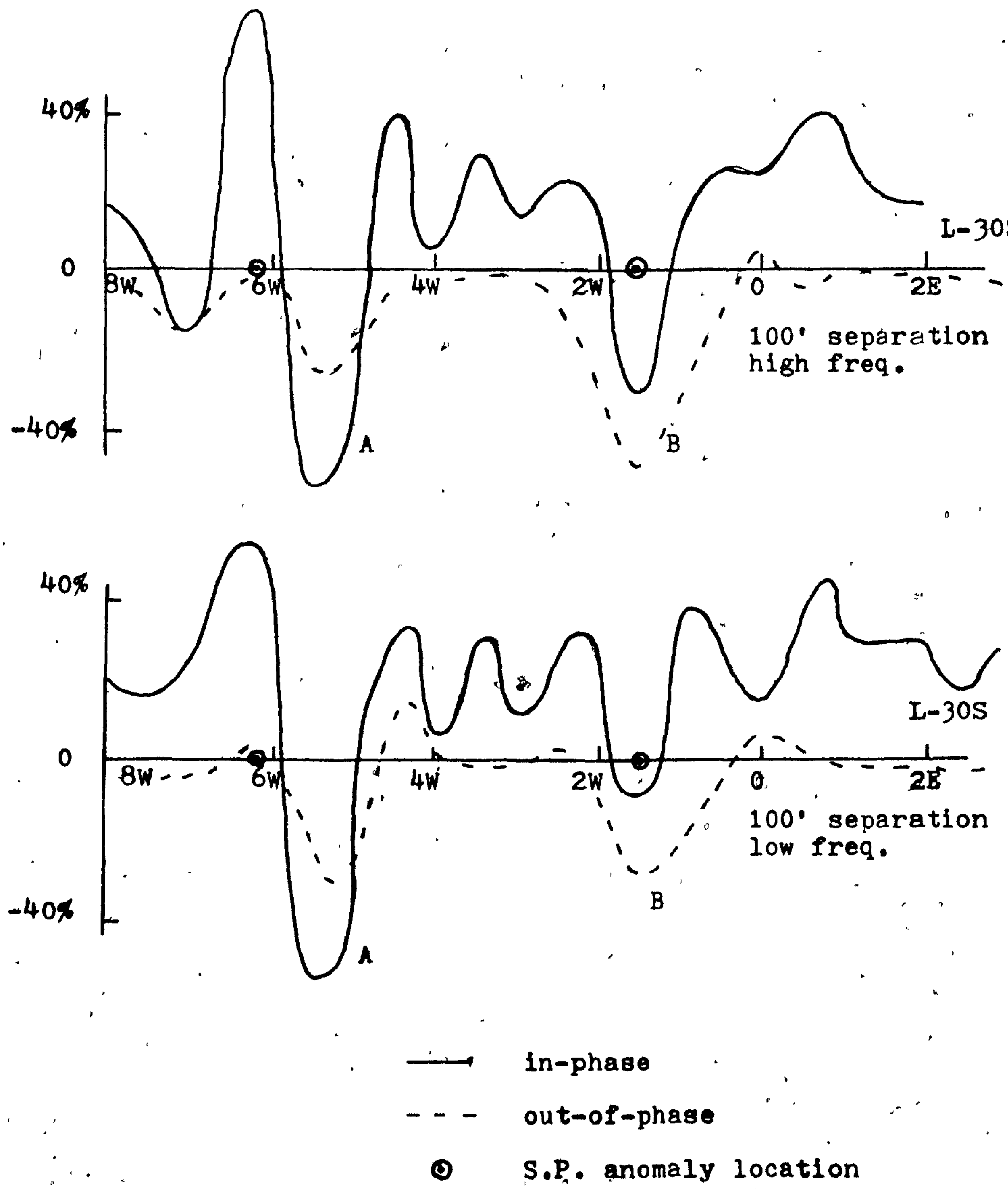

Scale 1" = 200'

Fig. 38. Horizontal Loop Profiles of L-30S (I)

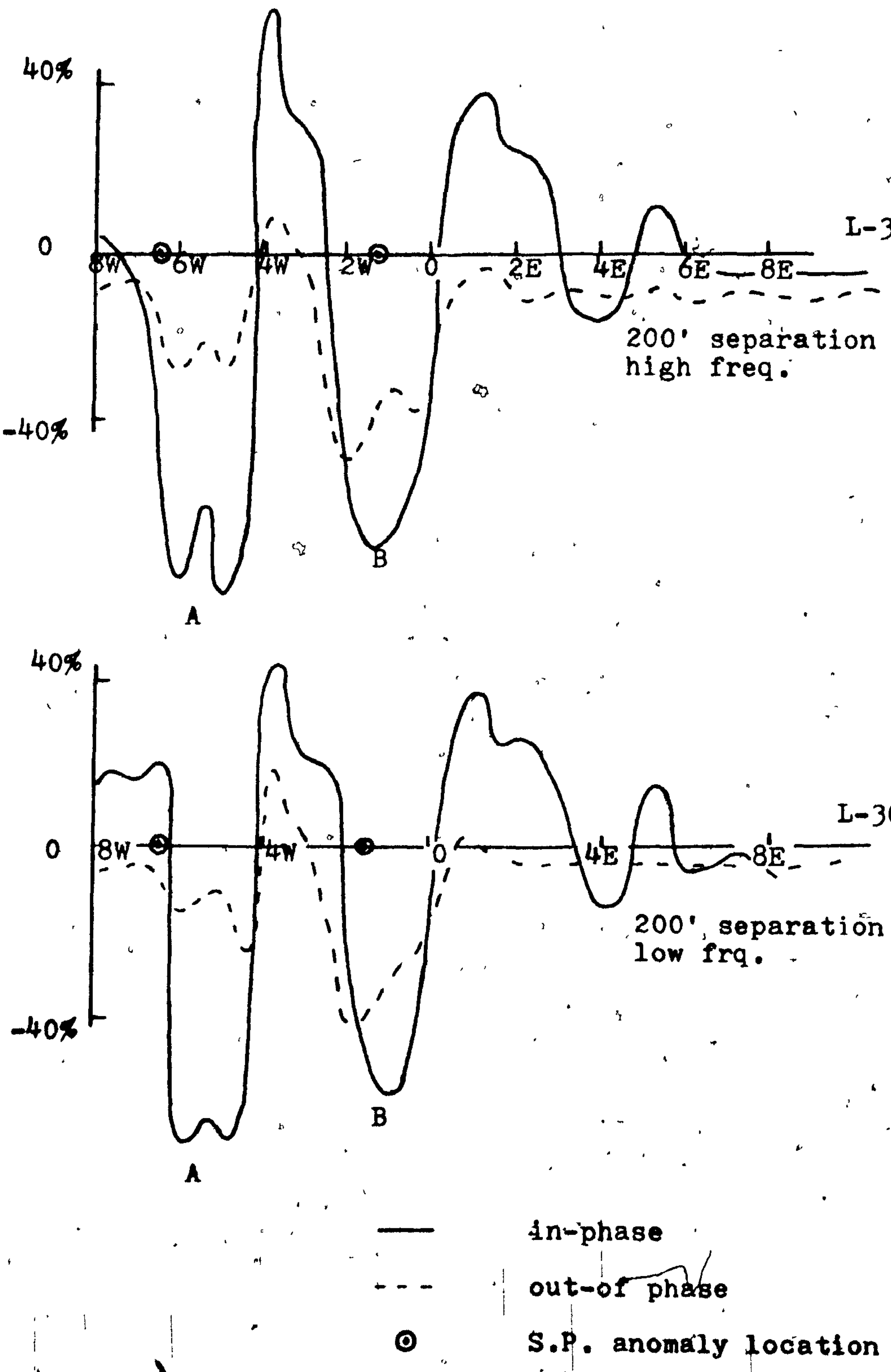

Scale 1" = 400'

Fig. 39. Horizontal Loop Profiles of L-30S (II)

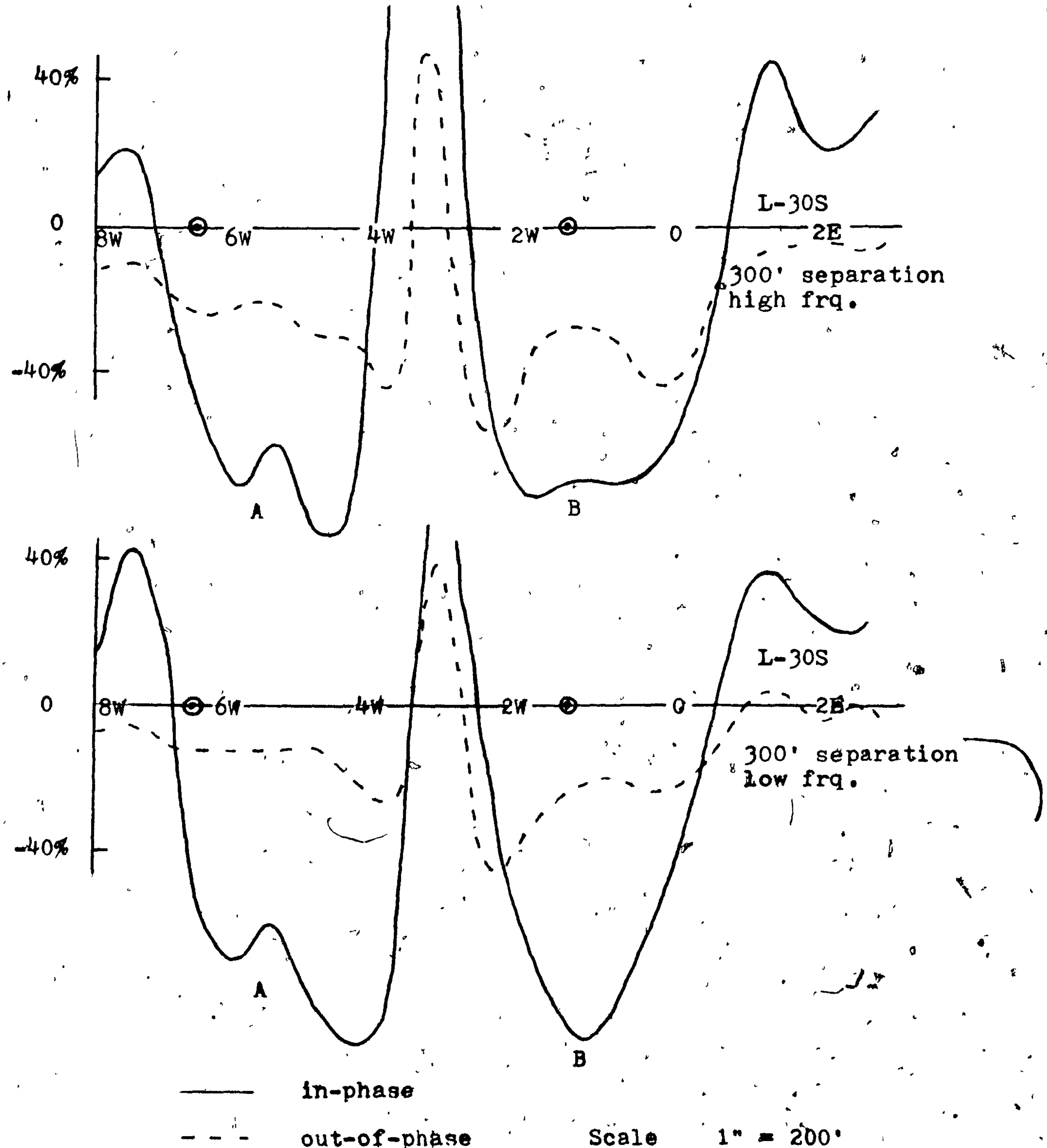

Fig. 40. Horizontal Loop Profiles of L-30S (III)

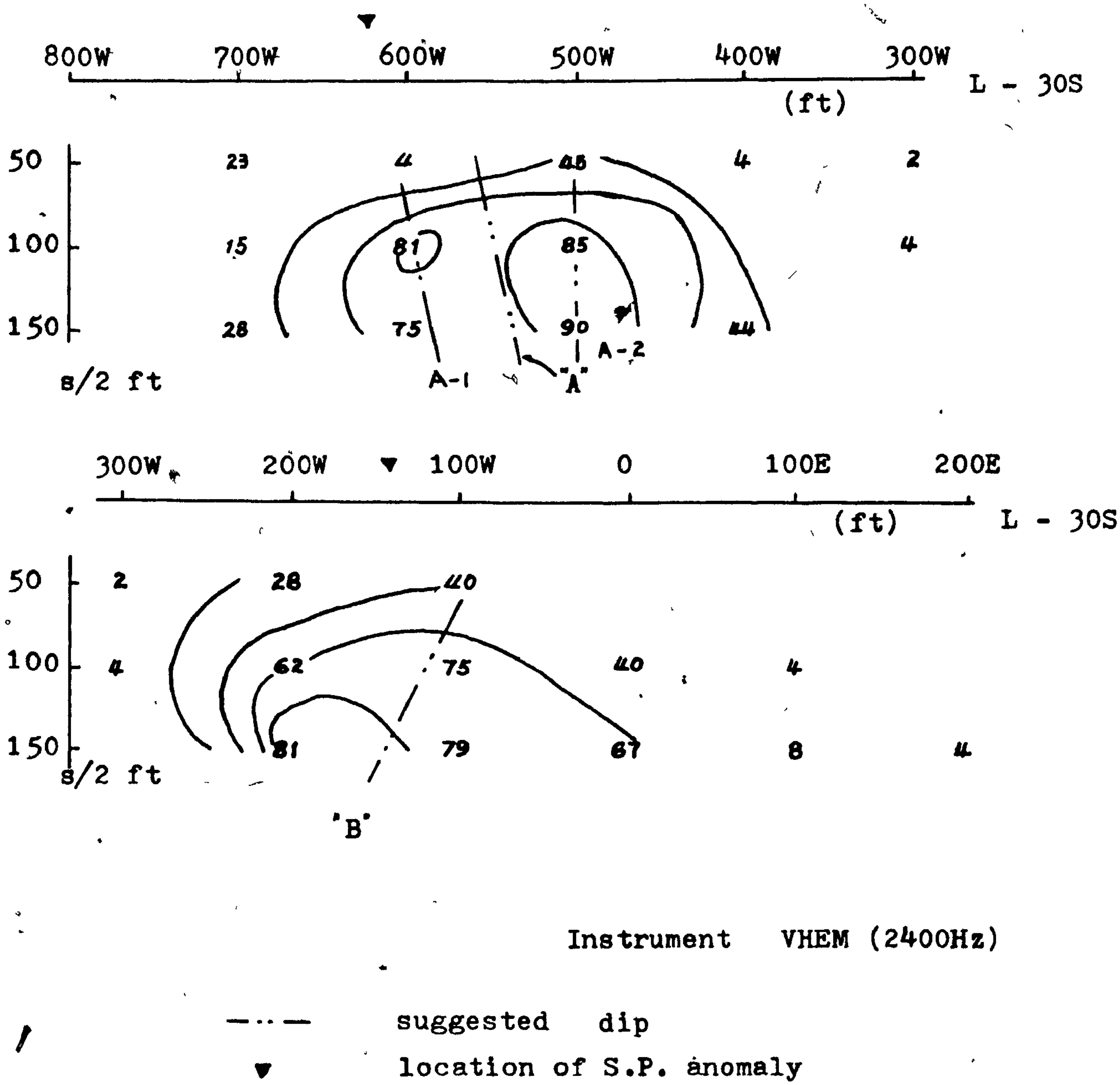

Fig. 41. Vertical pseudo section of Hicks Island (II)

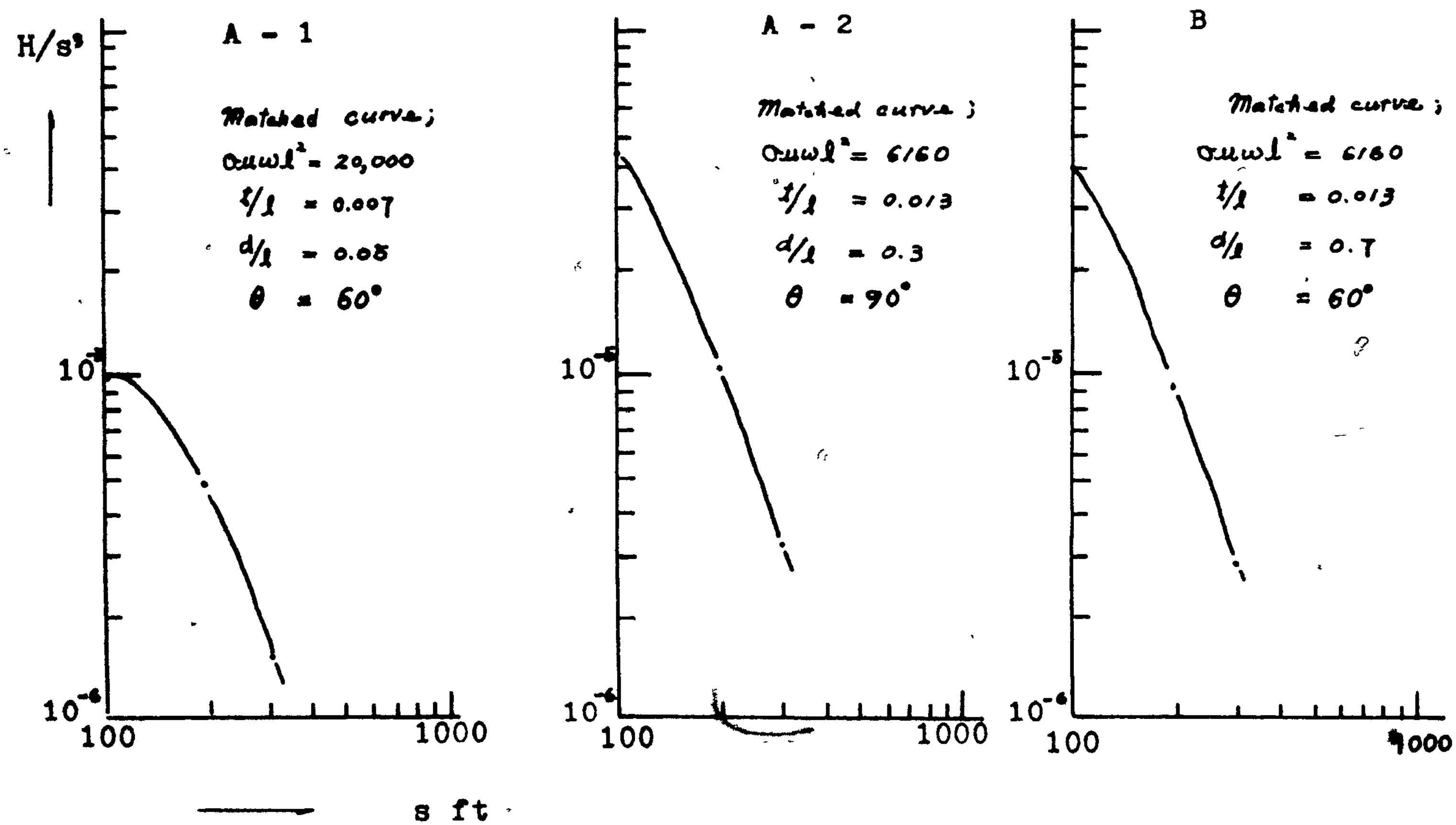

Fig. 42. H/s^3 - s curves of Hicks Island (II)

anomalies is likely to be different from the case in which the conductors are far apart.

An attempt was made to combine anomalies A-1 and A-2 as indicated by the center hatched line in Fig. 41. Then, the following results are obtained by averaging the two anomalies:

$l = 230$ ft, $\sigma \doteqdot 190$ mhos/m, $d \doteqdot 30$ ft, $t \doteqdot 4$ ft,

$\sigma t = 230$ mhos and $\theta \doteqdot 80$.

Using the conventional characteristic curves of Strangway with the horizontal profiles for anomaly A, θ is assumed to be 90°, because it is not defined by the conventional method due to complexities of the curves in the horizontal profiles, while the vertical pseudo section estimates $\theta = 90°$, and the other parameters are found as follows:

s(ft)	f (Hz)	$Re)_{max}$	$Im)_{max}$	[illegible]	d (ft)	σt (mhos)	t (ft)	σ (mhos/m)
100	2400	-60%	-32%	15	<10	26	10	5
	600	-68	-28	20	<10	140	10	50
200	2400	-80	-28	<53	<20	<46	120	<1
	600	-68	-24	30	<20	105	thin	
300	2400	-84	-44	<53	<30	<31	thin	
	600	-92	-28	<53	<30	<123	40	<10

In making the above table, some values of $\sigma\mu\omega st$ and all d are not well defined, because the values of $Re)_{max}$ and $Im)_{max}$ fall beyond the scales of the characteristic curves. Thus, the values of σt are not well defined. Although some of them are estimated, the variation of the σt values with frequency is large. Also, the variation of t values with separation is large. Furthermore, the values of σ are very low, since the ratios of $(Re/Im)_{max}$ are generally small.

Taking an average of six calculations from the above list -- two frequencies at each of three spacings -- one obtains as followings;

d $\ll$ 20 ft, $\sigma t < 79$ mhos, t $\doteqdot$ 30 ft, so that $\sigma < 9$ mhos/m.

For anomaly B, the conventional characteristic curves show the following results. θ is assumed to be 60° from the vertical pseudo section, because the dip angle may not be defined from the profiles due to complexity of the shoulder of the anomaly.

s(ft)	f(Hz)	$Re)_{max}$	$Im)_{max}$	$\sigma\mu\omega st$	d(ft)	σt(mhos)	t(ft)	σ(mhos/m)
100	2400	-52%	-48%	< 5	<10	<10	20	< 2
	600	-40	-32	10	<10	70	thin	
200	2400	-68	-48	<15	<20	<13	30	
	600	-60	-40	<53	<20	<185	20	<30
300	2400	-74	-56	<15	<30	<10	60	< 1
	600	-92	-48	<15	<30	<35	30	< 4

Like anomaly A, most estimates of $\sigma\mu\omega st$ and d are very crude, because the values of $Re)_{max}$ and $Im)_{max}$ are plotted beyond the scales of the characteristic curves. Therefore, the table shows that the values of σt, t and σ are not well defined.

Taking an average of six calculations for anomaly B in the same fashion as shown for anomaly A; $d < 20$ ft, $\sigma t < 52$ mhos and $t \doteq 30$ ft, so that $\sigma < 6$ mhos/m.

For both anomalies, A and B, comparing these results with the ones from the matching method, the former results gives smaller values in d, σt and σ but larger value in t than the latter ones. Thus, the conventional method indicates a conductor of poor conductivity and large width near the surface, while the method described in this thesis shows a very thin conductor of reasonably good conductivity which is buried at a depth of 40 ft.

Two S.P. anomalies are located at 620W and 150W, respectively. These locations are almost coincident with EM anomalies as indicated on the vertical pseudo section. The S.P. anomaly at 620W corresponded to anomaly A-1 but the anomaly A-2 does not show up in the S.P. survey.

B. Uranium Valley (Nemeiben Lake)

1) Location and general geology

The survey area is located at coordinates 55 degrees 20 minutes north and 105 degrees 23 minutes west, north of Nemeiben Lake, Saskatchewan. This area is 20 miles northeast of La Ronge and readily accessible from the air-base there. (Fig. 43)

The survey area is mainly composed of coarse-grained feldspathic quartz-biotite gneiss, probably derived from the sediments and volcanic rocks of the Wekusko group in which garnet commonly occurs. These gneisses are light grey to black and for the most part occur in alternate bands of fine grained (usually dark) and coarser grained (light) materials. (Fig. 44)

2) Geophysical results

The results measured by EM 17 with four coil separations

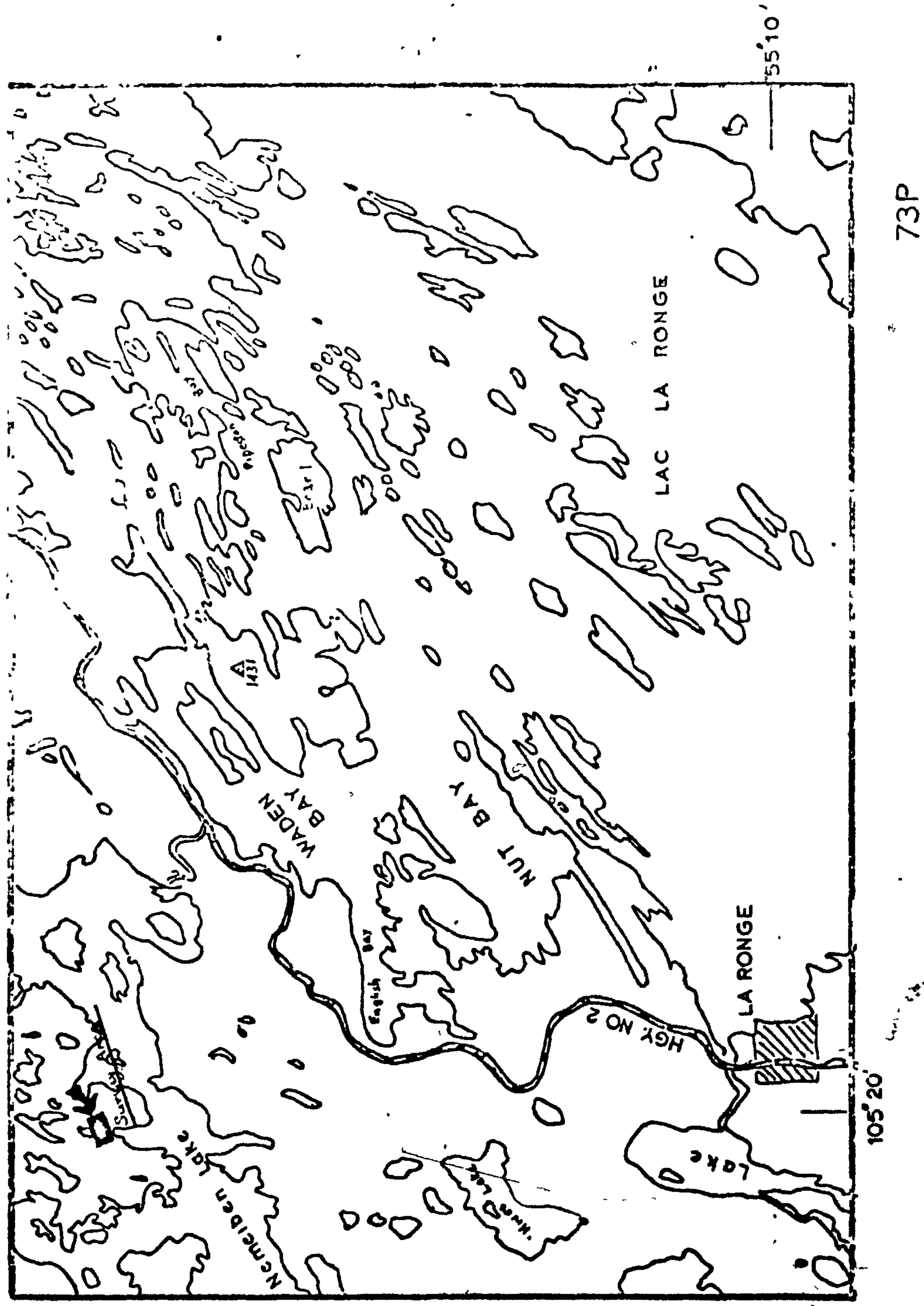

Scale 1 : 400,000

Fig. 43. Location map of Uranium Valley

GEOLOGICAL MAP

Scale

1" = 6.4 miles

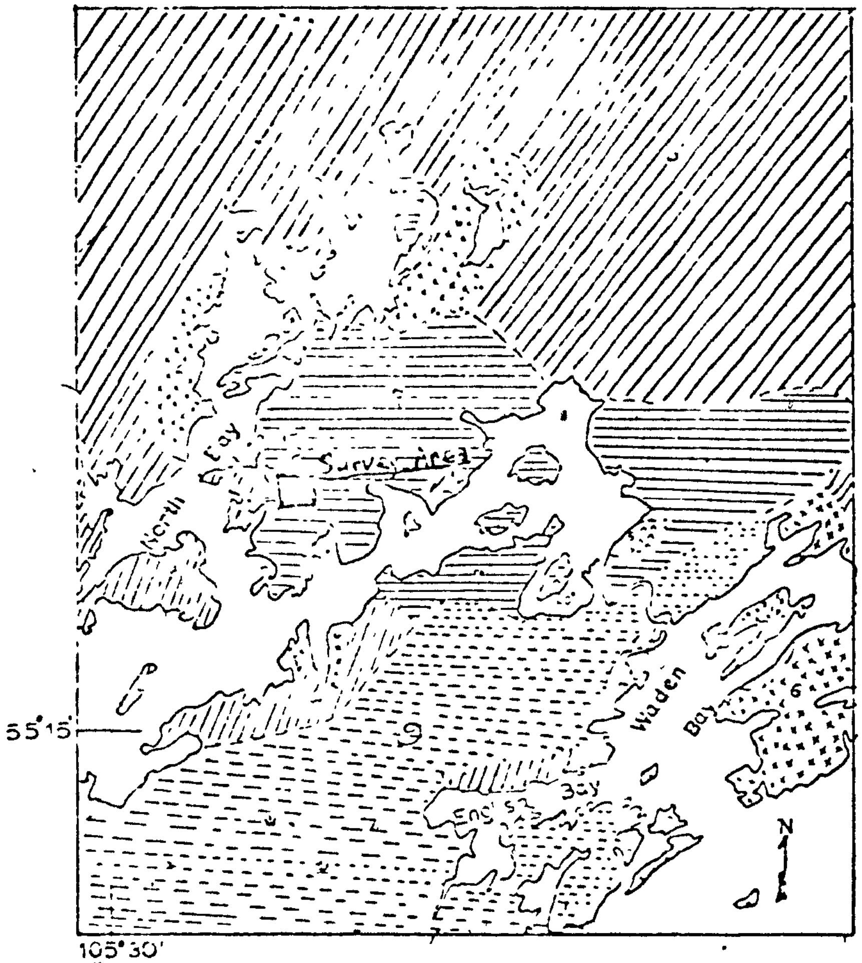

LEGEND

5	Diorite, gabbro, pyroxenite, peridotite
6	Pegmatitic granite, granite, syenite, granodiorite, diorite.
7	Quartz-biotite schist and gneiss, quartz-hornblende schist and gneiss, garnetiferous schist and gneiss probably altered Wekusko group strata.
8	Schist and gneiss (probably altered Wekusko group strata) intimately invaded by granite, aplite, pegmatite, etc.
9	Recent alluvium and glacial deposits.

Fig. 44 Geological map of Uranium Valley

on the traverse line 28S are represented in the profiles of Fig. 45 and vertical pseudo sections of Fig. 46, which reveal three anomalies, at 200E, 400E and 900E. The first two, however, are very weak. The strong anomaly at 900E is analyzed in Fig. 47 in the same fashion as the previous areas.

Considering the vertical pseudo section, the dip angle of the suspected conductor is nearly vertical. By means of the matching method mentioned previously, the final results of interpretation are as follows:

$l \doteqdot 330$ ft, $d \doteqdot 50$ ft, $\sigma \doteqdot 18$ mhos/m, $t \doteqdot 10$ ft, $\sigma t \doteqdot 55$ mhos and $\theta \doteqdot 80°$.

The relative conductivities estimated from the ratios of in-phase to out-of-phase amplitudes for three coi-separations are listed below:

s	Relative conductivity
200 ft	0.45
300 ft	0.63
400 ft	0.46

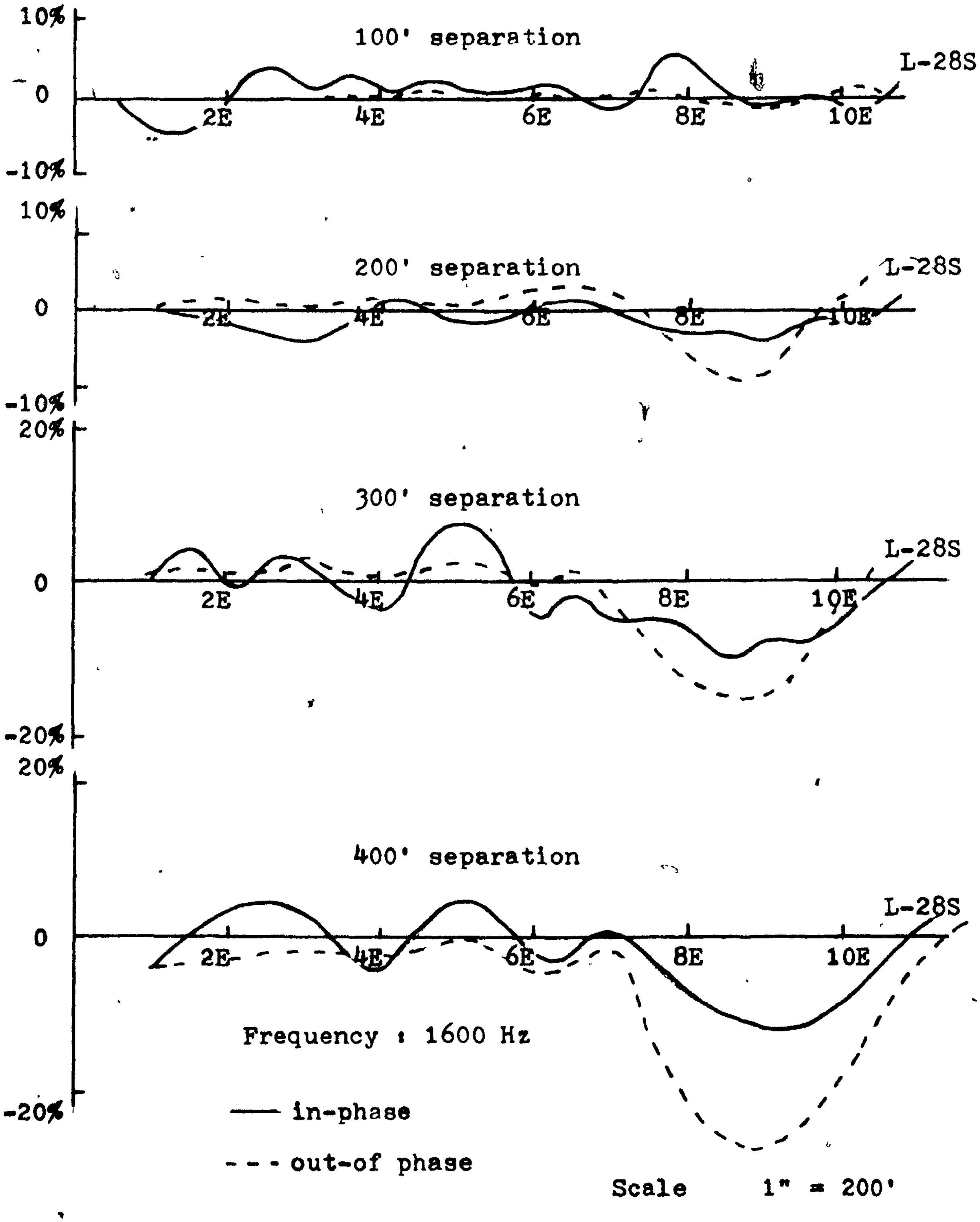

Fig. 45. Horizontal Loop Profiles of Uranium Valley

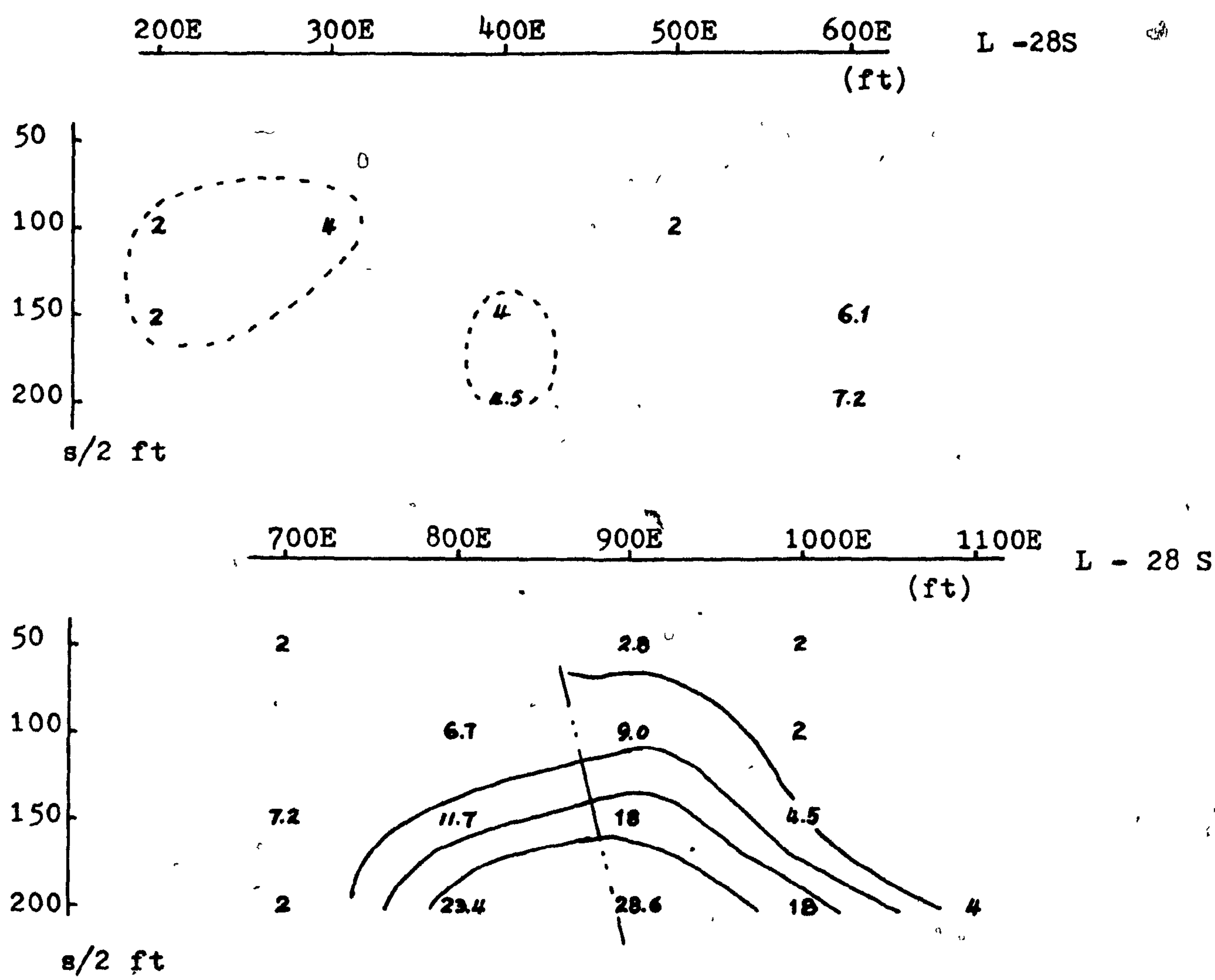

Instrument EM 17 (1600 Hz)

— -- — suggested dip

Fig. 46. Vertical pseudo section of Uranium Valley

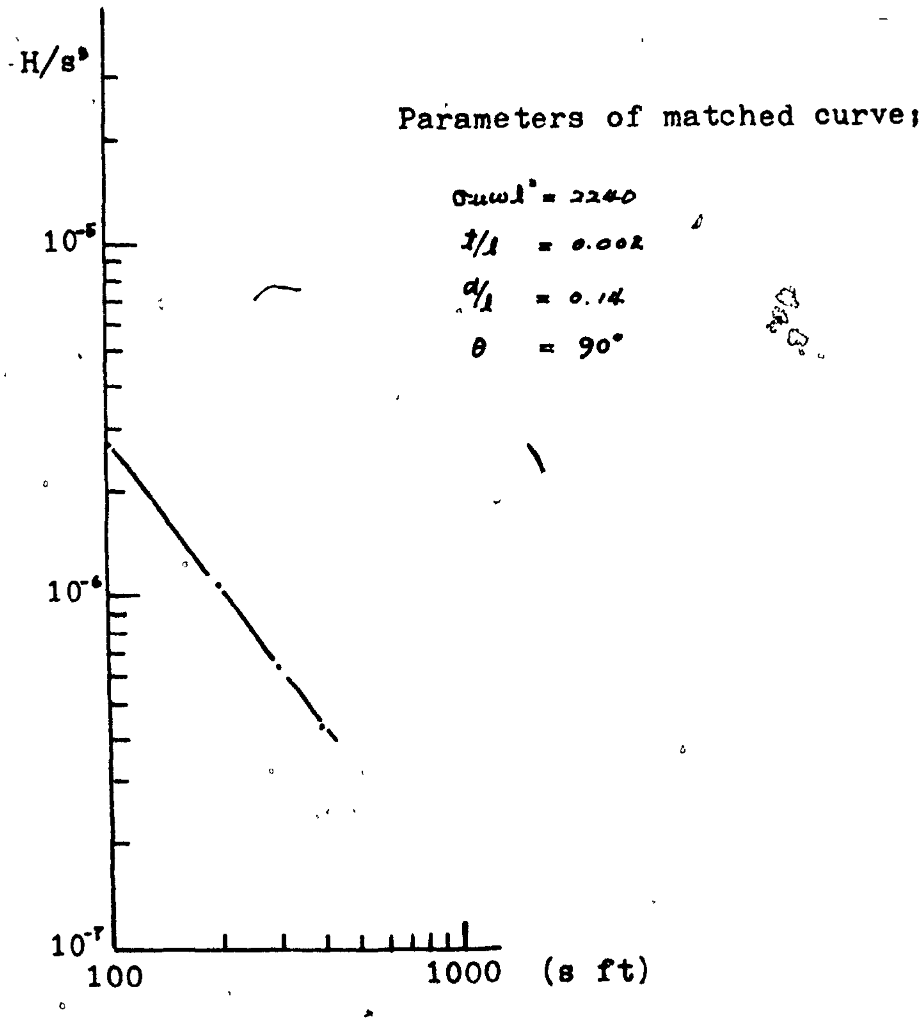

Fig. 47. H/s^3 - s curves of Uranium Valley

Clearly the ratios show that the suspected conductor is of low conductivity.

With the conventional interpretation technique which was used before, the following results are obtained:

f(Hz)	s(ft)	d(ft)	$\sigma\mu\omega st$	σt(mhos)	t(ft)	σ(mhos/m)
1600	200	20	1.5	2.0	160	0.04
	300	30	3.0	3.0	200	0.05
	400	40	3.0	2.0	thin	

The average value of t by the conventional method is about 120 ft, while the new method gives t = 10 ft. Compared to the results obtained by drilling, the latter value of t is reasonable. According to the results of the drill-hole (Fig. 48), a disseminated mineralization of chalcopyrite and pyrite is encountered at a depth of 120 ft and of about 10 ft thickness.

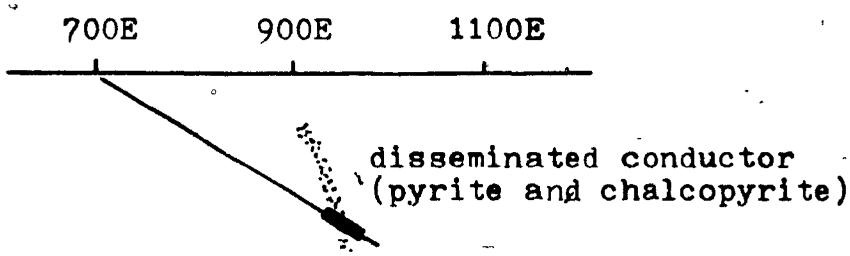

Fig. 48. Result of drill hole D.D.H. No. 5

C. Demers Creek

1) Introduction

The survey area is located on the boundary between Ham Township and Wolfe Township, Quebec and its geographic coordinates are 71° 39' W longitude and 45° 55' N latitude. (Fig. 49).

Previous work on the area included a geological survey and 9 drill holes by Trovsco Mines Ltd. in 1952. In that year, Koulomzine Geoffroy & Co. conducted magnetic and S.P. surveys for the same company. In 1964, Sullico Mines Ltd. carried out EM and magnetic surveys and in 1971, Jorex Syndicates made EM, geological and geochemical surveys.

It is reported that during the American Civil War, an open pit operation for copper had been conducted at the place where Demers Creek flows now, north along the creek from the survey area. However, there is no specific record of that mine operation. Due to this fact, several companies have tried to delineate copper bearing deposits in this vicinity.

According to available geological reports, this area is underlain mainly by Bennett schists of Cambrian age, which are composed of chlorite and sericite schists. (Fig. 50)

Fig.49 Location of the survey area

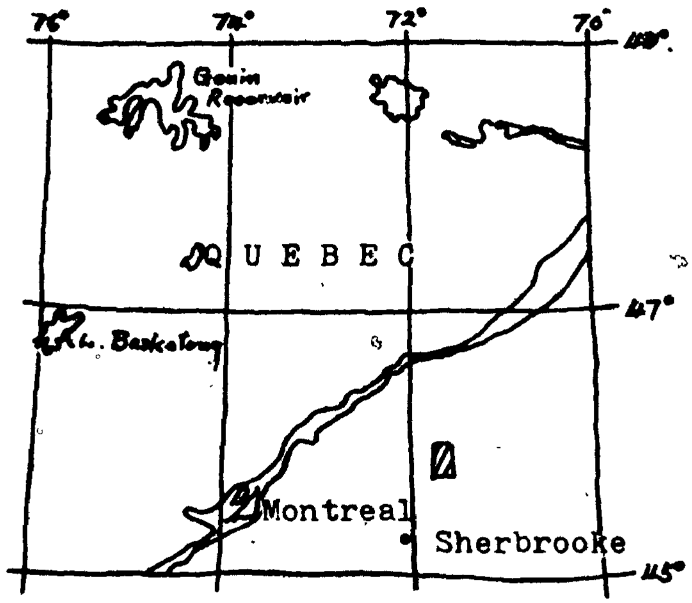

survey area

Scale 1" = 100 miles

Between the chlorite and the sericite schists, there are carbonate bands and dolomite, in which quartz veins and quartzite are interbedded. Such replacement might contain some chalcopyrite and bornite mineralization. In the schists, too, there is some interbedding of quartz and quartzite. It may be assumed that metamorphic-dynamic action has occurred by intrusion of peridotite or andesite which is the bedrock of this area.

Geophysical surveys, done earlier, showed EM anomalies at the contact between the schists and the carbonate or dolomite, and in the schists. The magnetic anomalies are produced by magnetites in the chlorite schist. A geochemical survey failed to outline significant copper anomalies. The drilling results, whose locations are shown in Fig. 50, however, indicated pyrite in the graphite schist and chalcopyrite and bornite in the dolomite.

2) Geophysical results

The results from L - 2E and L - 4E are displayed in Fig. 51 and Fig. 52 in profile form and the vertical pseudo sections are reproduced in Fig. 53. The data in the vertical pseudo sections are again analyzed by drawing the characteristic

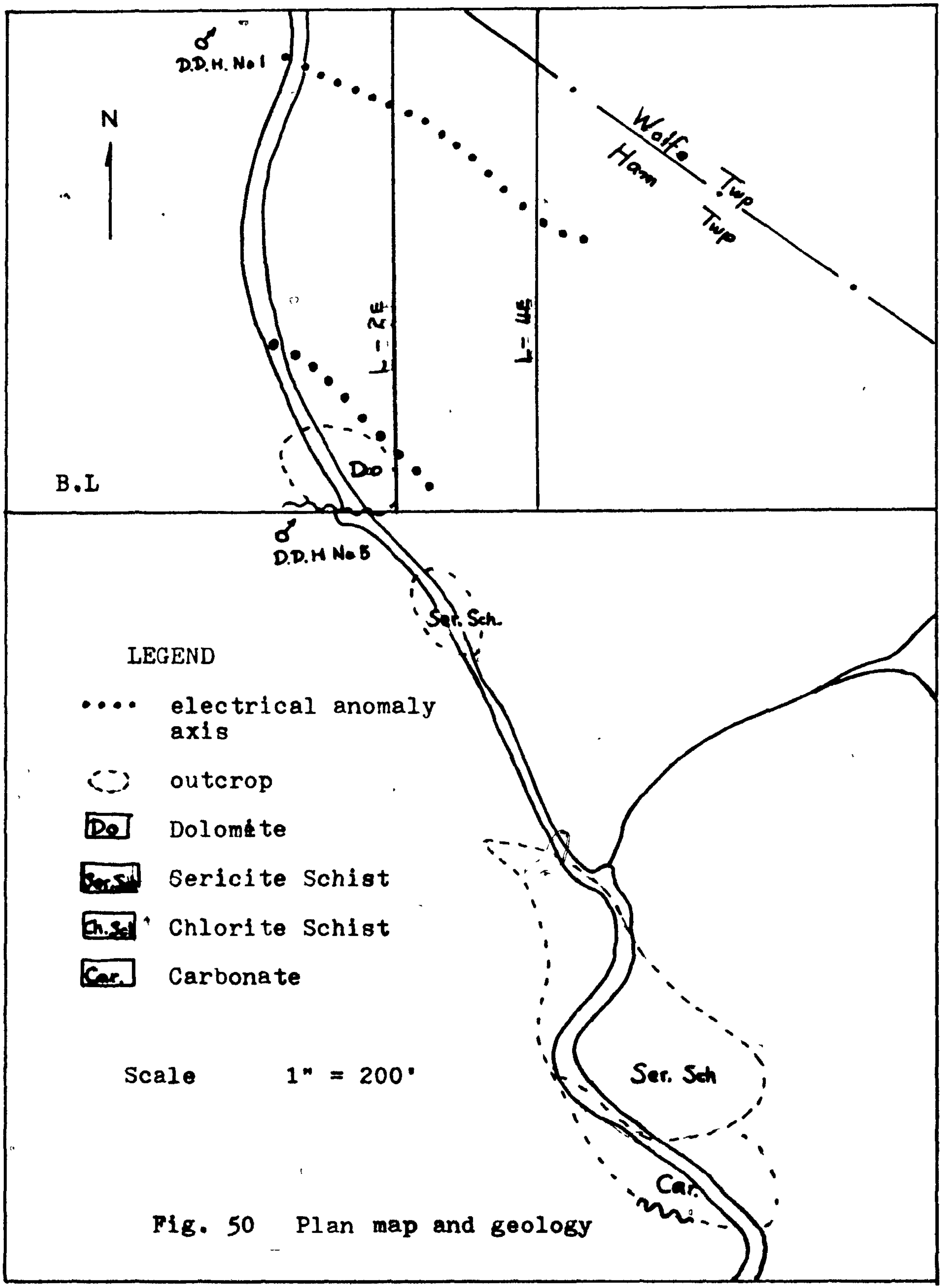

Fig. 50 Plan map and geology

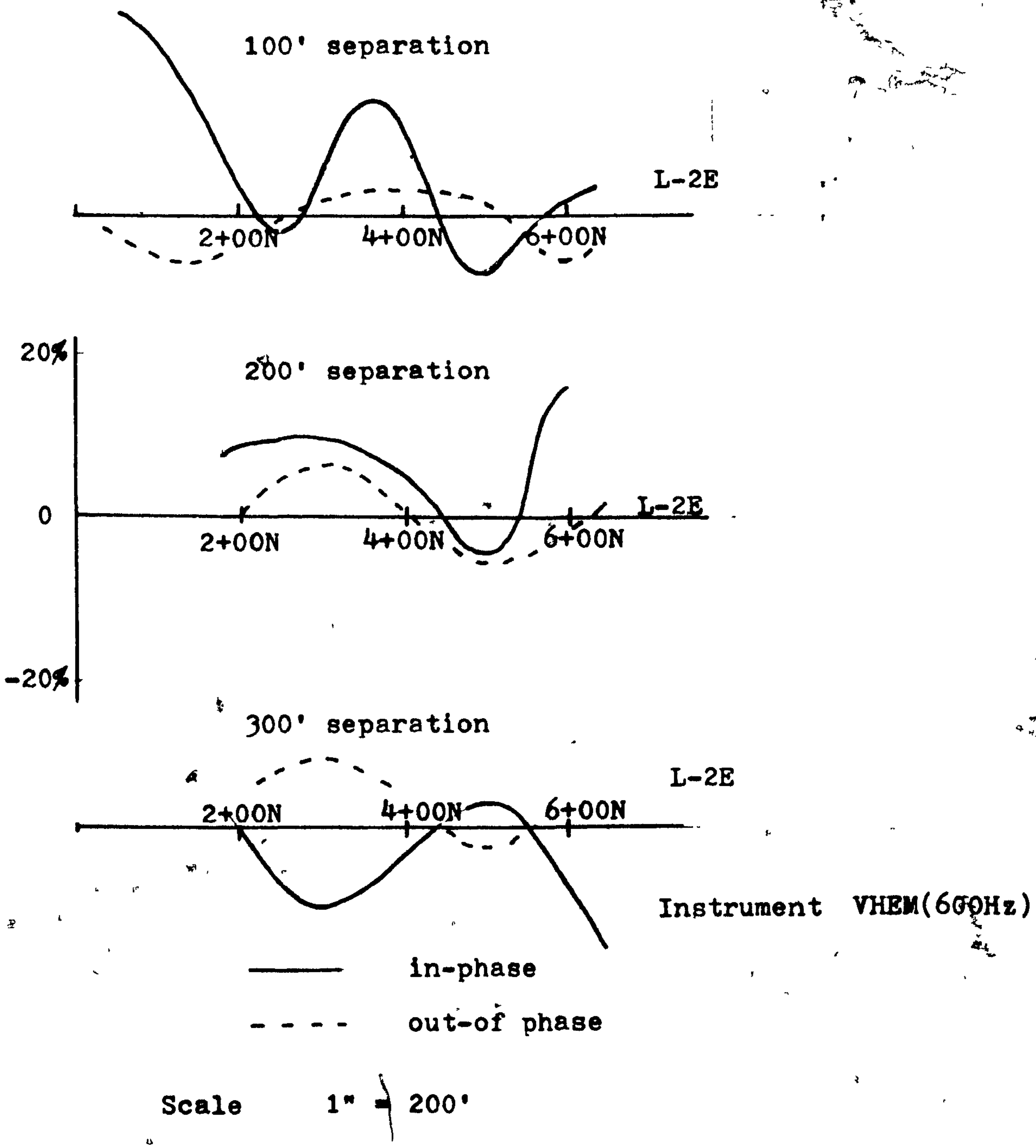

Fig. 51. Horizontal Loop Profiles of Demers Creek (I)

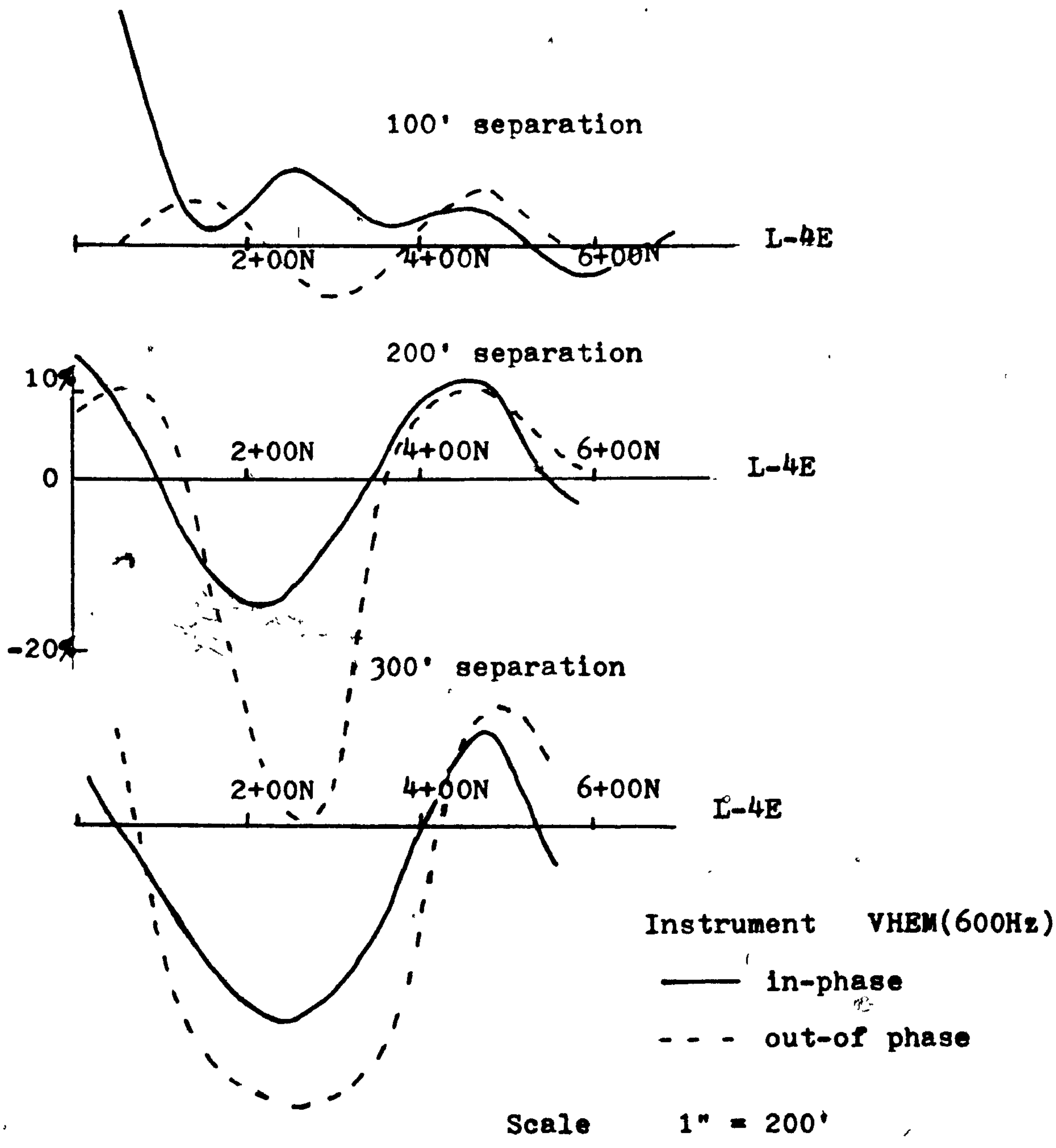

Fig. 52. Horizontal Loop Profiles of Demers Creek (II)

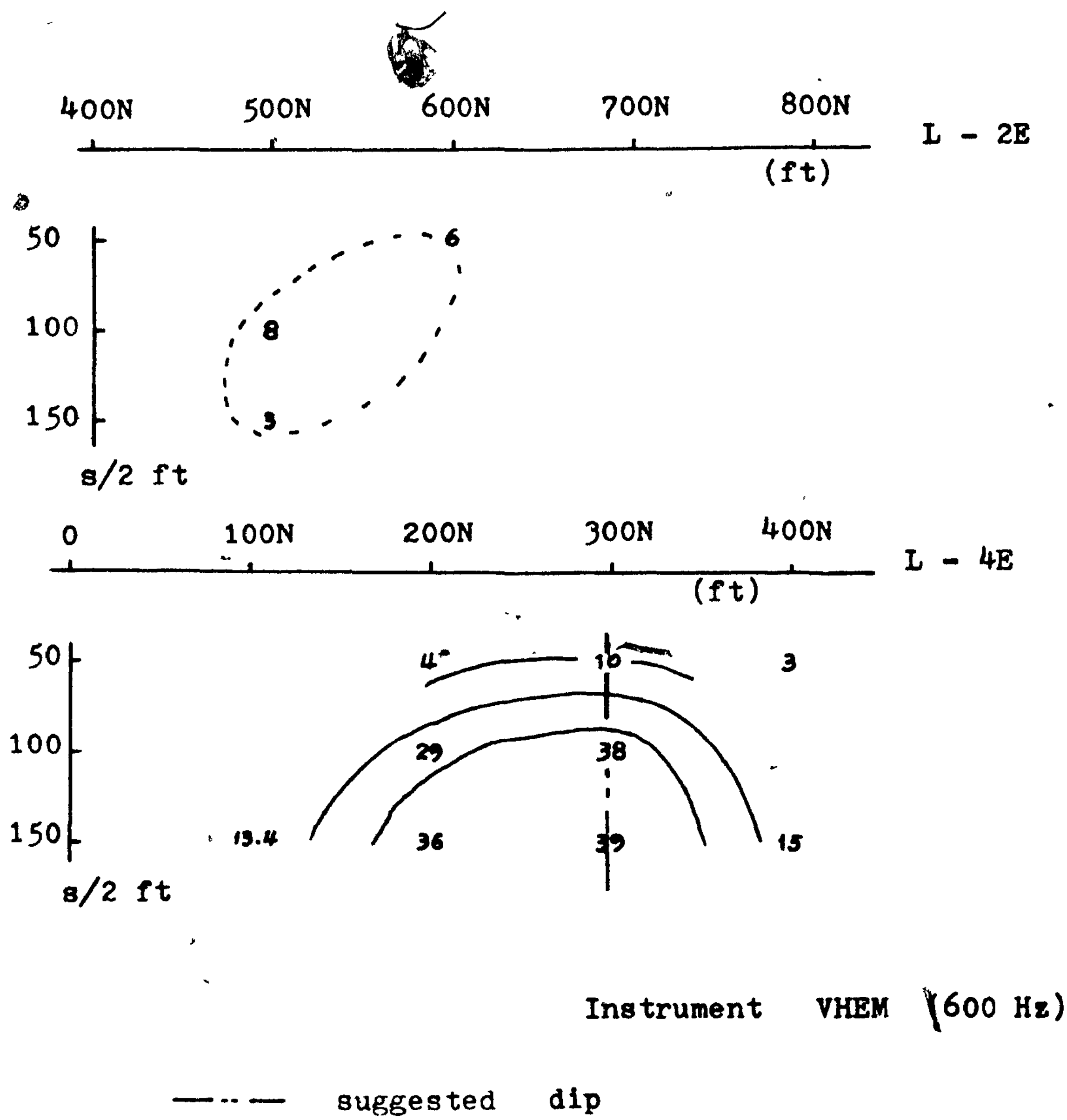

Fig. 53. Vertical pseudo sections of Demers Creek

curves for H/s^3 and s, shown in Fig. 54.

In the horizontal profiles, the anomaly on L - 2E is not distinguishable and it is probably caused by topography and conducting overburden, although it would be attractive to assume that it correlated with the neighboring anomaly on L - 4E. However, the anomly in L - 2E provides only one point in the characteristic curve H/s^3 - s which can be matched with any of the characteristic curves from model work and indicates small value of $\sigma\mu\omega l^2$. Therefore, the anomaly seems to be caused by either an extremely poor conductor or a very small one.

On L - 4E, the anomaly may be matched to a characteristic curve to give the following:

$l \doteqdot 160$ ft, $\sigma = 550$ mhos/m, $t \doteqdot 10$ ft, $d \doteqdot 20$ ft, $\sigma t = 1830$ mhos and $\theta = 90°$.

In order to compare the above results with those obtained from the conventional technique, the data in the horizontal profile of L - 4E are interpreted, using a phasor diagram for $\theta = 90°$, since the positive parts in the horizontal profiles show a steep dip angle. The results are as follows:

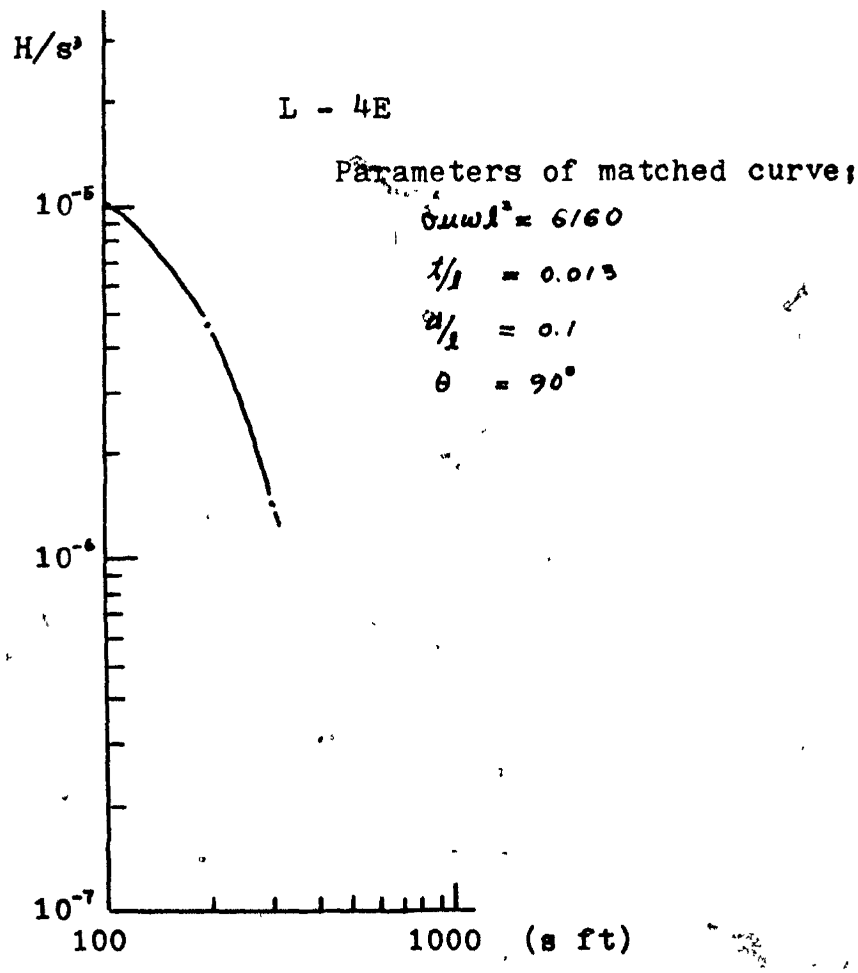

Fig. 54. H/s³ - s curve of Demers Creek

results are as follows:

f(Hz)	s(ft)	θ	d(ft)	$\sigma\mu\omega s t$	σt (mhos)	t(ft)	σ (mhos/m)
600	100	N.D.					
	200	90°	<20	3.0	1	50	0.07
	300	N.D	<30	4.0	1	60	0.06

Taking an average from the above list,

$d < 25$ ft, $t \doteqdot 55$ ft, $\sigma t = 1$ mhos, $\sigma \doteqdot 0.06$ mhos/m and $\theta = 90°$.

Comparing the results of the two methods, it is found that there are reasonable agreement in the values of d and θ but there are large differences in the values of t and σ, that the new method gives larger conductivity and smaller thickness, as usual, while the conventional method shows negligible conductivity and large thickness. Consequently the conventional method indicates extremely small values of σt, compared with the value from the new method.

For reference, the results from D.D.H. No.1, located in Fig. 50, carried out by Troysco Mines Ltd. in 1952 showed chalcopyrite and bornite mineralization, in small sections from 23' to 145' along the hole, which is inclined 45 degrees as indicated in the diagram.

Chapter 7. Application of the Method to Other Results

So far, the characteristic curves from the model work have been applied to the field results obtained by the author. In order to confirm the feasibility of the technique, it has also been applied to EM data from Cavendish, Ontario, Långsele and Kedträsk in Sweden. These results are described in the following.

1. Cavendish Township, Ontario

The results are a part of a case history which had been prepared by the staff of McPhar Geophysics Ltd. for the Canadian Centennial Conference on Mining and Groundwater Geophysics, 1967.

The test site is located in Cavendish Township, south of Gooderham, Ontario and approximately 100 miles northeast of Toronto.

The geology has been taken from the Ontario Department of Mines, Map No. 1957b. According to this map the grid area is underlain by Precambrian sediments consisting chiefly of crystalline limestones. The geologic trend is NNE and available dips are 60 to 65 degrees to the southeast, but no detailed subsurface information is available. Unfortunately, the area has not been thoroughly tested by drilling but one short vertical hole (i.e. about 50 ft) located near St. Croix Creek is reported to have intersected heavy sulphide mineralization.

The horizontal loop EM survey, which was operated at 600 Hz and three coil separations, 100', 200' and 300', produced the profiles which are shown in Fig. 55. From this data, the vertical pseudo section can be drawn as shown in Fig. 56, calculating the magnitude of the anomalous secondary field at the receiver. Applying the same method as before to the vertical pseudo section, the characteristic curve $H/s' - s$ is produced in Fig. 57, giving the following:

$l \doteqdot 310$ ft, $\sigma \doteqdot 3400$ mhos/m, $t \doteqdot 1$ ft, $d \doteqdot 6$ ft and $\sigma t = 1100$ mhos. θ is roughly $70°$ from the vertical pseudo section.

According to the conventional interpretation using the characteristic curve for $\theta = 60°$ (since the dip angle is not defined from the horizontal profiles because of

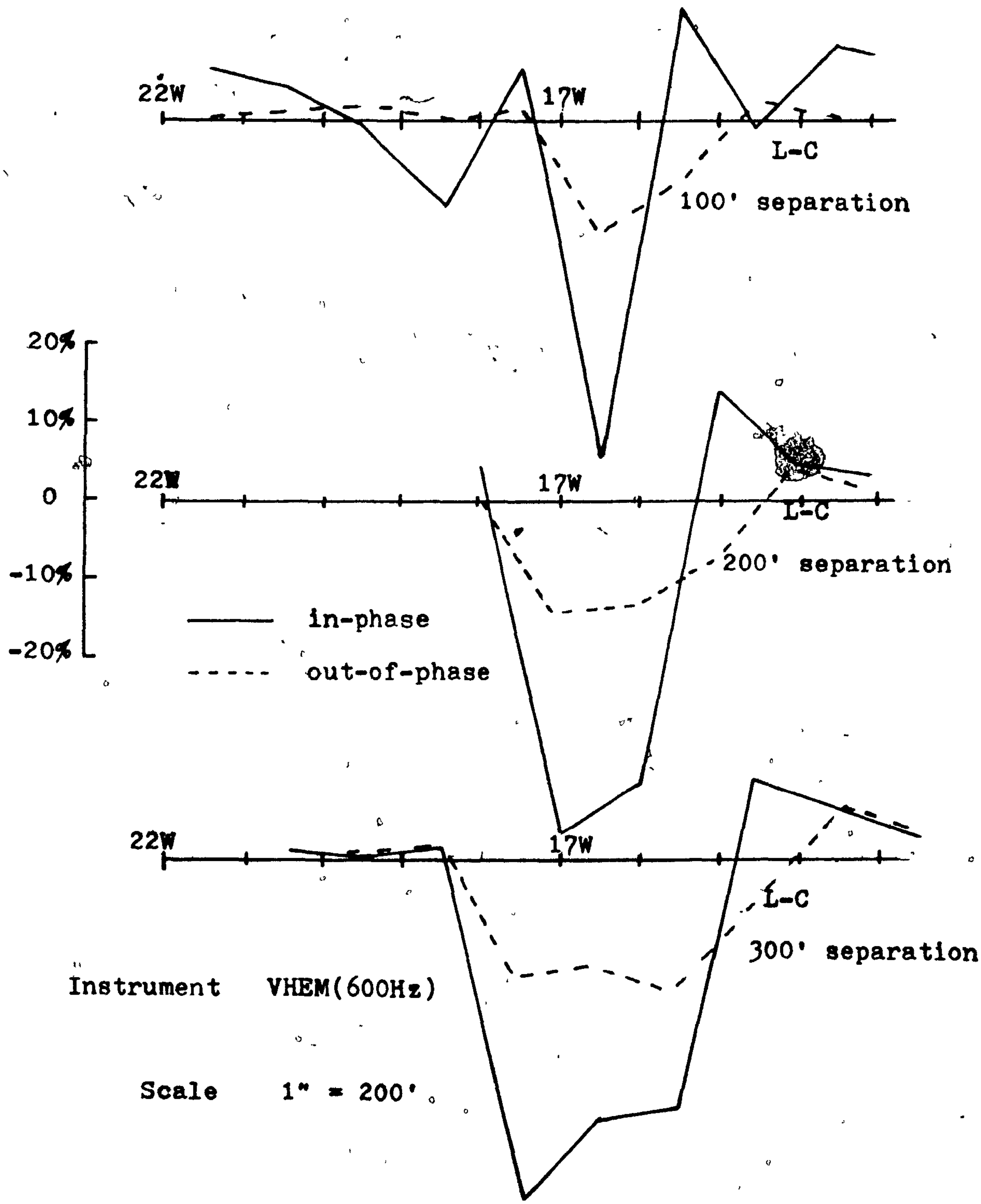

Fig. 55. Horizontal Loop Profiles, Cavendish Twp. Ont.

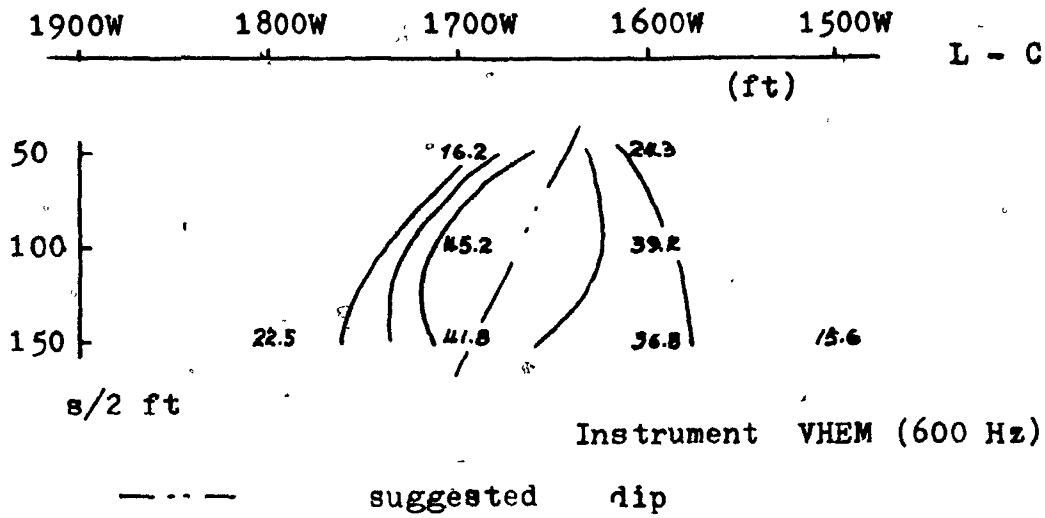

Fig. 56. Vertical pseudo section of Cavendish

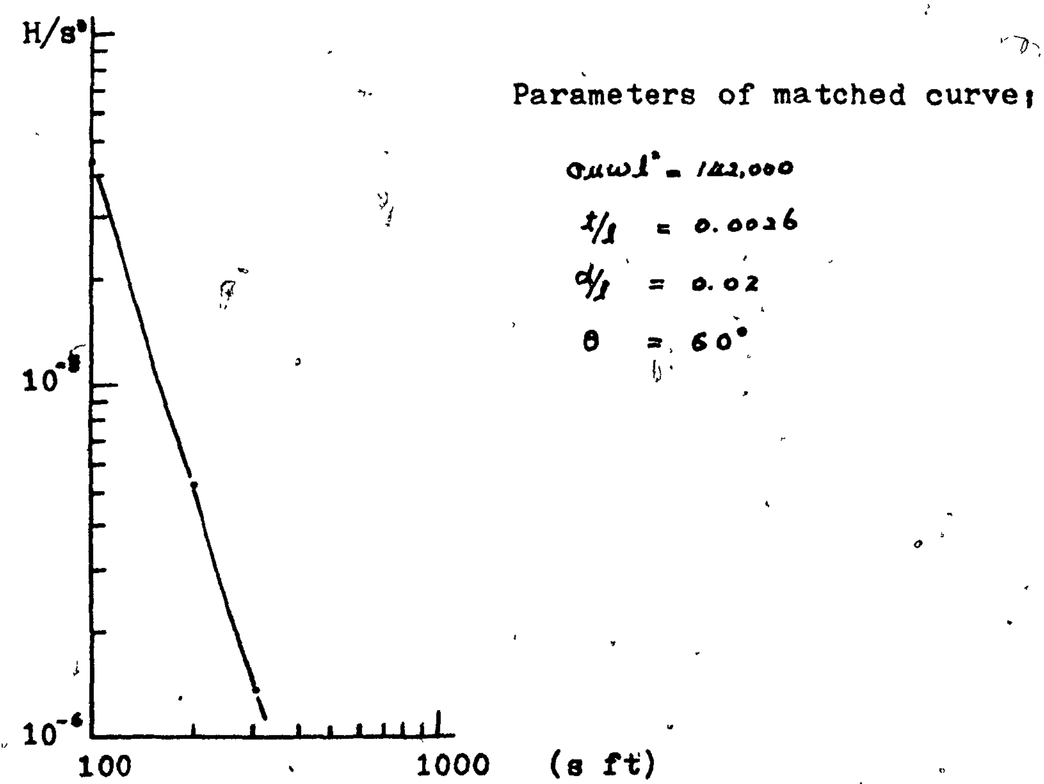

Fig. 57. H/s³ - s curve of Cavendish

incomplete shoulders on the anomaly, but the vertical pseudo section shows a dip angle close to 60°), the following results are obtained:

f(Hz)	s(ft)	d(ft)	[illegible]	σt(mhos)	t(ft)	σ([illegible]/m)
600	100	12	50	350	70	16
	200	24	50	180	70	8
	300	<30	40	90	80	4

Taking an average from the above list,

σ = 8 mhos/m, t = 73 ft, d < 22 ft and σt = 170 mhos.

Comparing these results with those on page 109, the conventional interpretation gives larger values of d and t, but much smaller values in σ and σt than the present type of interpretation, as before.

2. Långsele Ore, Sweden

This work was done by D. S. Parasnis (1971). Although general geological information about this ore body is not available, the geophysical results at hand provide a comparison with the method in this thesis.

Profiles for four transmitter-receiver separations are shown in Fig. 58; the vertical pseudo section and the field characteristic curve $H/s^2 - s$ are displayed in Figs. 59 and 60. Using the present type of interpretation, values of various parameters are as below:

$l = 40$ m, $\sigma = 135$ mhos/m, $t \doteqdot 5$ m, $d \doteqdot 15$ m $\sigma t \doteqdot 675$ mhos and $\theta \doteqdot 90^\circ$.

According to Parasnis' interpretation and the thickness estimation as before, the various parameters are as below. The average dip angle of this ore is reported to be 50° in the direction as shown in Figs. 58 and 59.

f(Hz)	s(m)	$Re)_{max}$	$Im)_{max}$	d(m)	σt(mhos)	t(m)	σ(mhos/m)
3600	60	-39 %	-8.9%	10.2	24.4	thin	
	40	-23	-8	10.4	25.0	10	2.5
	30	-15.5	-6.7	10.2	26.4	5	5.3
	20	-5.5	-0.5				

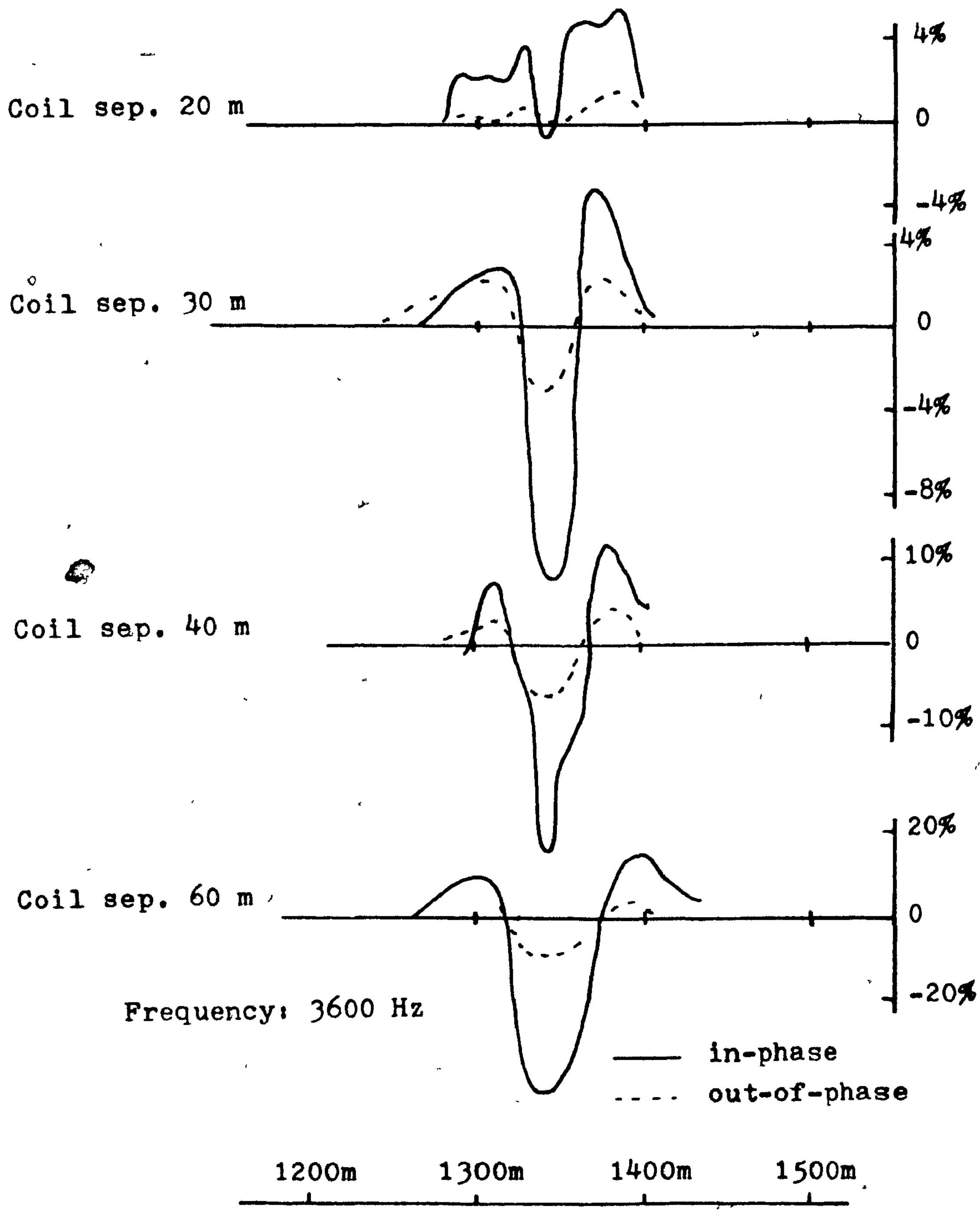

Fig. 58. Horizontal Loop Profiles of Långsele Ore

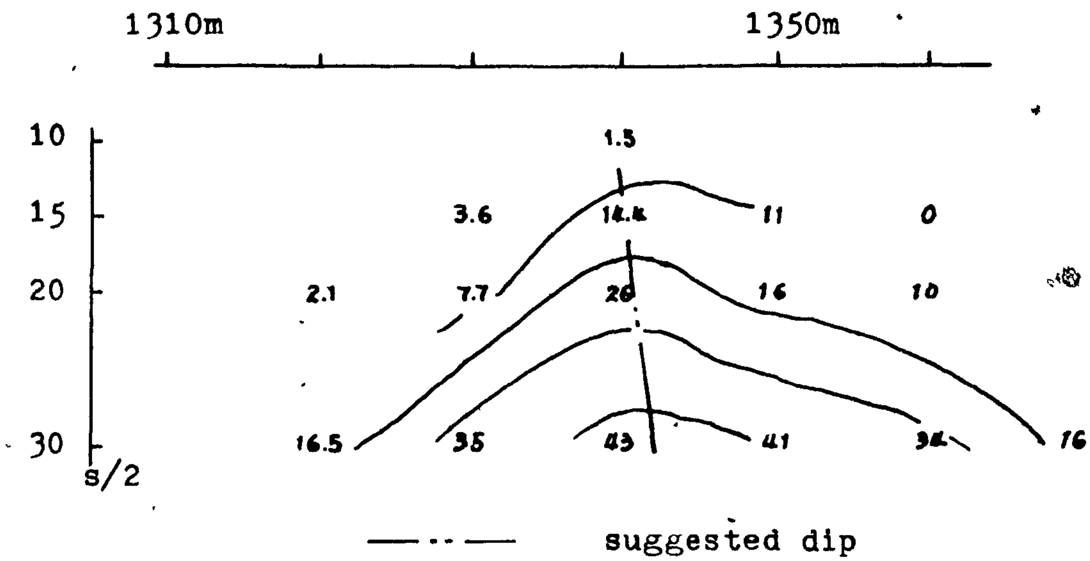

Fig. 59. Vertical pseudo section of Langsele ore

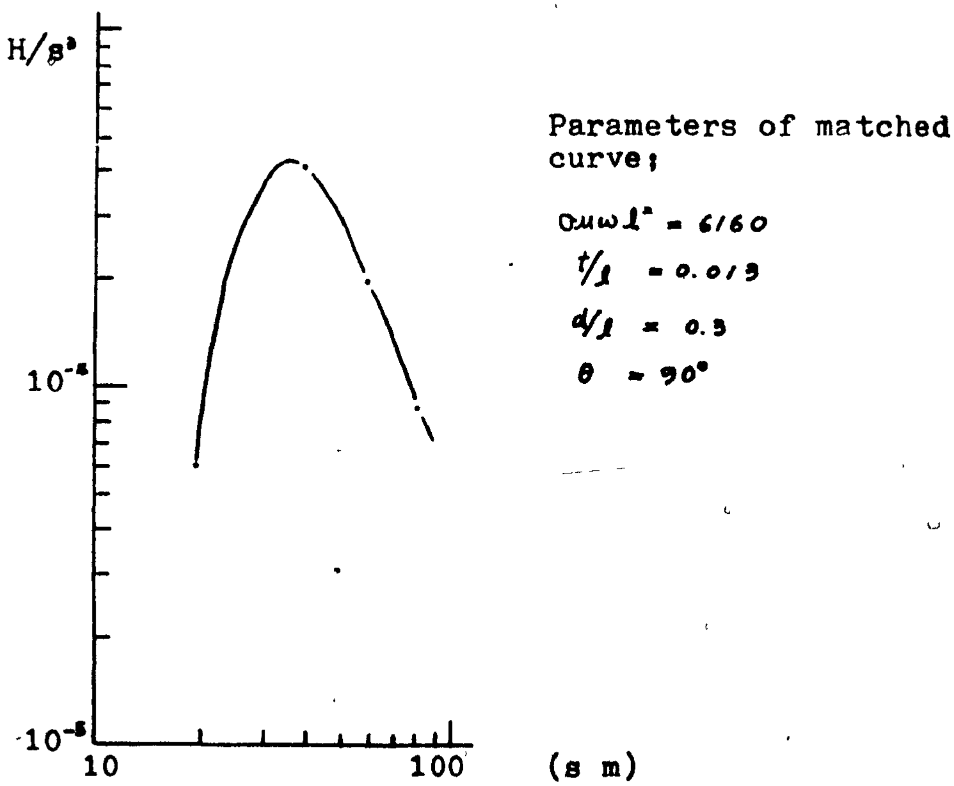

Fig. 60. H/s³ - s curve of Långsele ore

Taking an average from the above list to compare the values of σ, t, d and σt;

σ = 3.9 mhos/m, t = 5 m, d = 10.3 m and σt = 25.3 mhos.

The values of σ and σt of these results are, as usual, much smaller than those from the present type of interpretation, but the rest of the parameters, t and d show reasonable agreement with the latter method. Even though there is little difference in t between the two types of interpretation, the conductivity from Parasnis' interpretation is smaller than the one from the present interpretation.

3. Kedträsk pyrite orebody, Sweden

Like the Långsele orebody, no geographical information is available but some geological and geophysical information provided by Parasnis (1966) allows a comparison to be made with the results obtained by the present method.

According to Parasnis, the ore zone in quartzite has a strike-length of about 1.5 Km, an average width of some

45 m and the predominant conducting mineral is pyrite. The grade is fairly low across the entire width of the zone except within a 5 m thick lens on the footwall side, where the pyrite content is so high that only the lens produces the EM anomaly.

Profiles and vertical pseudo section are shown in Figs 61 and 62. The H/s' - s curve obtained from the latter appears in Fig. 63. Using the present technique the following results are obtained:

l = 170 m, σ = 180 mhos/m, t ≑ 0.5 m, d ≑ 3 m, σt ≑ 90 mhos and θ = 70°S.

Interpreting the results in Fig. 61 by the conventional method, the following results are obtained:

f(Hz)	s(m)	θ	d(m)	$\sigma\mu\omega st$	σt(mhos)	t(m)	σ(mhos/m)
3600	20		7	6.0	10	8	1.3
	30	80° S	7	12.0	14	thin	
	40	60° S	7	25	22	5	4.4
	60	90° S	6	30	18	2.5	7
Average		80° S	7		16	4	4

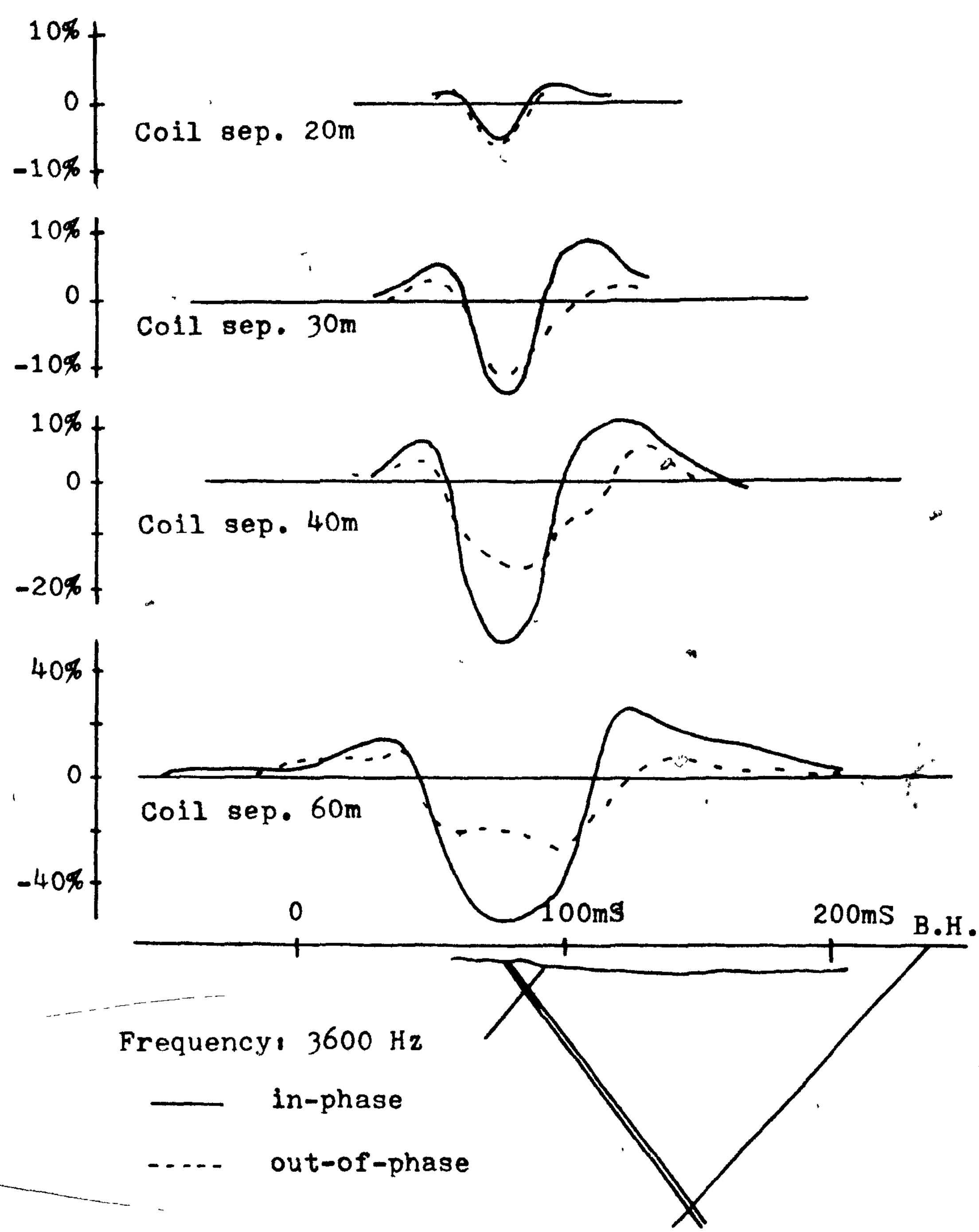

Fig. 61. Horizontal Loop Profiles of Kedträsk Pyrite

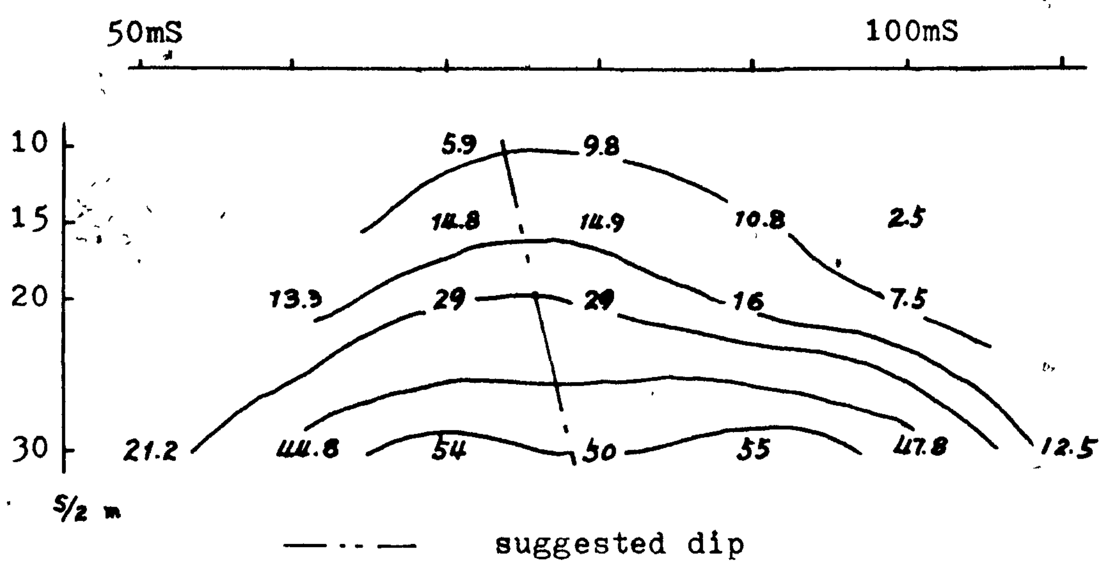

Fig. 62. Vertical pseudo section of Kedträsk

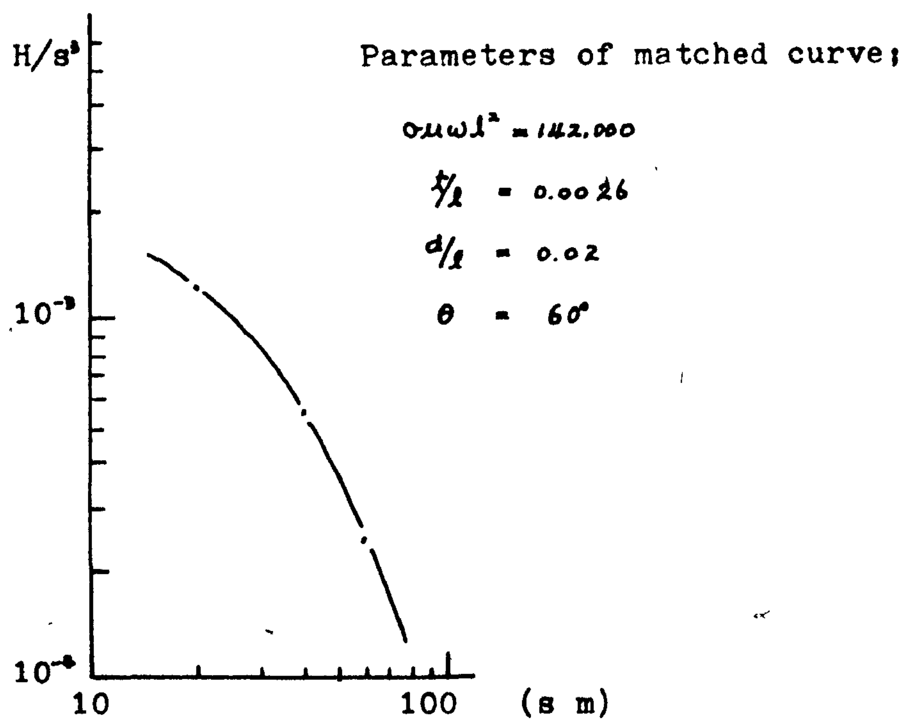

Fig. 63. H/s - s curve of Kedträsk

Comparing the two sets of results of page 117, the same discrepancies show up as before, since the present interpretation gives larger values of σ and σt, but smaller values of t and d than the conventional method.

Chapter 8. Conclusion

When we consider the EM response from a very thin plate with finite conductivity and finite dimensions, it is impossible at present to solve the general partial differential equation which express the electromagnetic phenomena, because of the complex boundary conditions. The dimensional analysis of this problem was carried out/to reduce the many original parameters to five new ones.

In order to investigate the result of the dimensional analysis, the geometrical factor was calculated for horizontal loop EM response over a thin conductor with infinite conductivity, strike length and depth extent. The separation between the transmitter and the receiver was varied to produce a set of curves $H(l/s)^3$ - s/l with varying d/s.

Extending these results further to the more general case of finite conductivity, the unknown function of the new parameters was determined from model measurements to find the effect of the new parameters on the curves which express the relation between $H(l/s)^3$ and s/l.

As a result of model measurements, various sets of the curves $H(l/s)^3$ - s/l were produced which could be used to interpret field results from several selected areas, using the horizontal-loop EM system with multi-separation of transmitter and receiver.

It was then possible to calculate the depth, thickness, conductivity and the depth extent of the suspected conductor. In addition, the dip angle and location of the conductor could be estimated by plotting the vertical pseudo section.

A summary of the interpretation results is tabulated below.

Anomaly	Interpretation	θ	d	σt(mhos)	σ(mhos/m)	t	l
Anomaly A of Claim line, Hicks Island #1	Thesis method	70°	9'	1370	760	6'	175'
	Conventional method		<20	88	8	45'	
Anomaly B of Claim line, Hicks Island #2	Thesis method	80°	25'	2600	780	11'	83'
	Conven. method		<15'	43	1	100'	
Anomaly A of L - 30S, Hicks Island #3	Thesis method	80°	30'	230	190	4'	230'
	Conven. method		<20'	<79	< 9	30'	

Anomaly	Interpretation	θ	d	σt (mhos)	σ (mho/m)	t	l
Anomaly B of L - 30S, Hicks Island #4	Thesis method	70°	40'	2600	860	10'	50'
	Conven. method		<20'	<52	<6	30'	
L - 28 S, Uranium Val. #5	Thesis method	80°	50'	55	18	10'	330'
	Conven.		30'	2.3	0.05	120'	
L - 4E, Demers Creek #6	Thesis method	90°	20'	1830	550	10'	160'
	Conven. method	90°	25'	1	0.06	55'	
L - C, Cavendish #7	Thesis method	70°	6'	1100	3400	1'	310'
	Conven. method		22'	170	8	73'	
Langsele #8	Thesis method	90°	15m	675	135	5m	40m
	Conven. method		10m	25	5	5m	
Kedträsk #9	Thesis method	70°	3m	90	180	0.5m	170m
	Conven. method	80°	7m	16	4	4m	

As shown on the above table, the dip angles are not defined for the conventional method of interpretation, because the horizontal profiles do not show simple shoulders of the anomlies in most cases. However, when the conventional method defines θ in a few examples, it shows reasonable agreement with θ obtained by the new method, as shown in the Demers Creek and the Kedträsk orebody. The θ values are estimated by drawing trends of the contours in the vertical pseudo sections, although there is considerable ambiguity in drawing the trends.

Considering the depth estimates, d, there is reasonable agreement between the two interpretation techniques in five of the nine examples (#1, 5, 6, 8, 9), although the conventional characteristic curves generally produce smaller d values, with the exception of Cavendish Township.

Estimate of thickness t by the new technique produces much smaller values than usually obtained, except in the case of the Långsele zone. This is undoubtedly due to the fact that no thick sheets were used in the model work, in which the largest value of t corresponded to about 2 ft. Conversely, the σ values are all far too large because of the high conductivities of the model sheets. The large differences between σt determined by the two interpretation methods could probably be modified to some extent by additional model measurements with thicker sheets and sheets of lower conductivity (stainless steel, graphite). However, it is unlikely that the σ values obtained by the two schemes would ever agree -- except in the case of very thin mineralized zones -- since the dimensions of t obtained from horizontal loop profiles is generally too large.

In the estimation of all the parameters, σ, d, t and l the selection of the best matched curve from the characteristic curves obtained by the model work can be made by calculating the l_h and l_v and picking the curve with the minimum difference between them, even though there are many curves, which may match reasonably well.

In general, compared to conventional horizontal loop interpretation techniques, the new method has two distinct advantages. First, it is possible to determine the depth extent of the conductor and second the thickness and conductivity of the sheet are obtained separately rather than the conventional conductivity- thickness product. In addition, the use of several transmitter-receiver spacings and resultant pseudo depth plot permit a better estimate of dip angle than horizontal profiles.

On the other hand, in speaking about the characteristic curves $H(l/s)^2$ - s/l, since they are specified by $\sigma\omega l^2$, t/l and d/l, which are more than two original factors, one model curve can cover a lot of different cases in the values of σ, l, d and t. However, in order to have a complete suite of characteristic curves, it would be required to do some more measurements with variation of the parameters.

Appendix A

Calculation of F at various depths

```
C     CALCULATION OF FS AT VARIOUS VALUES OF D
      REAL D(13),S(10)
      WRITE(6,24)
24    FORMAT('1'///' ',12X,'APPENDIX A')
      WRITE(6,25)
25    FORMAT('0',12X,'THE VALUES OF FS')
      WRITE(6,39)
39    FORMAT('0',6X,'D',10X,'S',10X,'FS')
      READ(5,21) (D(I),I=1,13)
21    FORMAT(13F5.1)
      READ(5,20) (S(J),J=1,10)
20    FORMAT(10F6.1)
      K=0
      DO 6 I=1,13
      DO 6 J=1,10
      K=K+1
      A= S(J)**8*(D(I)+S(J)*5/16)**2
      B=((S(J)/2)**2+(D(I)+S(J)*5/16)**2)**5
      FS=A/B
      IF(K.GT.25) GO TO 40
27    WRITE(6,26) D(I),S(J),FS
26    FORMAT('0',3F10.3)
      GO TO 6
40    K=1
      WRITE(6,30)
30    FORMAT('1'//////'0',6X,'D',10X,'S',10X,'FS')
      GO TO 27
6     CONTINUE
      STOP
      END

*OPTIONS IN EFFECT*  ID,EBCDIC,SOURCE,NOLIST,NODECK,LOAD,NOMAP
*OPTIONS IN EFFECT*  NAME = MAIN    , LINECNT =       56
*STATISTICS*   SOURCE STATEMENTS =       29,PROGRAM SIZE =      1064
*STATISTICS*  NO DIAGNOSTICS GENERATED
```

APPENDIX A

THE VALUES OF FS

C	S	FS
0.0	100.000	19.229
0.0	200.000	19.229
0.0	300.000	19.229
0.0	400.000	19.229
0.0	500.000	19.229
0.0	600.000	19.229
0.0	700.000	19.229
0.0	800.000	19.229
0.0	900.000	19.229
0.0	1000.000	19.229
10.000	100.000	12.996
10.000	200.000	16.281
10.000	300.000	17.341
10.000	400.000	17.848
10.000	500.000	18.143
10.000	600.000	18.335
10.000	700.000	18.470
10.000	800.000	18.570
10.000	900.000	18.646
10.000	1000.000	18.707
20.000	100.000	7.417
20.000	200.000	12.996
20.000	300.000	15.187
20.000	400.000	16.281
20.000	500.000	16.923

D	S	FS
20.000	600.000	17.341
20.000	700.000	17.633
20.000	800.000	17.848
20.000	900.000	18.013
20.000	1000.000	18.143
30.000	100.000	3.929
30.000	200.000	9.956
30.000	300.000	12.996
30.000	400.000	14.635
30.000	500.000	15.627
30.000	600.000	16.281
30.000	700.000	16.741
30.000	800.000	17.081
30.000	900.000	17.341
30.000	1000.000	17.546
40.000	100.000	2.033
40.000	200.000	7.417
40.000	300.000	10.920
40.000	400.000	12.996
40.000	500.000	14.304
40.000	600.000	15.187
40.000	700.000	15.814
40.000	800.000	16.281
40.000	900.000	16.639
40.000	1000.000	16.923

D	S	FS
50.000	100.000	1.057
50.000	200.000	5.428
50.000	300.000	9.048
50.000	400.000	11.423
50.000	500.000	12.996
50.000	600.000	14.084
50.000	700.000	14.872
50.000	800.000	15.462
50.000	900.000	15.919
50.000	1000.000	16.281
60.000	100.000	0.560
60.000	200.000	3.929
60.000	300.000	7.417
60.000	400.000	9.956
60.000	500.000	11.730
60.000	600.000	12.996
60.000	700.000	13.928
60.000	800.000	14.635
60.000	900.000	15.187
60.000	1000.000	15.627
70.000	100.000	0.304
70.000	200.000	2.829
70.000	300.000	6.032
70.000	400.000	8.617
70.000	500.000	10.528

D	S	FS
70.000	600.000	11.937
70.000	700.000	12.996
70.000	800.000	13.810
70.000	900.000	14.451
70.000	1000.000	14.966
80.000	100.000	0.170
80.000	200.000	2.033
80.000	300.000	4.878
80.000	400.000	7.417
80.000	500.000	9.404
80.000	600.000	10.920
80.000	700.000	12.086
80.000	800.000	12.996
80.000	900.000	13.719
80.000	1000.000	14.304
90.000	100.000	0.098
90.000	200.000	1.464
90.000	300.000	3.929
90.000	400.000	6.356
90.000	500.000	8.366
90.000	600.000	9.956
90.000	700.000	11.206
90.000	800.000	12.198
90.000	900.000	12.996
90.000	1000.000	13.646

D	S	FS
100.000	100.000	0.058
100.000	200.000	1.057
100.000	300.000	3.157
100.000	400.000	5.428
100.000	500.000	7.417
100.000	600.000	9.048
100.000	700.000	10.362
100.000	800.000	11.423
100.000	900.000	12.285
100.000	1000.000	12.996
200.000	100.000	0.001
200.000	200.000	0.058
200.000	300.000	0.372
200.000	400.000	1.057
200.000	500.000	2.033
200.000	600.000	3.157
200.000	700.000	4.312
200.000	800.000	5.428
200.000	900.000	6.467
200.000	1000.000	7.417
300.000	100.000	0.000
300.000	200.000	0.006
300.000	300.000	0.058
300.000	400.000	0.226
300.000	500.000	0.560

D	S	FS
300.000	600.000	1.057
300.000	700.000	1.685
300.000	800.000	2.398
300.000	900.000	3.157
300.000	1000.000	3.929

Appendix B

Calculation of H(l/s) for s/l at various d/l

```
FORTRAN IV G LEVEL  21                MAIN            DATE = 73130         16/24/04            PAGE 0001

              C       CALCULATION OF M,P,R
                      FS(A,B)=(A**8*(B+A*5/16)**2)/((A/2)**2+(B+A*5/16)**2)**5
                      REAL D(17),S(11),L,M
                      WRITE(6,24)
               24     FORMAT('1'//'0',50X,'TABLE 1')
                      WRITE(6,25)
               25     FORMAT('0',10X,'THE VALUES OF M')
                      WRITE(6,30)
               30     FORMAT('0',5X,'M',10X,'P',9X,'R')
                      READ(5,21) (D(I),I=1,17)
               21     FORMAT(16F5.1/F5.1)
                      READ(5,20) (S(J),J=1,11)
               20     FORMAT(11F5.1)
                      L=1000.0
                      K=0
                      DO 10 I=1,17
                      DO 10 J=1,11
                      K=K+1
                      P=D(I)/L
                      R=S(J)/L
                      M=FS(S(J),D(I))*(L/S(J))**3
                      IF(K.GT.25) GO TO 50
               45     WRITE(6,26) M,P,R
               26     FORMAT('0',3F10.3)
                      GO TO 10
               50     K=1
                      WRITE(6,60)
               60     FORMAT('1'///'0',5X,'M',10X,'P',9X,'R')
               10     CONTINUE
                      STOP
                      END

 *OPTIONS IN EFFECT*  ID,EBCDIC,SOURCE,NOLIST,NODECK,LOAD,NOMAP
 *OPTIONS IN EFFECT*  NAME = MAIN  - , LINECNT =       56
 *STATISTICS*    SOURCE STATEMENTS =       30,PROGRAM SIZE =      1258
 *STATISTICS*  NO DIAGNOSTICS GENERATED
```

THE VALUES OF M

M	P	R
**********	0.0	0.020
300443.375	0.0	0.040
189021.563	0.0	0.060
37555.051	0.0	0.080
19228.680	0.0	0.100
2403.587	0.0	0.200
712.174	0.0	0.300
300.448	0.0	0.400
153.830	0.0	0.500
89.022	0.0	0.600
56.060	0.0	0.700
132122.500	0.010	0.020
84805.688	0.010	0.040
41890.855	0.010	0.060
22309.699	0.010	0.080
12095.535	0.010	0.100
2035.105	0.010	0.200
642.252	0.010	0.300
278.881	0.010	0.400
145.147	0.010	0.500
84.886	0.010	0.600
53.849	0.010	0.700
37208.605	0.020	0.020
16515.303	0.020	0.040
14616.023	0.020	0.060

M	P	R
7417.480	0.020	0.100
1524.441	0.020	0.200
562.468	0.020	0.300
254.388	0.020	0.400
135.383	0.020	0.500
30.231	0.020	0.600
51.408	0.020	0.700
743.744	0.030	0.020
3538.376	0.030	0.040
4393.410	0.030	0.060
4683.996	0.030	0.080
392[illegible].884	0.030	0.100
1244.465	0.030	0.200
491.316	0.030	0.300
229.673	0.030	0.400
125.013	0.030	0.500
75.374	0.030	0.600
43.808	0.030	0.700
121.631	0.040	0.020
901.076	0.040	0.040
1720.065	0.040	0.060
2064.414	0.040	0.080
2033.335	0.040	0.100
927.186	0.040	0.200

M	P	R
203.055	0.040	0.400
114.435	0.040	0.500
70.308	0.040	0.600
46.106	0.040	0.700
27.328	0.050	0.020
270.125	0.050	0.040
651.756	0.050	0.060
936.231	0.050	0.080
1056.981	0.050	0.100
678.446	0.050	0.200
335.128	0.050	0.300
178.478	0.050	0.400
103.964	0.050	0.500
65.206	0.050	0.600
43.357	0.050	0.700
7.704	0.060	0.020
92.968	0.060	0.040
265.985	0.060	0.060
442.297	0.060	0.080
559.774	0.060	0.100
491.111	0.060	0.200
274.721	0.060	0.300
155.558	0.060	0.400
93.837	0.060	0.500

M	P	R
40.605	0.060	0.700
2.572	0.070	0.020
35.864	0.070	0.040
117.617	0.070	0.060
218.400	0.070	0.080
304.070	0.070	0.100
353.575	0.070	0.200
223.416	0.070	0.300
134.648	0.070	0.400
84.224	0.070	0.500
55.262	0.070	0.600
37.888	0.070	0.700
0.977	0.080	0.020
15.204	0.080	0.040
55.305	0.080	0.060
112.634	0.080	0.080
169.858	0.080	0.100
254.167	0.080	0.200
130.655	0.080	0.300
115.898	0.080	0.400
75.234	0.080	0.500
50.557	0.080	0.600
35.235	0.080	0.700
0.412	0.090	0.020

M	P	R
27.540	0.090	0.060
50.516	0.090	0.080
97.617	0.090	0.100
132.946	0.090	0.200
145.514	0.090	0.300
99.314	0.090	0.400
66.930	0.090	0.500
46.091	0.090	0.600
32.670	0.090	0.700
0.189	0.100	0.020
3.416	0.100	0.040
14.432	0.100	0.060
33.766	0.100	0.080
57.669	0.100	0.100
132.123	0.100	0.200
116.928	0.100	0.300
84.806	0.100	0.400
59.340	0.100	0.500
41.891	0.100	0.600
30.211	0.100	0.700
0.026	0.130	0.020
0.546	0.130	0.040
2.658	0.130	0.060
7.125	0.130	0.080

M	P	R
51.305	0.130	0.200
60.468	0.130	0.300
52.109	0.130	0.400
40.730	0.130	0.500
30.994	0.130	0.600
23.574	0.130	0.700
0.005	0.160	0.020
0.122	0.160	0.040
0.649	0.160	0.060
1.900	0.160	0.080
4.014	0.160	0.100
21.232	0.160	0.200
31.593	0.160	0.300
31.771	0.160	0.400
27.571	0.160	0.500
22.582	0.160	0.600
13.121	0.160	0.700
0.001	0.200	0.020
0.024	0.200	0.040
0.135	0.200	0.060
0.427	0.200	0.080
0.973	0.200	0.100
7.209	0.200	0.200
13.761	0.200	0.300

M	P	R
16.267	0.200	0.500
14.616	0.200	0.600
12.572	0.200	0.700
0.000	0.230	0.020
0.008	0.230	0.040
0.049	0.230	0.060
0.162	0.230	0.080
0.385	0.230	0.100
3.436	0.230	0.200
7.615	0.230	0.300
10.230	0.230	0.400
10.967	0.230	0.500
10.508	0.230	0.600
9.497	0.230	0.700
0.000	0.260	0.020
0.003	0.260	0.040
0.020	0.260	0.060
0.068	0.260	0.080
0.167	0.260	0.100
1.728	0.260	0.200
4.335	0.260	0.300
6.424	0.260	0.400
7.433	0.260	0.500
7.558	0.260	0.600

M	P	R
0.000	0.300	0.020
0.001	0.300	0.040
0.007	0.300	0.060
0.024	0.300	0.080
0.062	0.300	0.100
0.744	0.300	0.200
2.136	0.300	0.300
3.538	0.300	0.400
4.478	0.300	0.500
4.893	0.300	0.600
4.911	0.300	0.700

Appendix C

Vertical pseudo sections of in-phase

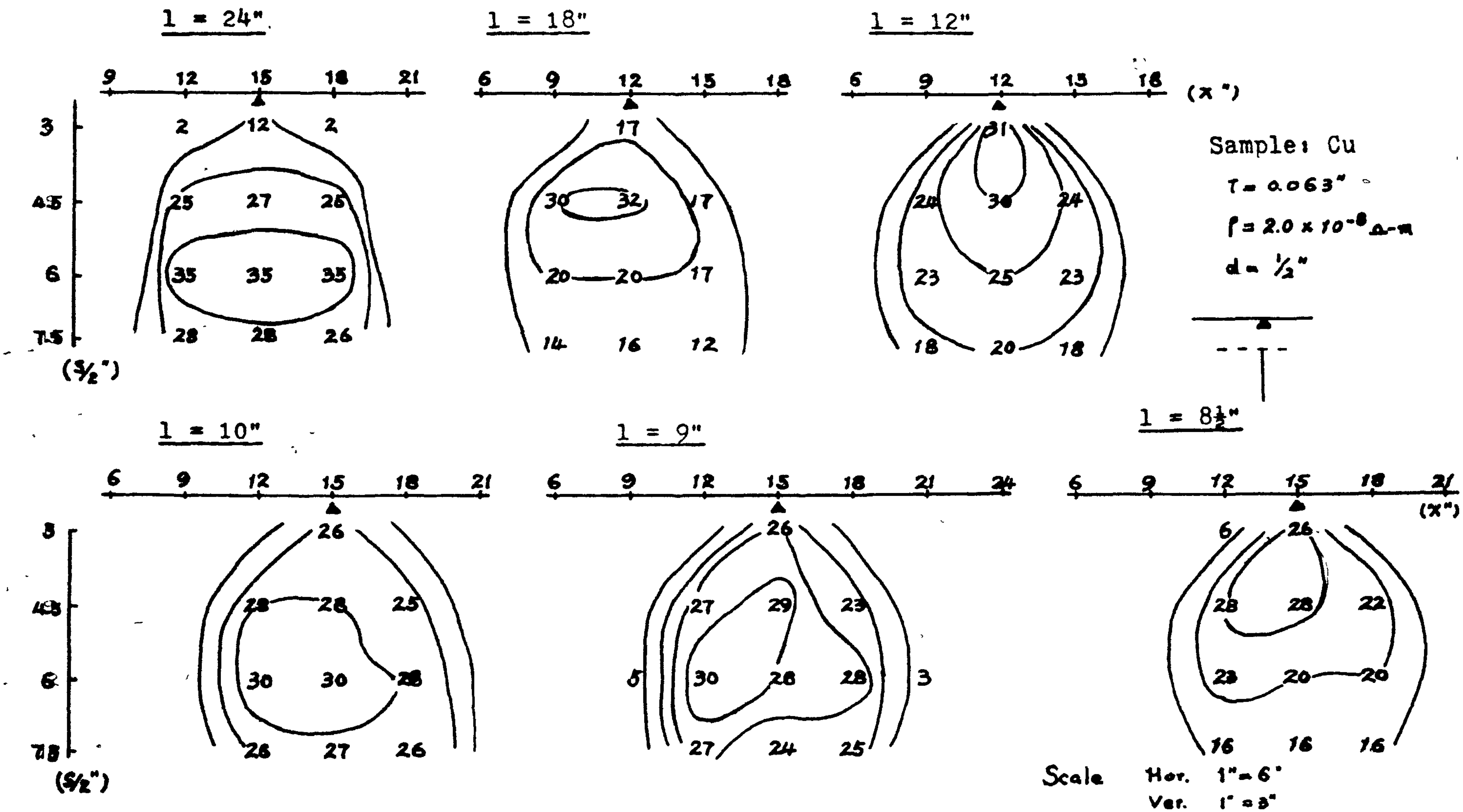

Variation of depth extent for $\theta = 90^\circ$ (I)

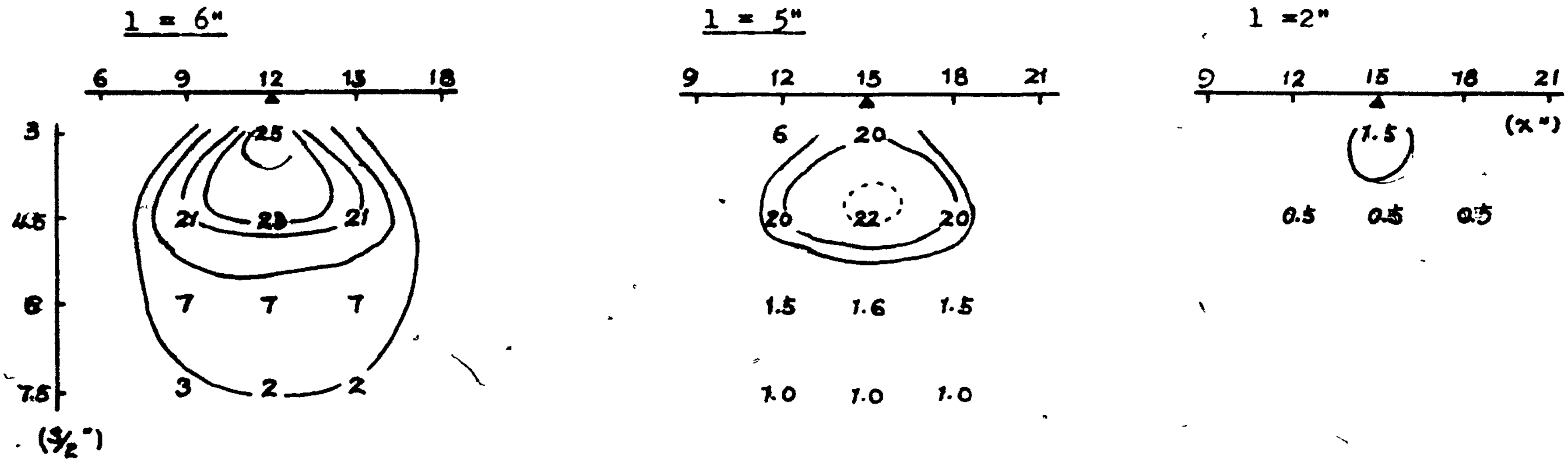

Sample: Cu
$t = 0.063"$
$\rho = 2.0 \times 10^{-8}\ \Omega\text{-m}$
d= 1/2"

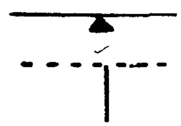

Scale Hor. 1" = 6"
Ver. 1" = 3"

Variation of depth extent for $\theta = 90°$ (II)

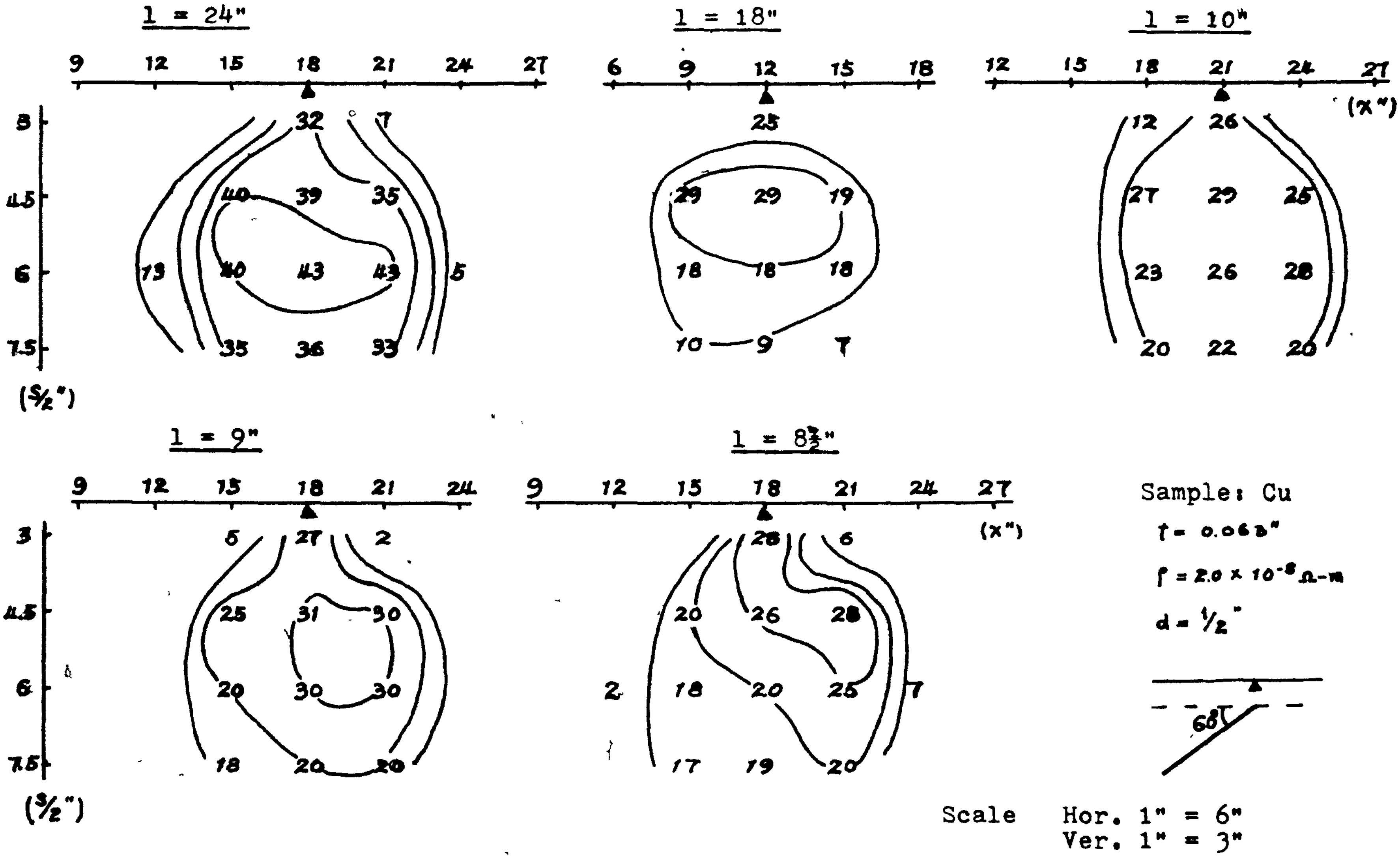

Variation of depth extent for $\theta = 60^\circ$ (I)

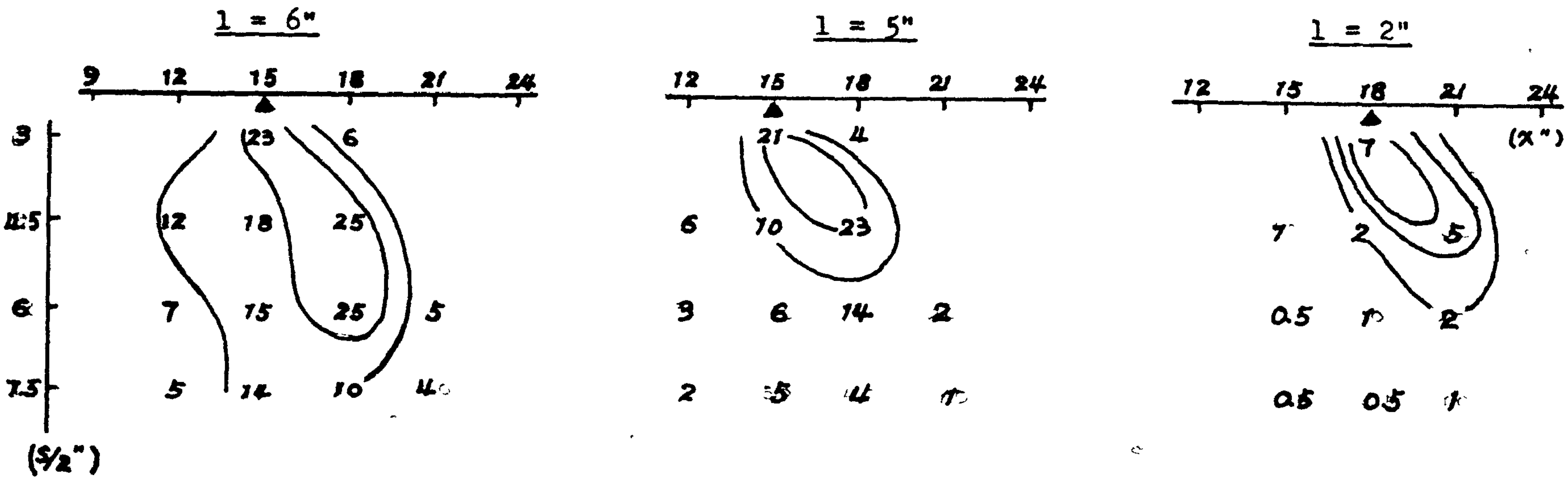

Sample: Cu
T = 0.063"
ρ = 2.0 × 10⁻⁸ Ω-m
d = ½ "

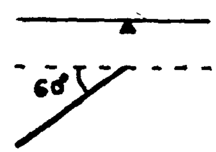

Scale Hor. 1" = 6"
ver. 1" = 3"

Variation of depth extent for θ = 60°(II)

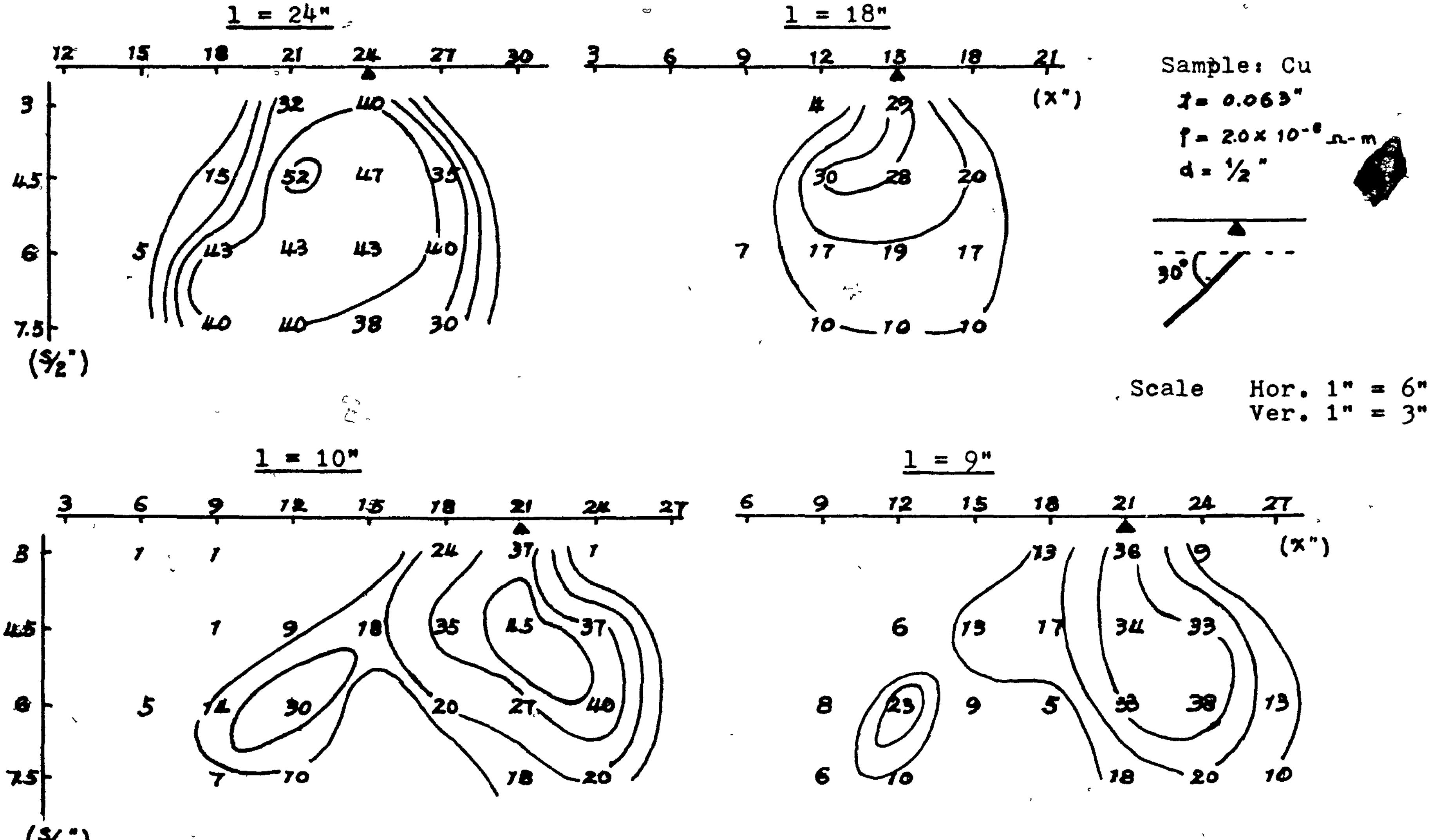

Variation of depth extent for $\theta = 30^\circ$ (I)

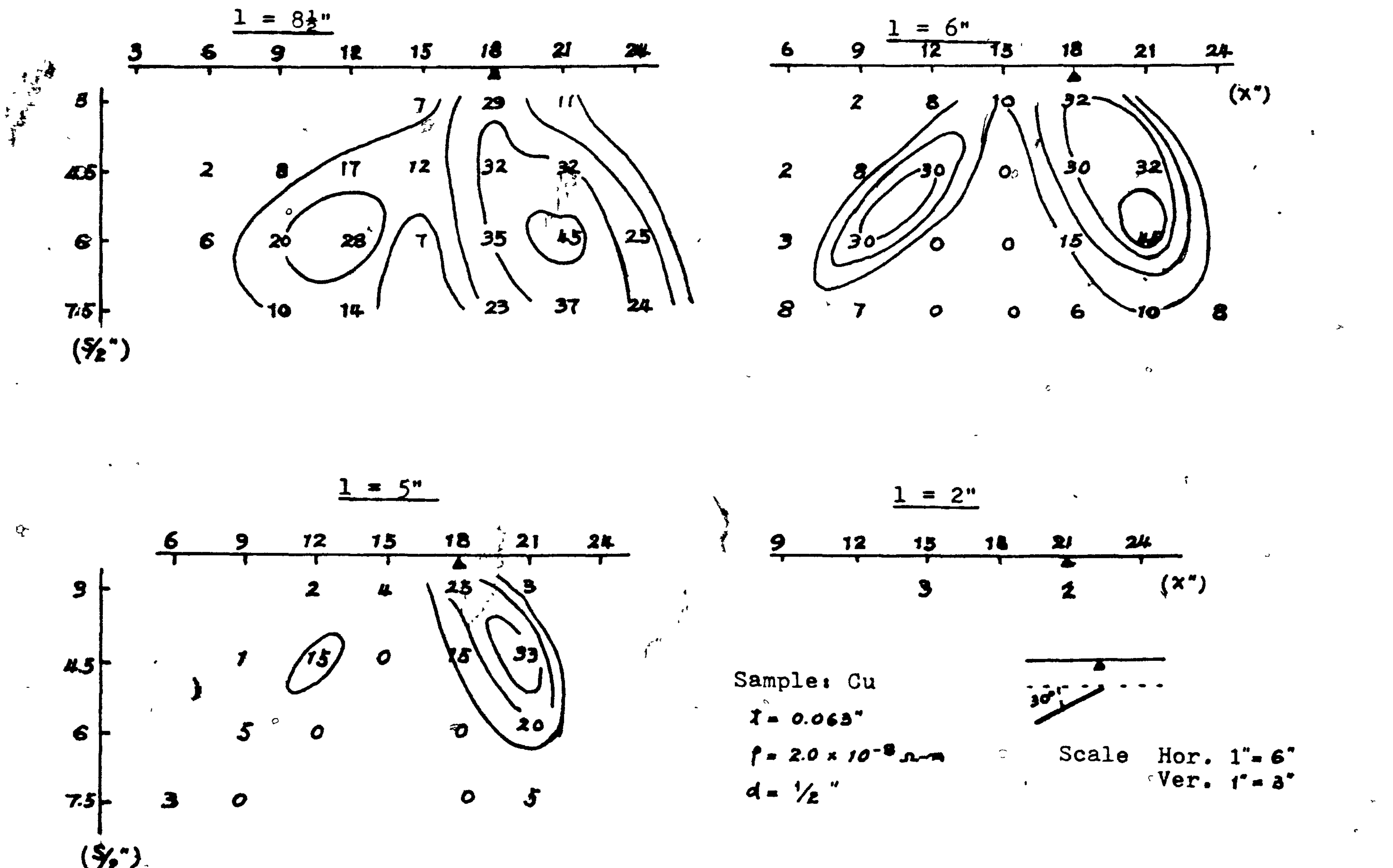

Variation of depth extent for $\theta = 30^\circ$ (II)

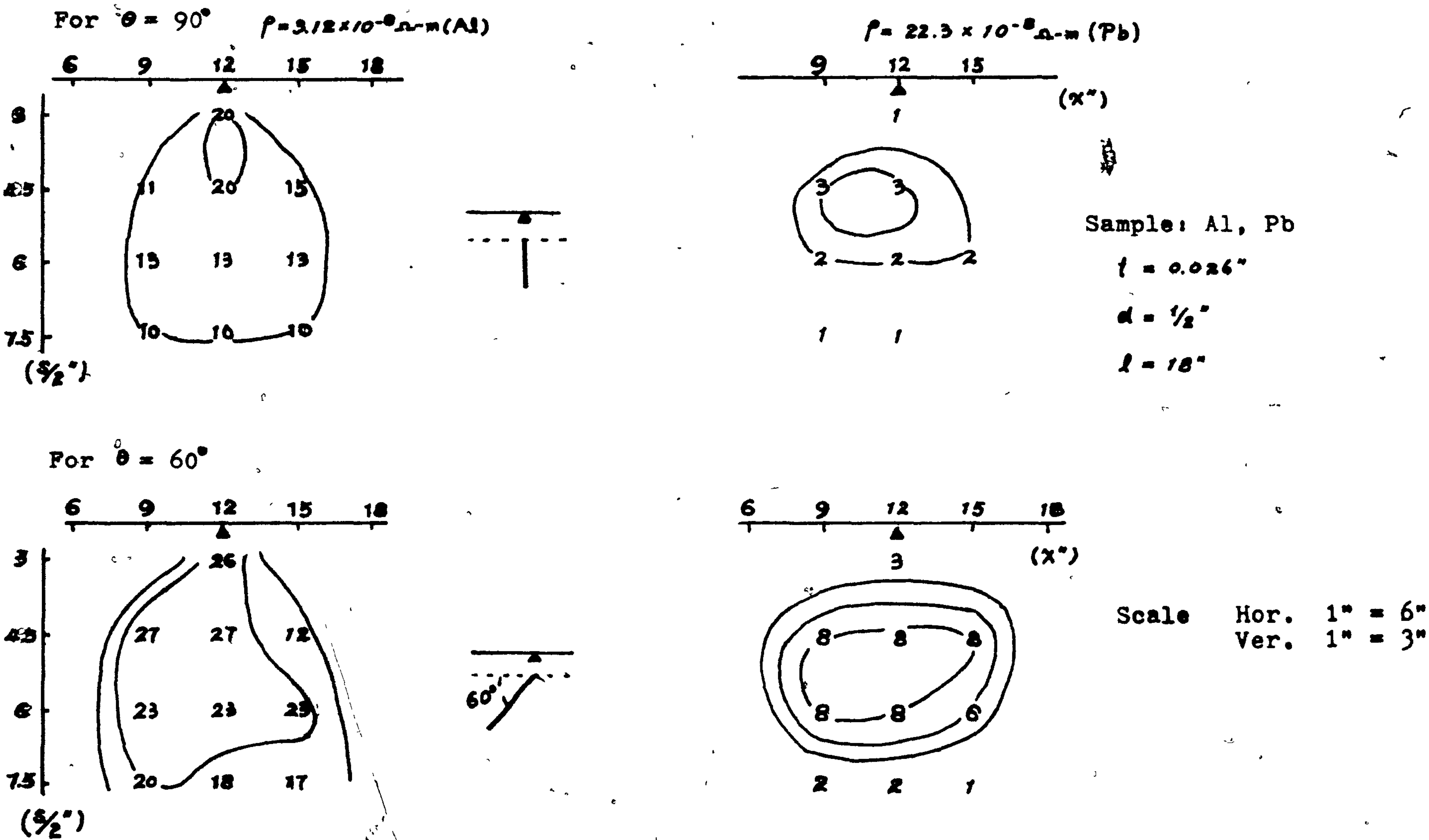

Variation of conductivity (I)

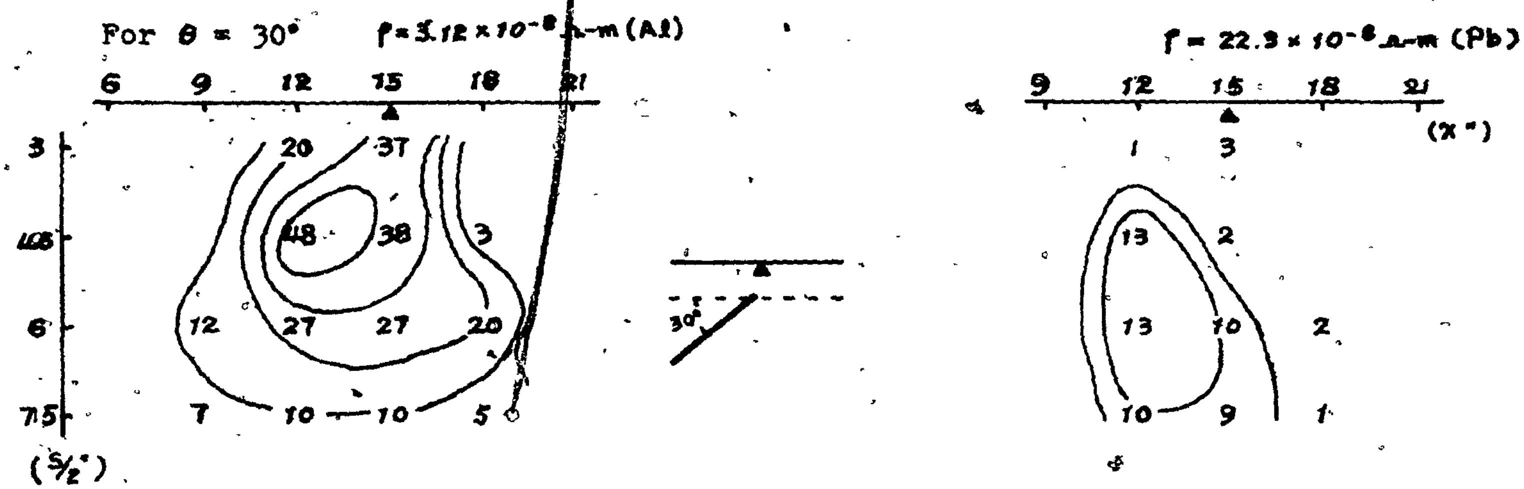

Sample: Al, Pb

$t = 0.026"$

$d = 1/2"$

$\ell = 18"$

Scale Hor. 1" = 6"
Ver. 1" = 3"

Variation of conductivity (II)

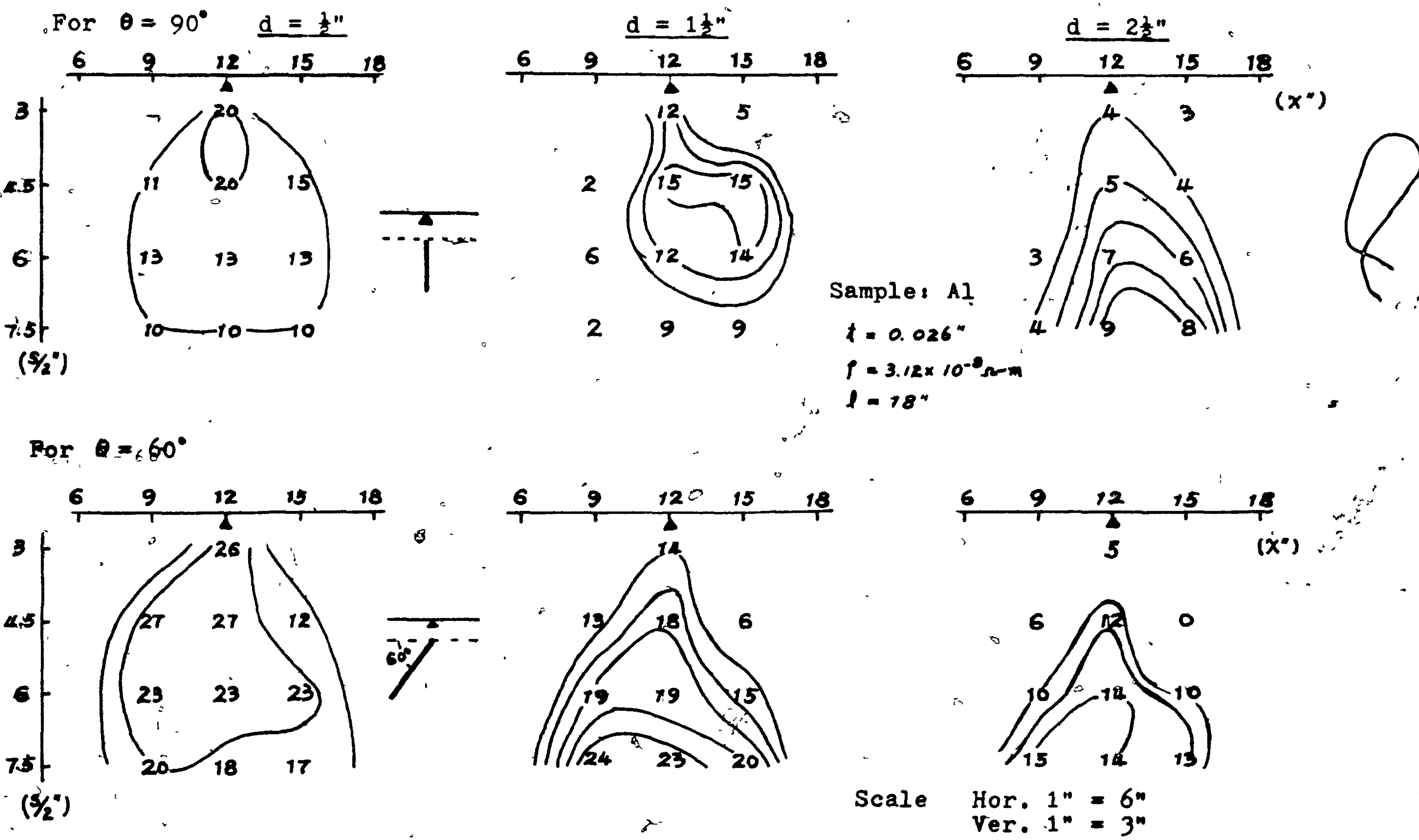

Variation of depth (I)

For $\theta = 30°$

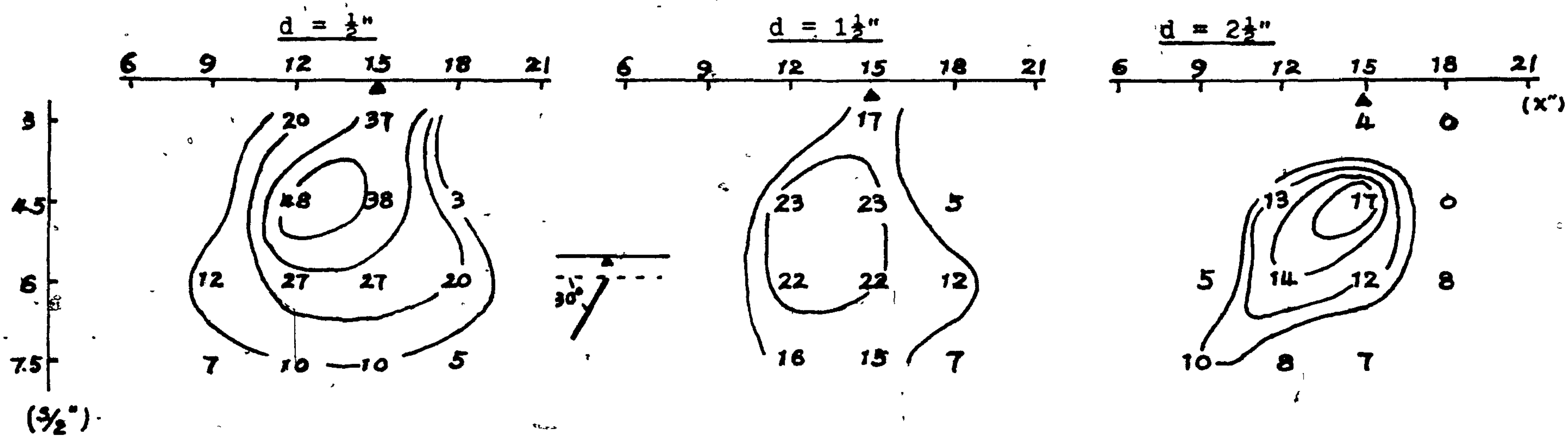

Sample: Al

$t = 0.026"$

$\rho = 3.12 \times 10^{-8}$ Ω-m

$l = 18"$

Scale Hor. 1" = 6"
Ver. 1" = 3"

Variation of depth (II)

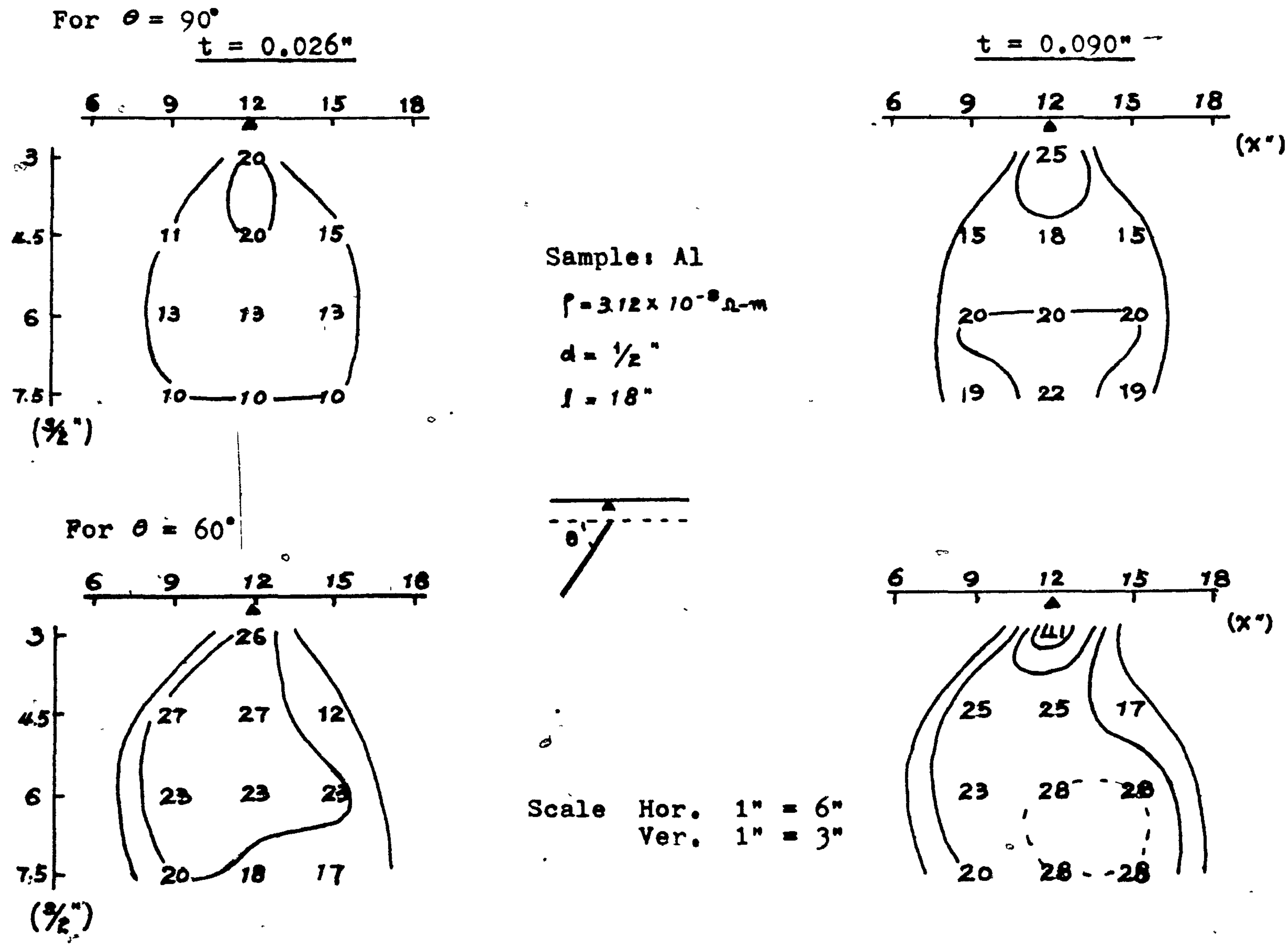

Variation of thickness (I)

For $\theta = 30^{\circ}$

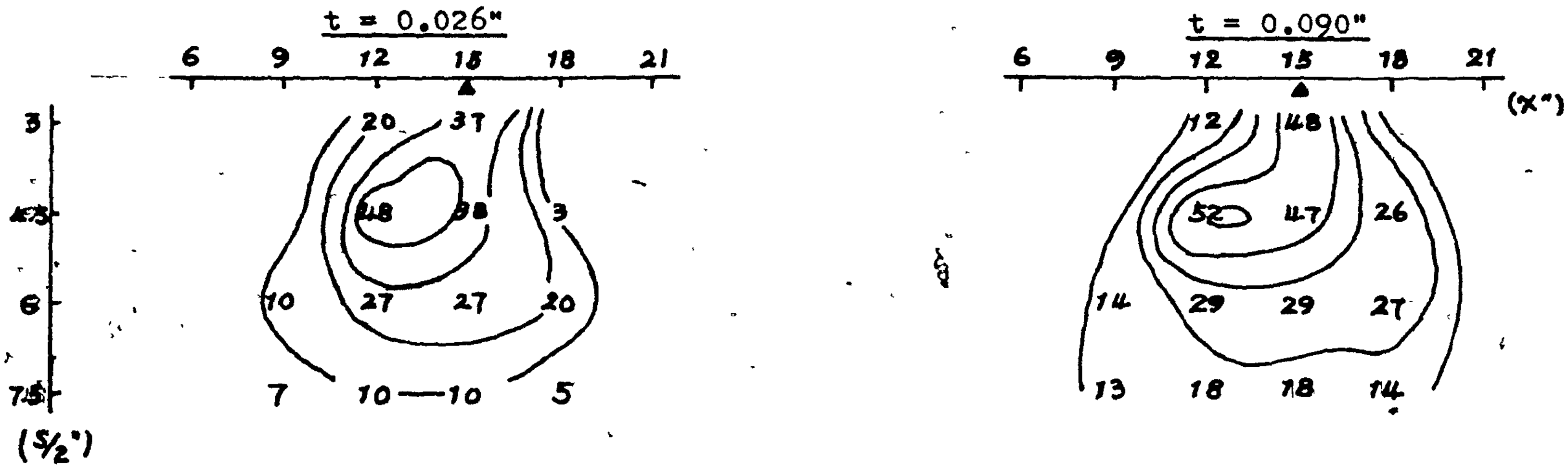

Sample: Al

$\rho = 3.12 \times 10^{-8}\ \Omega\text{-m}$

$d = 1/2"$

$l = 18"$

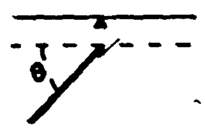

Scale Hor. 1" = 6"
Ver. 1" = 3"

Variation of thickness (II)

Appendix D

Vertical pseudo section of out-of-phase

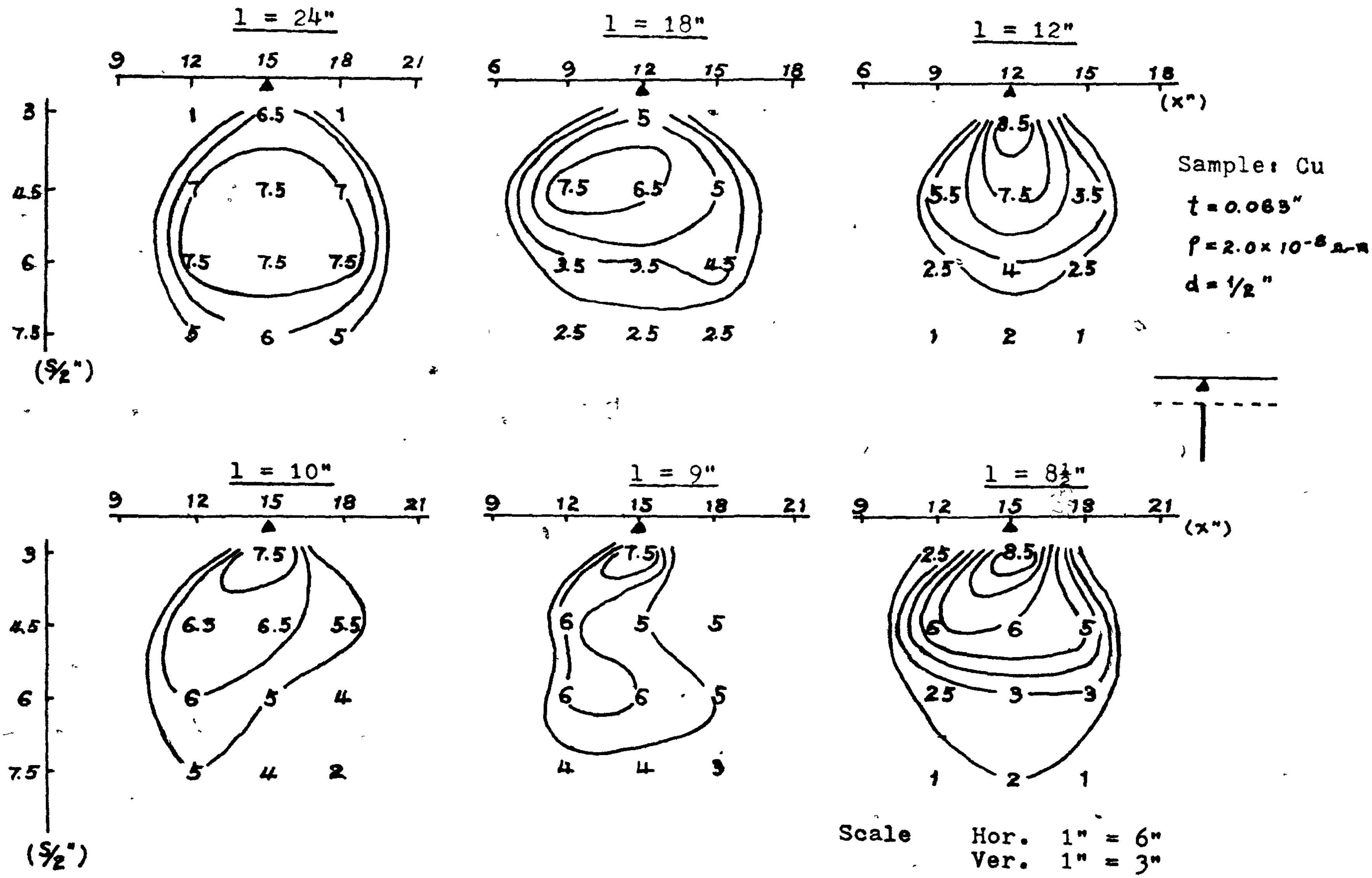

Variation of depth extent for θ = 90°

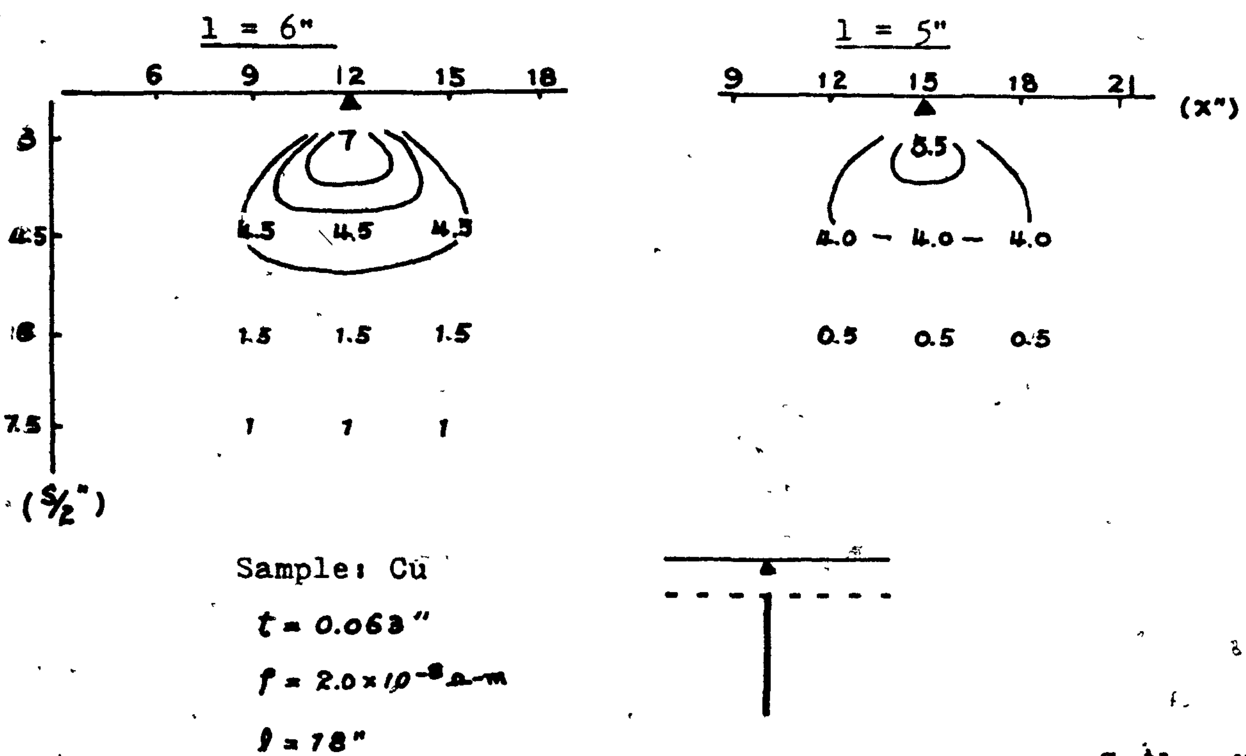

Scale Hor. 1" = 6"
Ver. 1" = 3"

Variation of depth extent for $\theta = 90°$

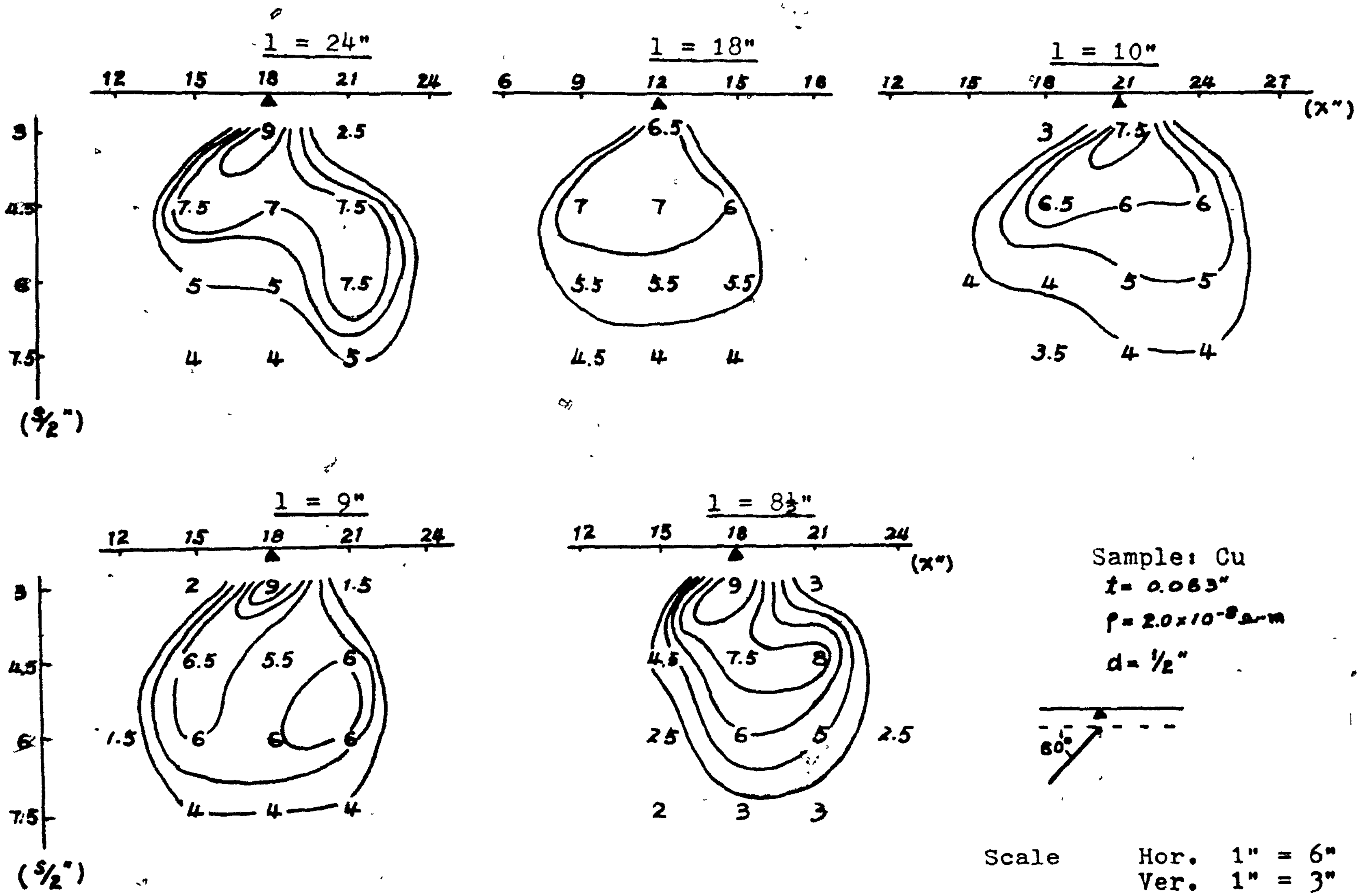

Variation of depth extent for $\theta = 60°$

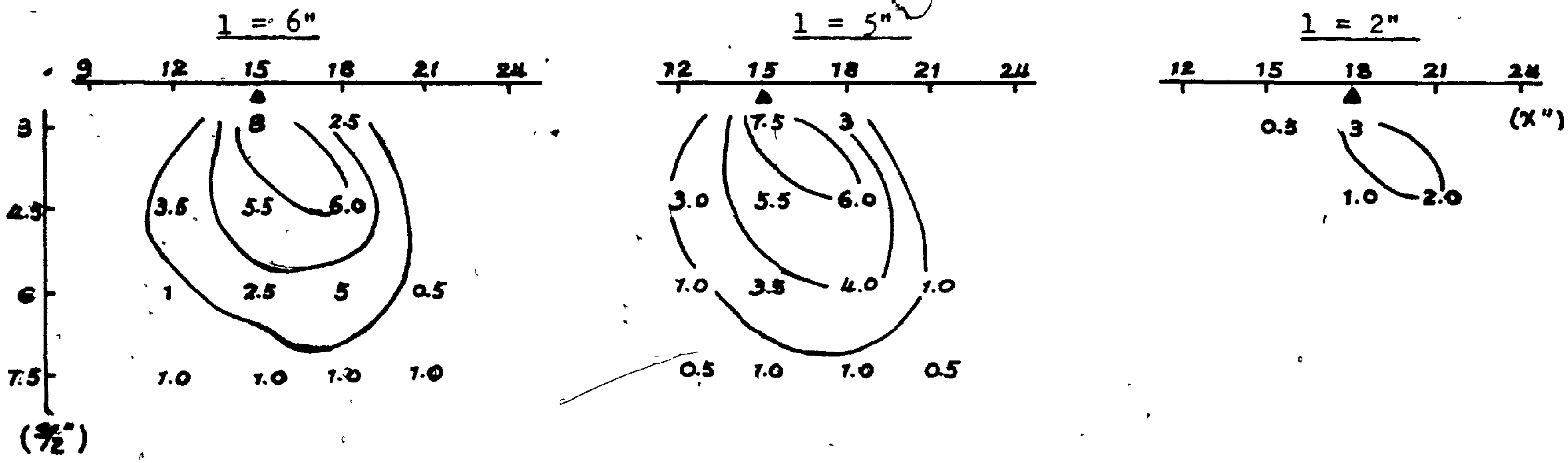

Sample: Cu

$t = 0.063"$

$\rho = 2.0 \times 10^{-8} \Omega m$

$d = 1/2"$

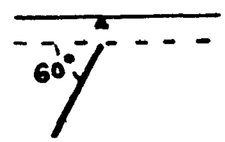

Scale Hor. 1" = 6"
Ver. 1" = 3"

Variation of depth extent for $\theta = 60°$

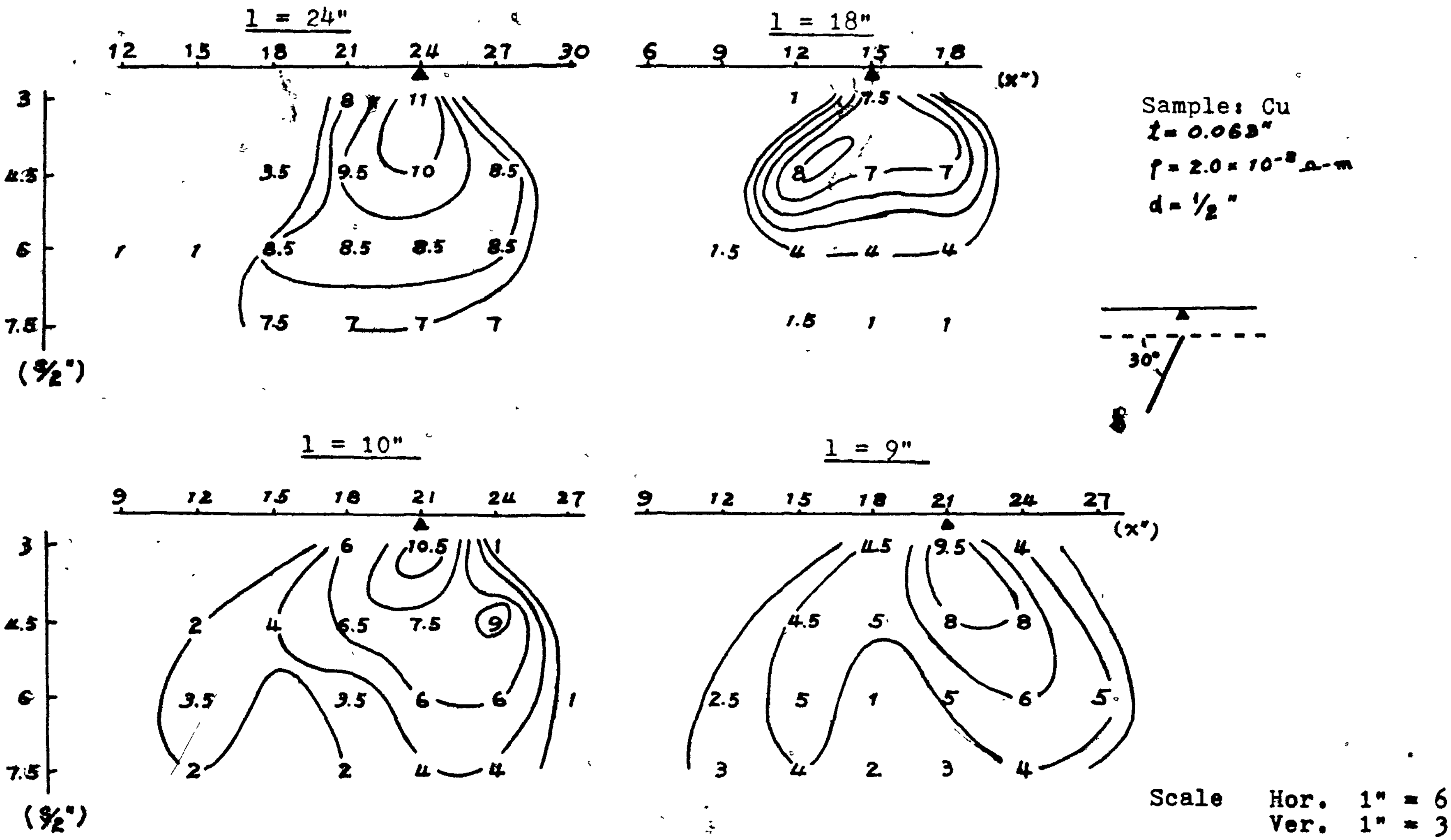

Variation of depth extent for $\theta = 30°$

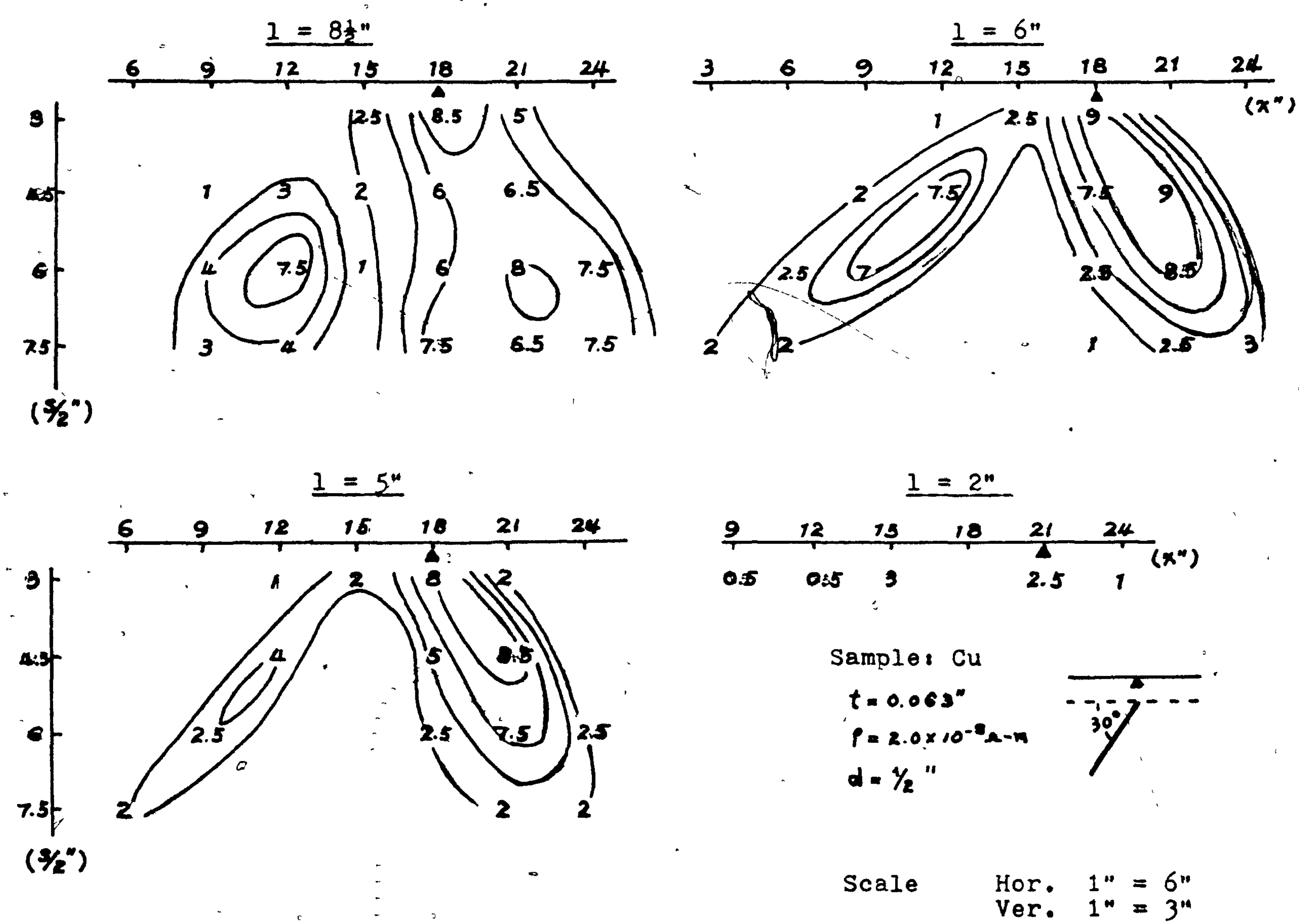

Variation of depth extent for $\theta = 30°$

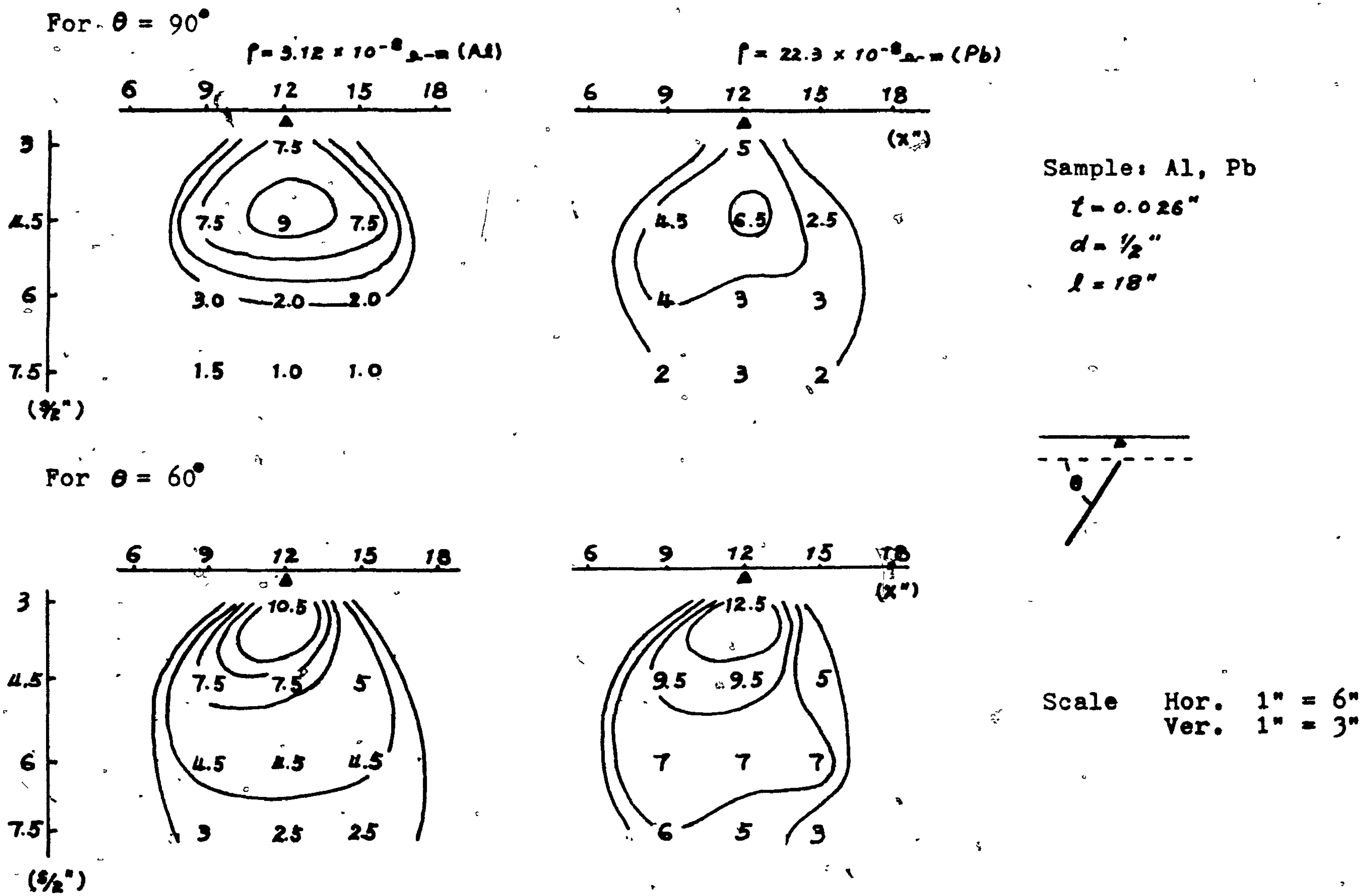

Variation of conductivity

For $\theta = 30°$

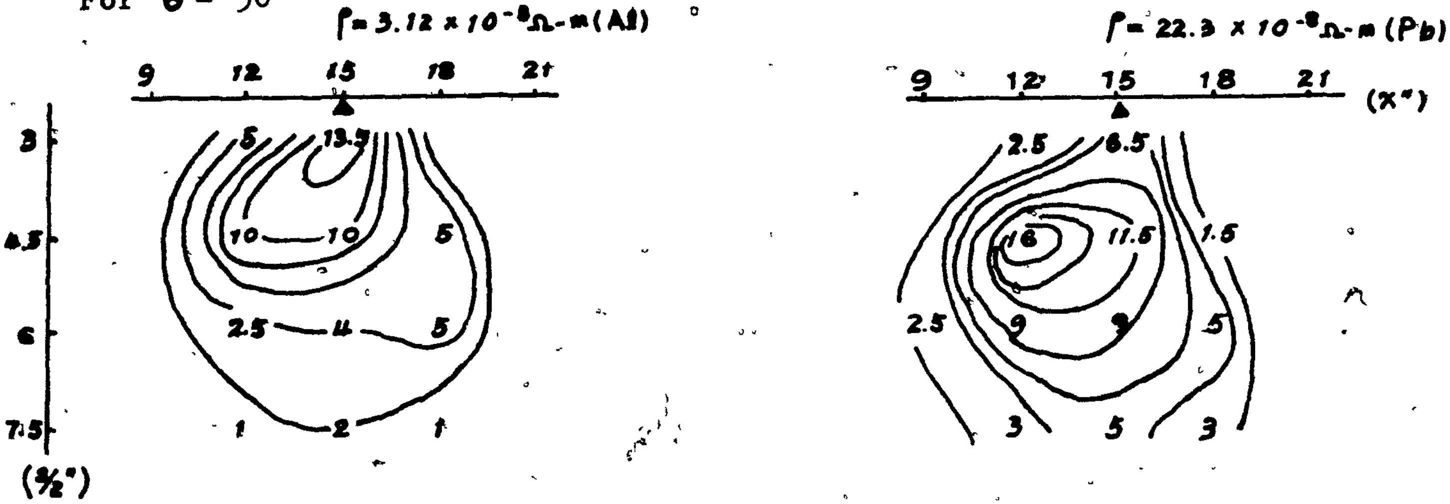

Sample: Al, Pb

$t = 0.026"$

$d = 1/2"$

$l = 18"$

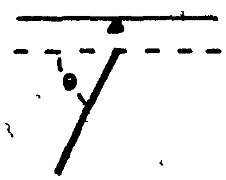

Scale Hor. 1" = 6"
Ver. 1" = 3"

Variation of donductivity

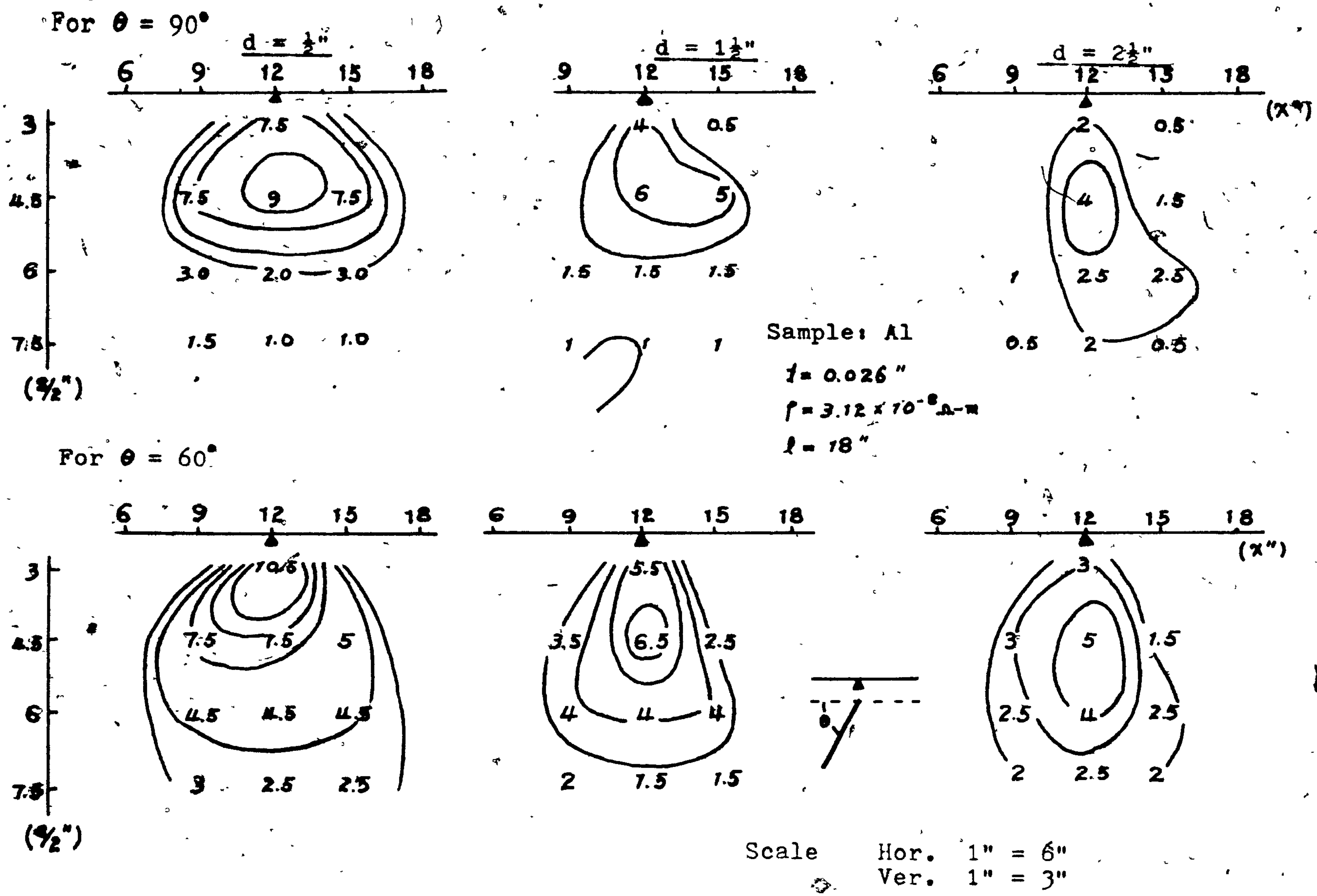

Variation of depth

For θ = 30°

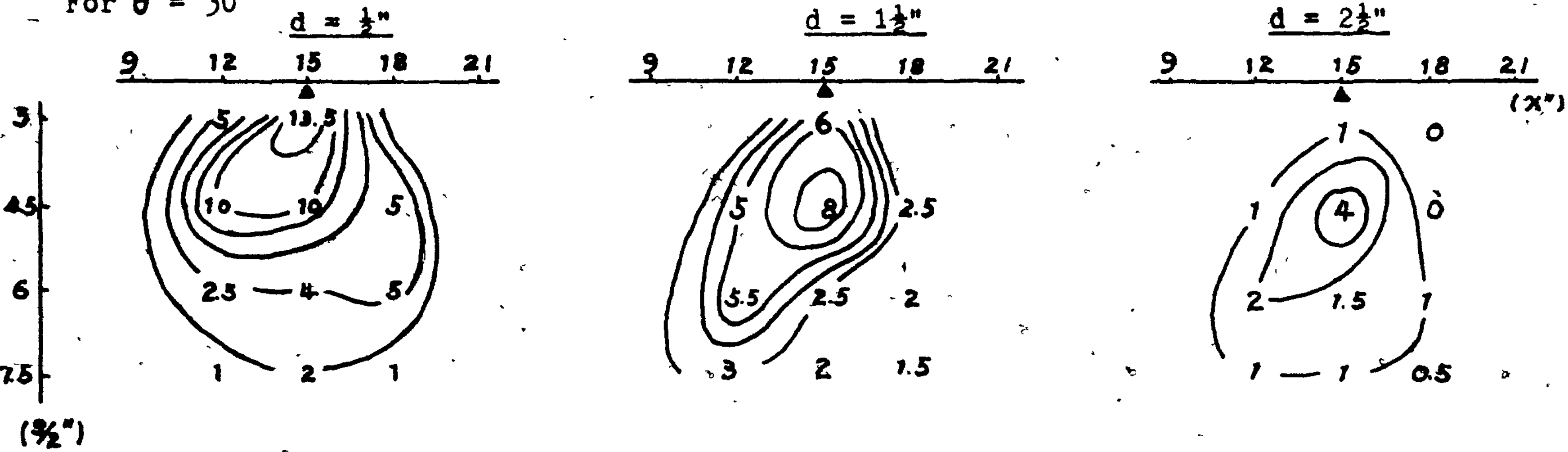

Sample: Al

t = 0.026"

ρ = 2.12 × 10^{-8} Ω-m

l = 18"

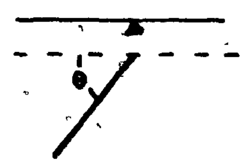

Scale Hor. 1" = 6"
Ver. 1" = 3"

Variation of depth

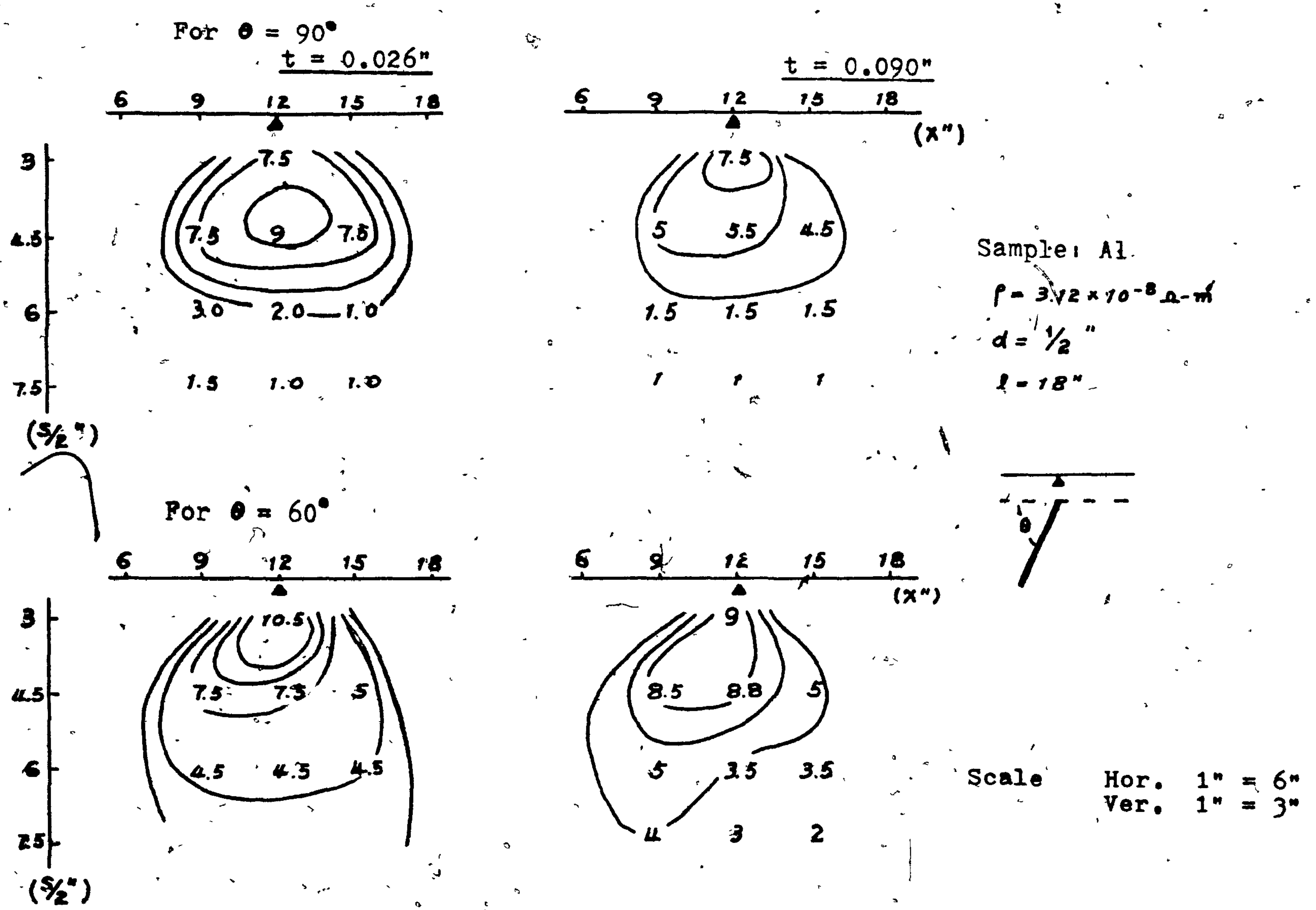

Variation of thickness

For $\theta = 30°$

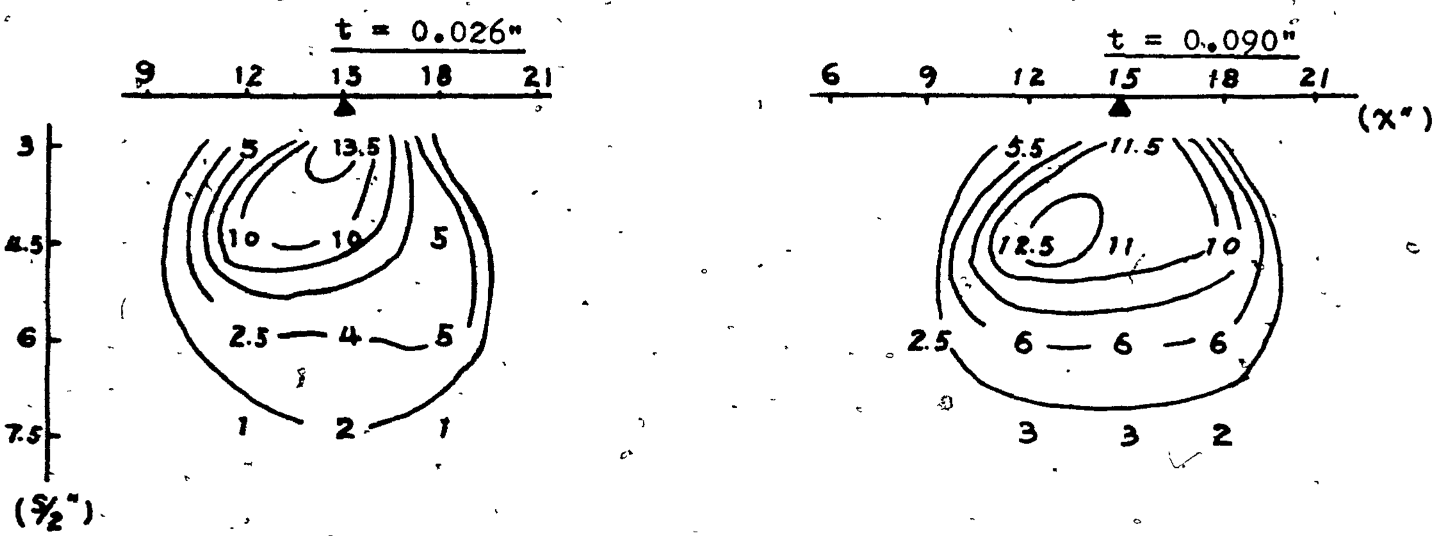

Sample: Al

$\rho = 3.12 \times 10^{-8}\ \Omega\text{-m}$

$d = 1/2"$

$l = 18"$

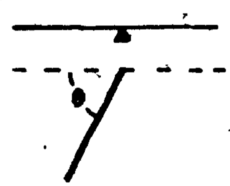

Scale Hor. 1" = 6"
Ver. 1" = 3"

Variation of thickness

Appendix E

Vertical pseudo section of magnitude of secondary magnetic field $\tilde{S}$

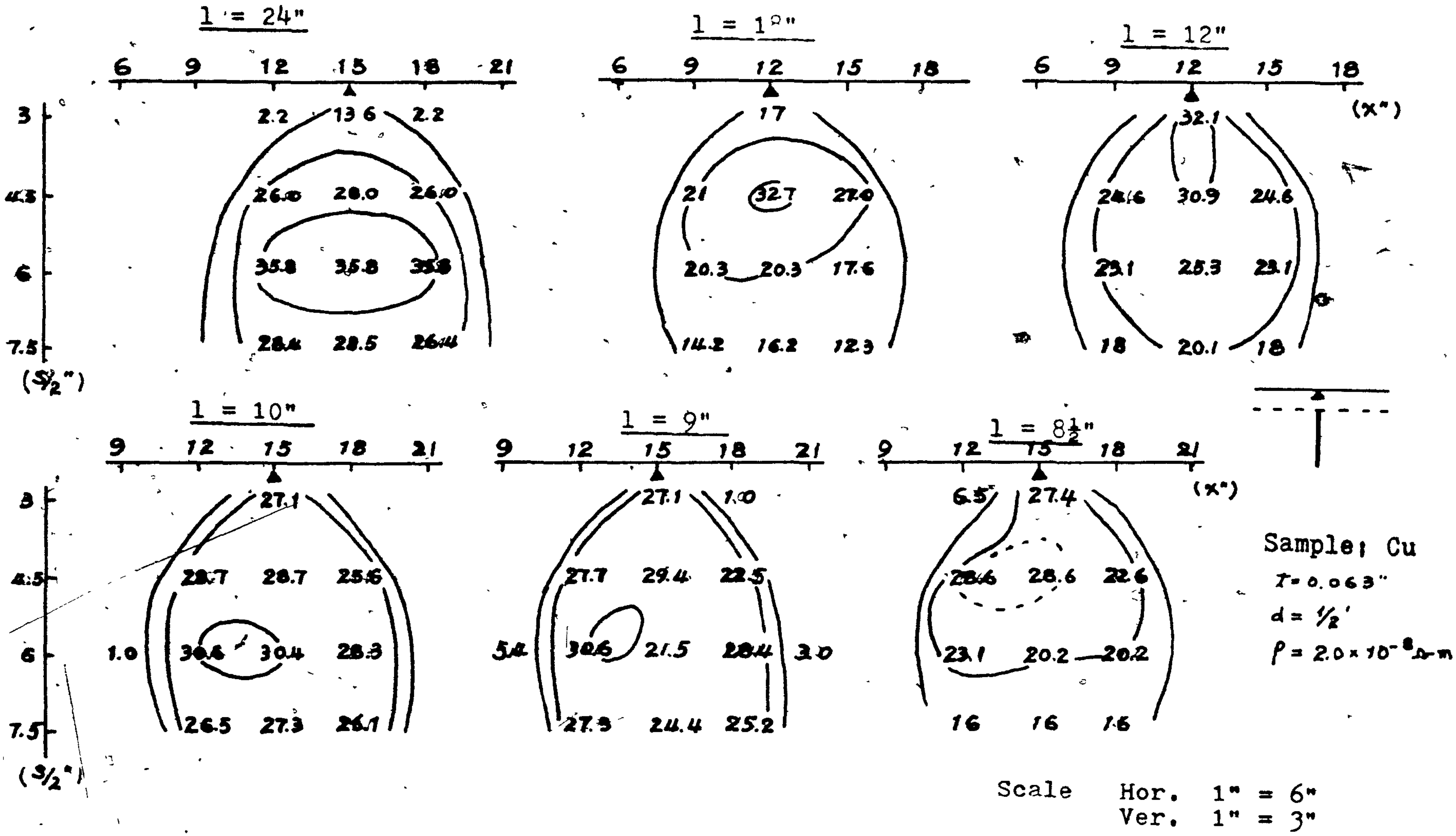

Variation of depth extent for $\theta = 90^{\circ}$

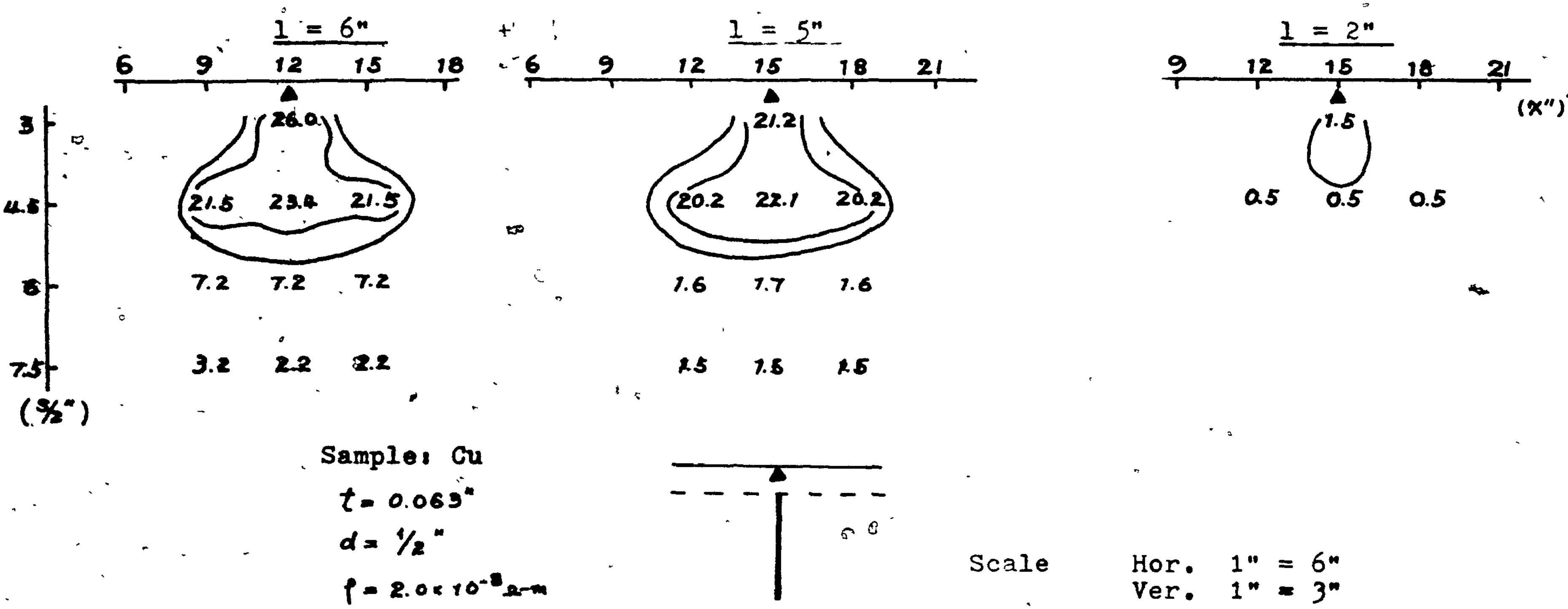

Variation of depth extent for θ = 90°

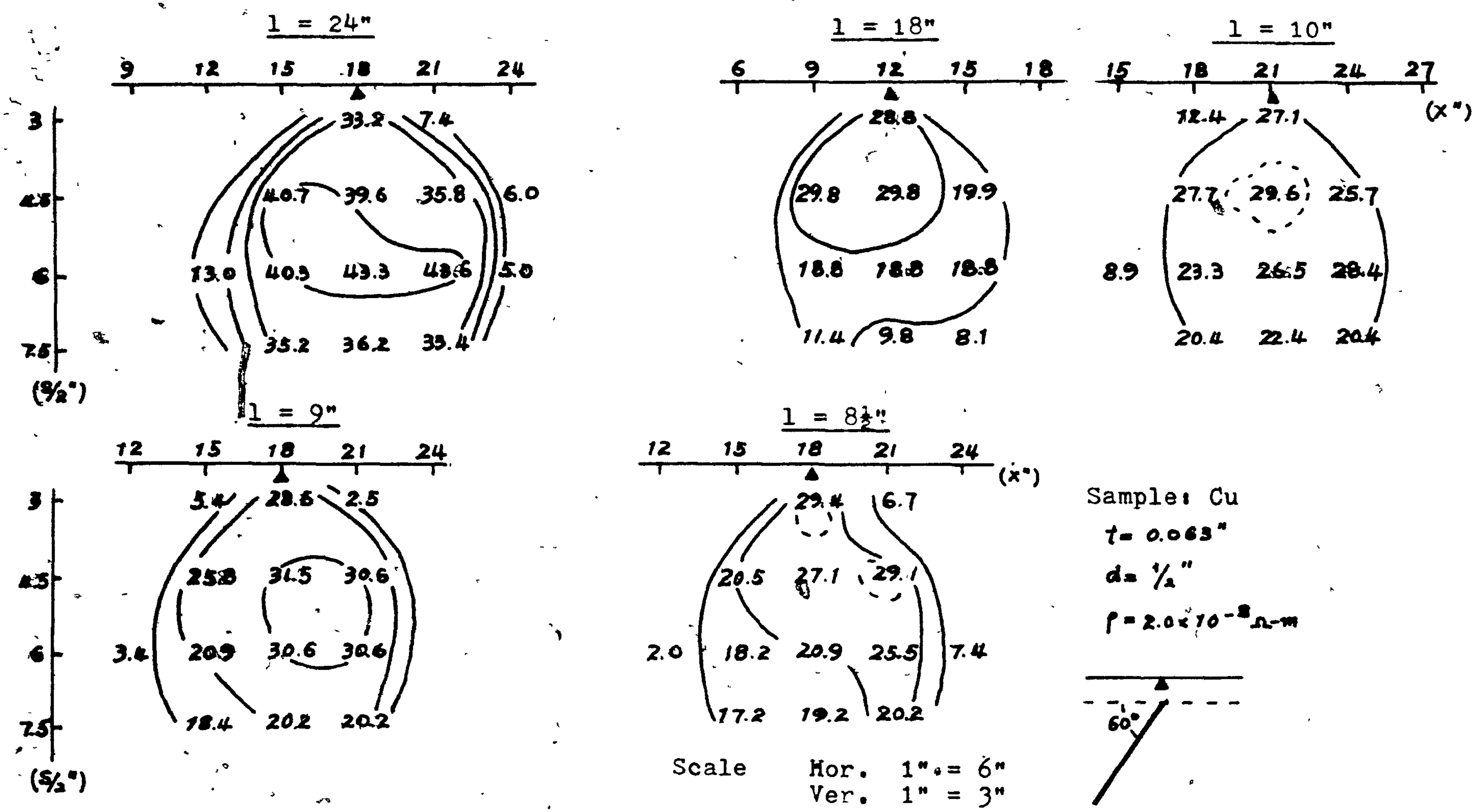

Variation of depth extent for θ = 60°

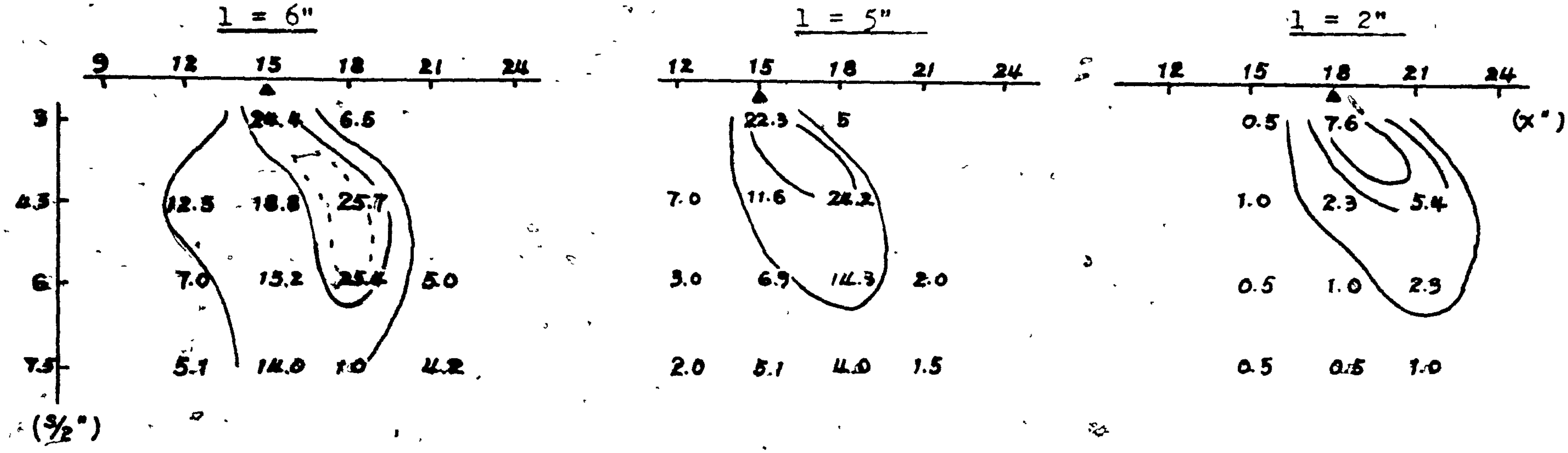

Sample: Cu

$t = 0.063"$

$d = 1/2"$

$\rho = 2.0 \times 10^{-8}\ \Omega\text{-m}$

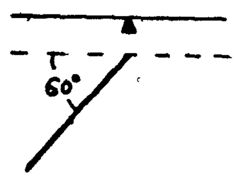

Scale Hor. 1" = 6"
Ver. 1" = 3"

Variation of depth extent for $\theta = 60°$

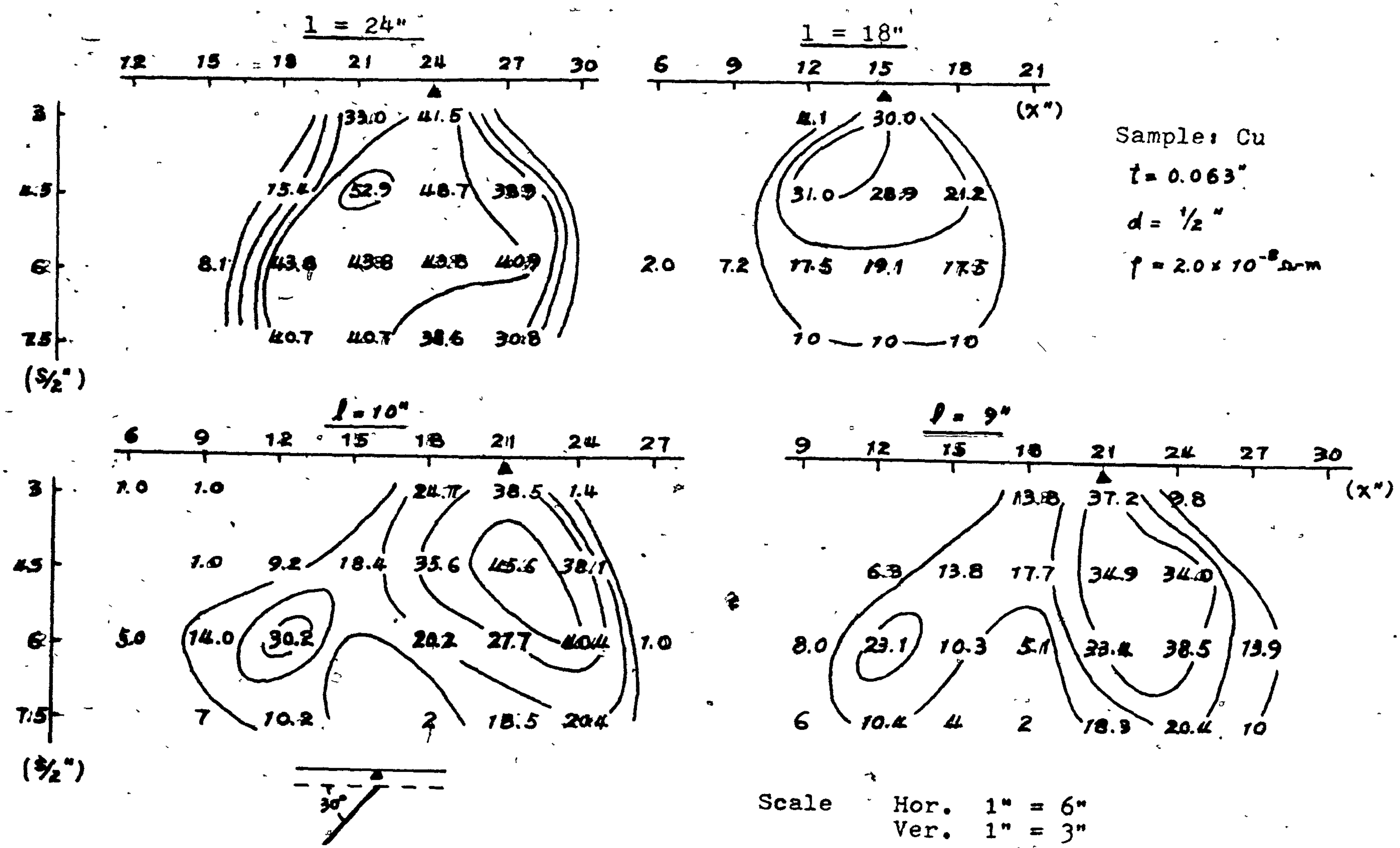

Variation of depth extent for $\theta = 30°$

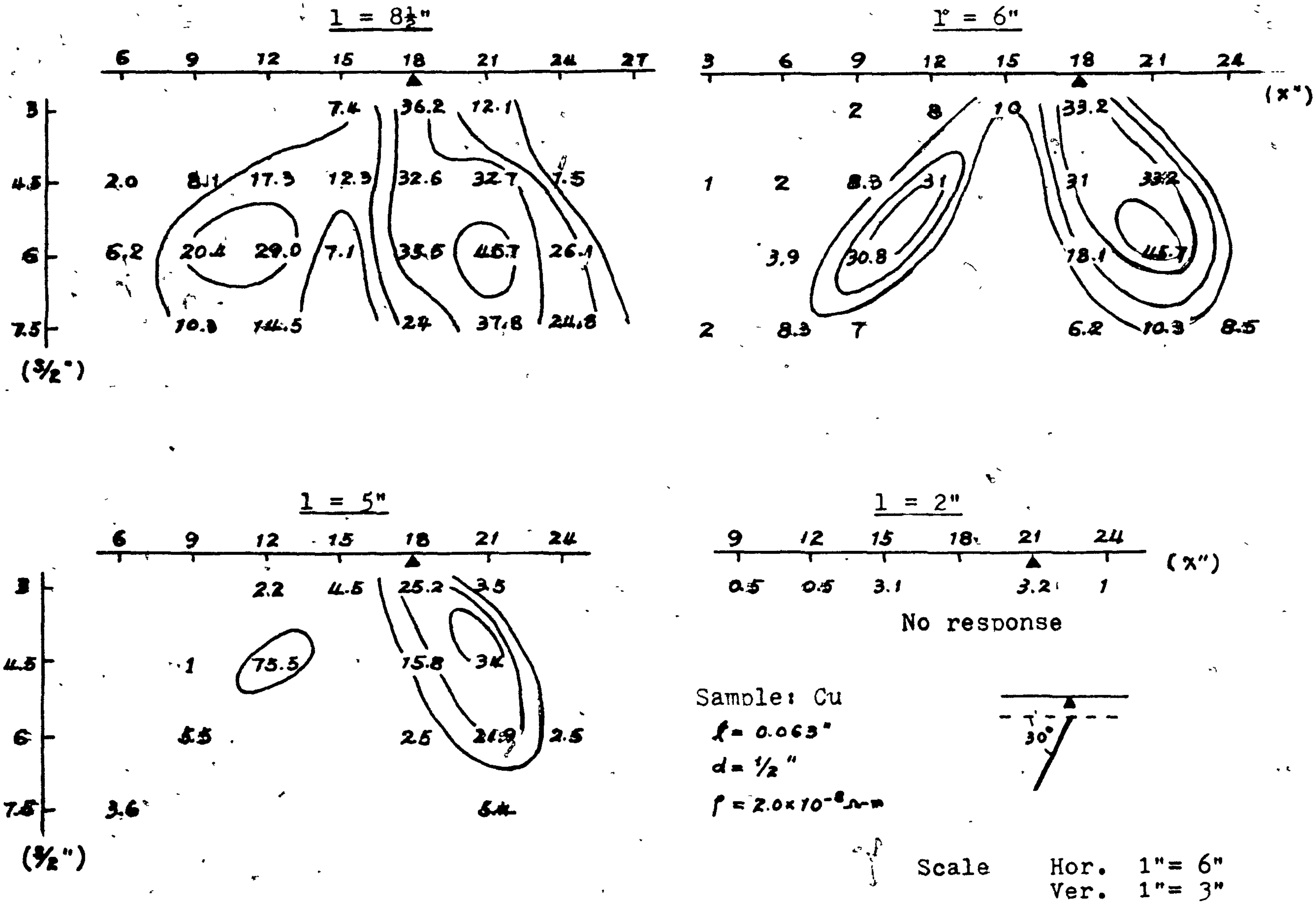

Variation of depth extent for $\theta = 30°$

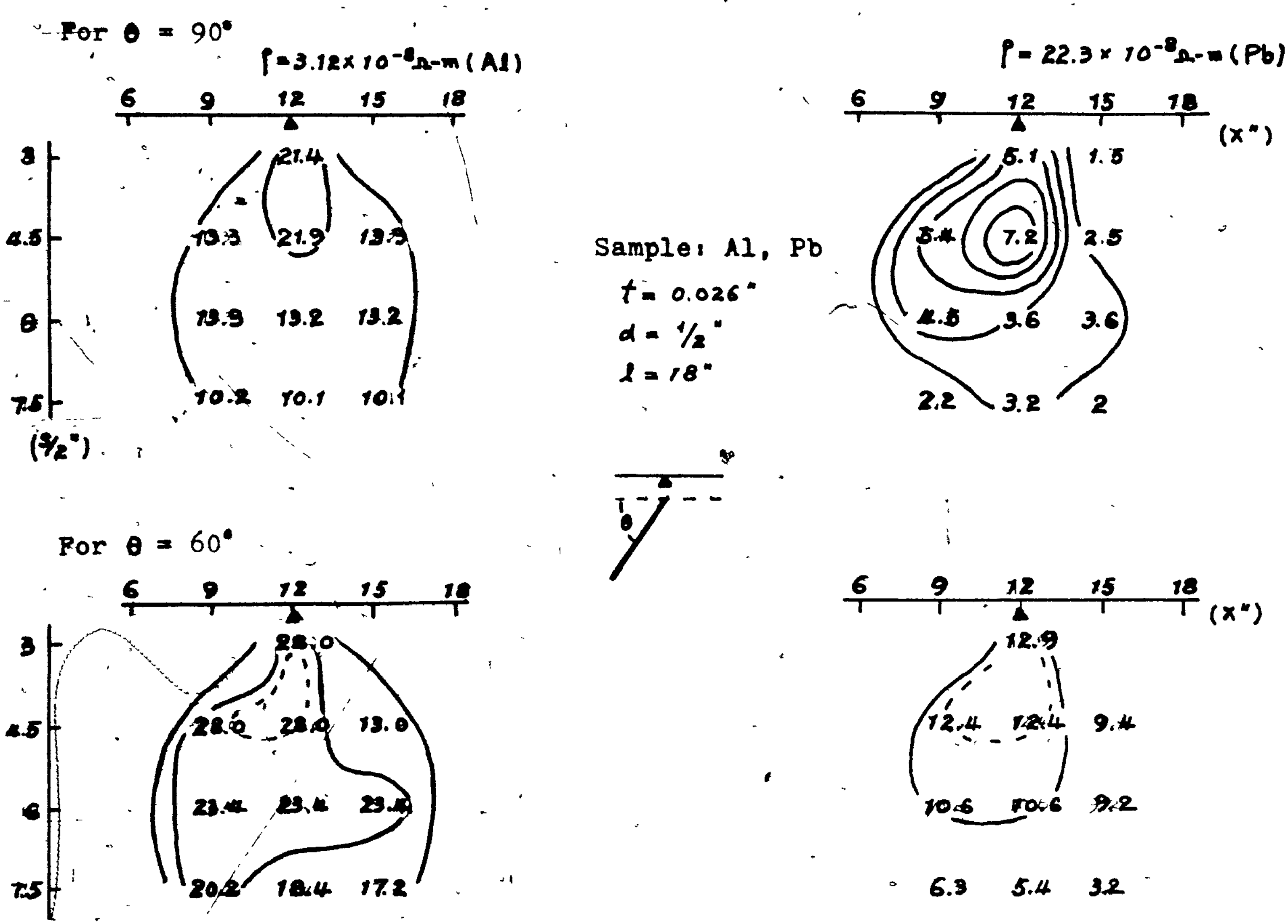

Scale Hor. 1" = 6"
Ver. 1" = 3"

Variation of conductivity

For $\theta = 30^\circ$ $\rho = 3.12 \times 10^{-8}\,\Omega\text{-m}$ (Al) $\rho = 22.3 \times 10^{-8}\,\Omega\text{-m}$ (Pb)

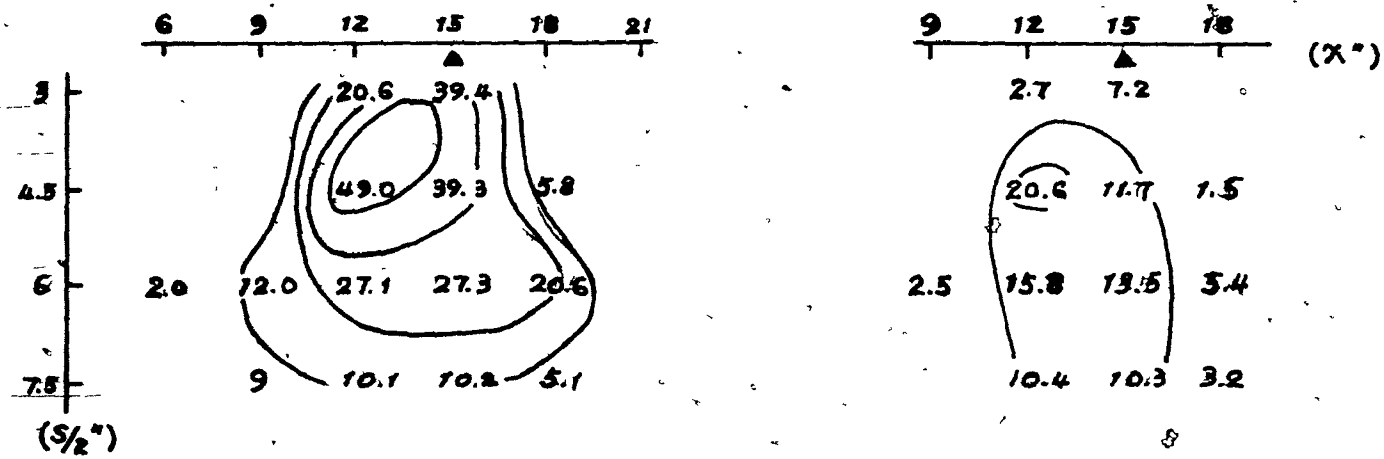

Sample: Al, Pb

$t = 0.026"$

$d = 1/2"$

$\ell = 18"$

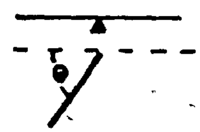

Scale Hor. 1" = 6"
Ver. 1" = 3"

Variation of conductivity

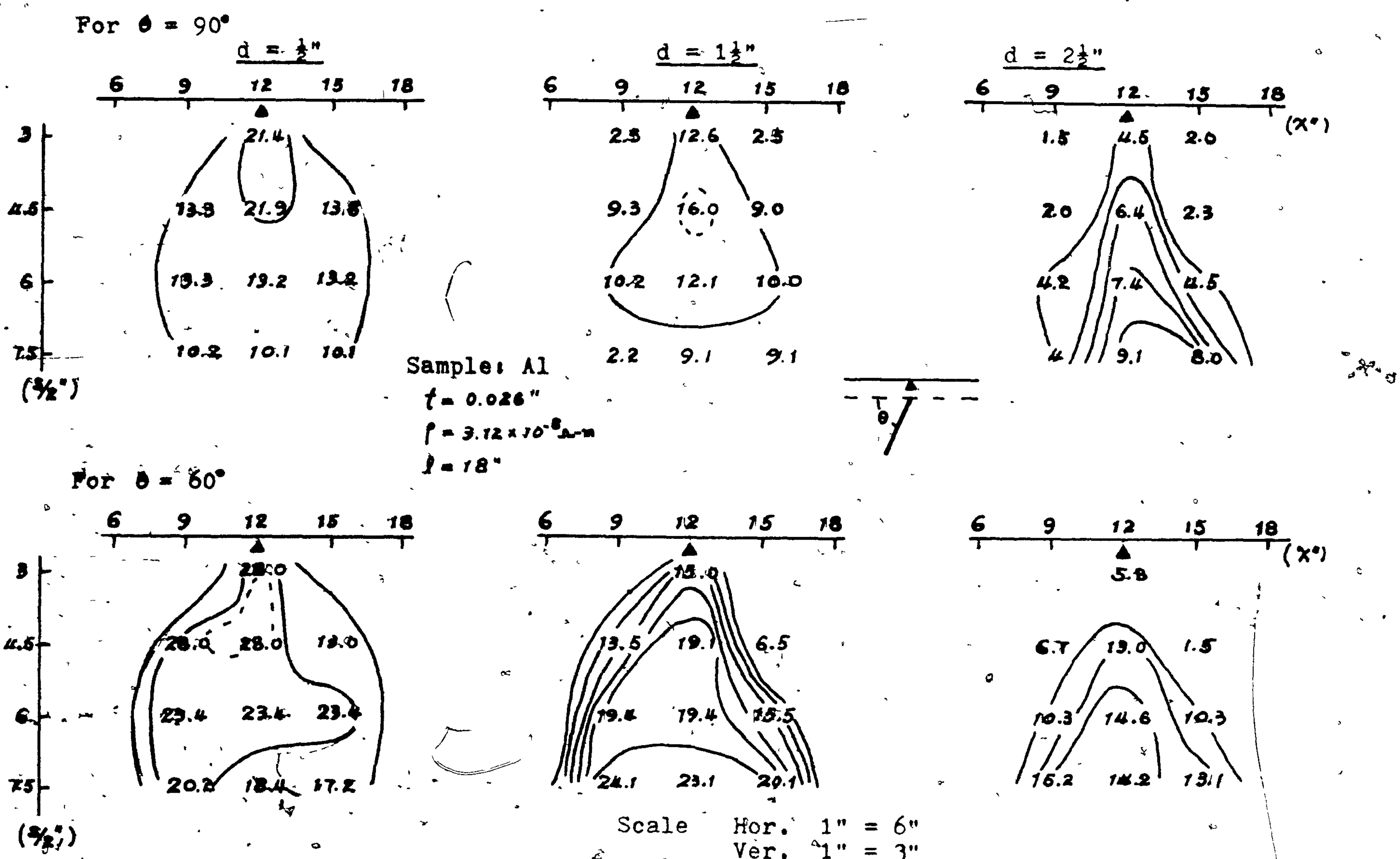

Variation of depth

For $\theta = 30°$

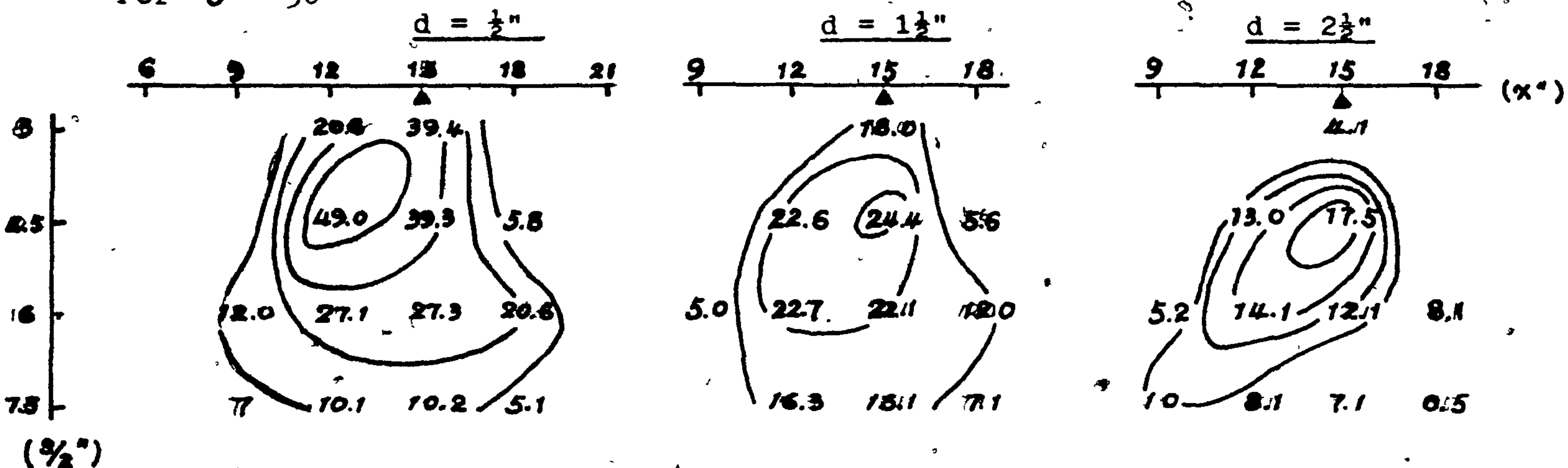

Sample: Al

$t = 0.026"$

$\rho = 3.12 \times 10^{-8}\ \Omega\text{-m}$

$l = 18"$

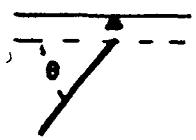

Scale Hor. 1" = 6"
Ver. 1" = 3"

Variation of depth

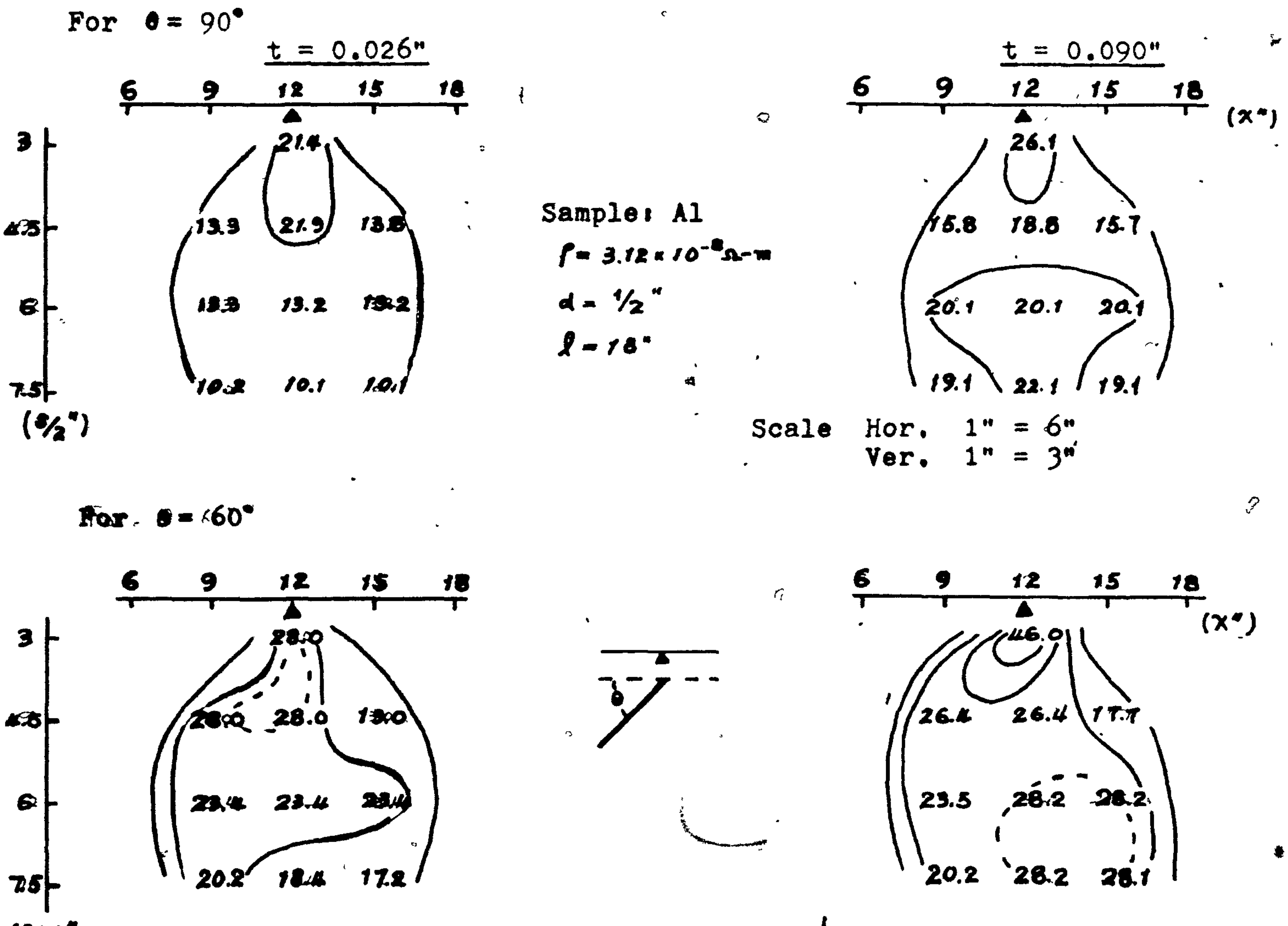

Variation of thickness

For θ = 30°   t = 0.026"   t = 0.090"

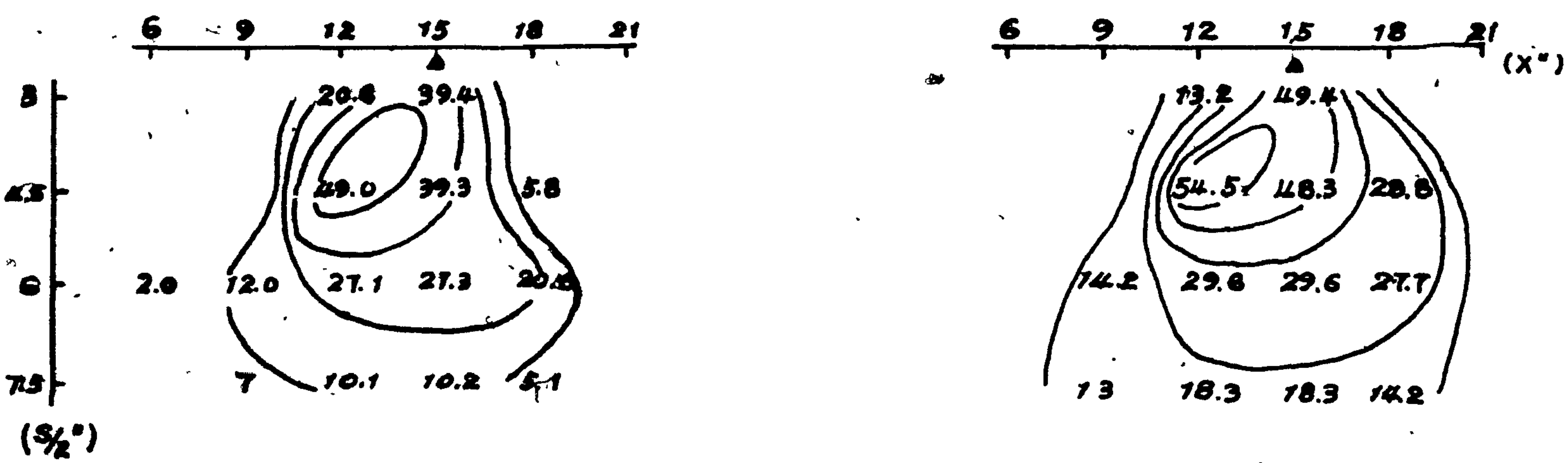

Sample: Al
$\rho = 3.12 \times 10^{-8}\ \Omega\text{-m}$
d = ½"
l = 18"

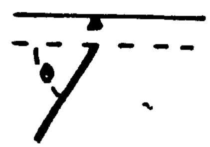

Scale Hor. 1" = 6"
Ver. 1" = 3"

Variation of thickness

BIBLIOGRAPHY

1. Bateman, A. M.(1947), Economic mineral deposits, John Wiley & Sons Inc. New York

2. Beaudet, R.(1952), Engineer's report on the property of Troysco Mines Ltd., Quebec Department of Mines

3. Beaudet, R.(1953), Logs of diamond drill holes made on copper property, Quebec Department of Mines

4. Bergman, D. J.(1971), Report on geochemical and geophysical surveys, Jorex Syndicate, Ham Township, Que., unpublished

5. Bridgman, P. W.(1922), Dimensional analysis, Yale University Press

6. Carriere, G.(1965), Reports on the exploration work performed on lots 27 and 28, Range IV, Ham Township and on lots 8, 9, and 10, Range XI, Wolfestown Township, Ministére des Richesses Naturelles, Québec

7. Cooke, H.C. & Clark, T.C.(1935), Geological Map 419a, Warwick sheet, Geological Surveys of Canada

8. Corson, D. & Lorrain, P.(1962), Introduction to electromagnetic fields and waves, W. H. Freeman & Co.

9. Cress, P., Dirksen, P. & Graham, J.(1970), Fortran IV with Watfor and WATF IV, Prentice-Hall Inc.

10. Duncan, W. J.(1953), Physical similarity & dimensional analysis, Edward Arnold & Co.

11. Grant & West(1965), Interpretation theory in applied geophvsics, McGraw Hill

12. Grover, F. W.(1946), Inductance calculations, Dover Publications Inc., New York

13. Hedstrom, H. & Parasnis, D.(1958), Some model exneriments relating to EM prospecting with soecial reference to air borne work, Geoph. Pros., v.6, no.4

14. Jackson, T. D.(1967), Classical electrodynamics, John Wiley & Sons Inc.

15. Kemp, D. J.(1971), A letter to Jorex Syndicate, unpublished

16. Kim, K.(1970), Report on the test survey at La Ronge, Sask., unpublished

17. Koefoed, O. & Kegge, G.(1968), The electrical current pattern induced by an oscillating magnetic dipole in a semi-infinite thin plate of infinitesimal resistivity, Geoph. Pros., v.16, no.1

18. Koefoed, O. & Struyk, A.(1969), The electrical current pattern induced by an oscillating magnetic dipole in a semi-infinite conductive thin plate, Geoph. Pros., v.17, no.2

19. Koulomzine, T. & Fox, T. V.(1952), Report on the magnetometer & spontaneous polarization surveys of part of the property of Troysco Mines Ltd., Wolfestown & Ham Townships, Wolfe County, Quebec, Ministére des Richesses Natralles, Québec

20. McPhar Staff(1967), A geophysical case history, Cavendish Township, Ont., McPhar Geophysics Ltd.

21. Parasnis, D. S.(1956), The electrical properties of some sulphide and oxide minerals and their ores, Geoph. Pros., v.4

22. Parasnis, D. S.(1966), Mining geophysics, Elsevier Publishing

23. Parasnis, D. S.(1971), Analysis of some multi-frequency, multi-separation EM surveys, Geoph. Pros., v.19, no.2

24. Paterson, N. R.(1959), Comments on paper "Some model experiments......" by Hedstrom & Parasnis, Geoph. Pros., v.7, no.4

25. Paterson, N. R.(1961), Experimental and field data for the dual-frequency phase-shift method of air-borne EM prospecting, Geophysics, v.7, no.4

26. Slichter, L. B. & Knopoff, L.(1959), Field of an alternating magnetic dipole on the surface of layered earth, Geophysics, v. 24

27. Strangway, D. W.(1966), E.M. parameters of some sulfide ore bodies, Mining Geophysics, v. 1, S.E.G.

28. Wait, J.(1954), Mutual coupling of loops over a homogeneous ground, Geophysics, v. 20

29. Wait, J.(1955), Mutual coupling of loops over a homogeneous ground, Geophysics, v. 21

30. Ward, S. H. & Rogers, G. R.(1967) (in) Mining Geophysics v. 2, ch. 1, S.E.G.

31. Wesley, J. P.(1958a), Response of a dyke to an oscillating dipoles, Geophysics, v. 23, no. 1

32. Wesley, J. P.(1958b), Response of a thin dyke to an oscilating dipoles, Geophysics, v. 23, no. 1